FUNCTIONAL FIBROUS MATERIALS WITH CONTROLLED MOISTURE AND LIQUID TRANSPORT PROPERTIES

A Dissertation

Presented to the Faculty of the Graduate School

of Cornell University

In Partial Fulfillment of the Requirements for the Degree of

Doctor of Philosophy

by

Lihong Lao

August 2019

FUNCTIONAL FIBROUS MATERIALS WITH CONTROLLED MOISTURE AND LIQUID TRANSPORT PROPERTIES

Lihong Lao, Ph. D.

Cornell University 2019

Thermal comfort is an essential property in almost every clothing application due to the wearer's physiological need. The thermal microclimate between the body and the external environment can be regulated by clothing systems. There are various functional requirements for clothing systems for different applications. In particular, the huge demand of high-performance and smart clothing has raised up the development of new fibrous systems with better functionalities, of which, moisture and liquid transport properties are of critical importance. In this dissertation, several new fibrous materials with controlled moisture and liquid transport properties are developed for better thermal comfort.

Firstly, a superhydrophilic wrinkle-free cotton fabric has been developed via a nanofluid treatment, which solves the dilemma of achieving both wrinkle-free property and superhydrophilicity on a cotton fabric in a conventional wrinkle-free finishing process.

Secondly, a “skin-like” fibrous system with directional liquid transport property has been designed via surface finishing and selective plasma treatment; the material is able to directionally transport water from the one side to the other, but repels water absorption or penetration in the opposite direction. Finally, a breathable fabric with smart pores to mimic leaf stomata has been explored via hydrogel coating technique; the artificial stomata has the ability to open and close the pores spontaneously according to the humidity change, therefore provides the self-regulating ability for moisture management. All these developments are based on the material design and surface chemistry to enable the different functionalities for the fibrous systems.

BIOGRAPHICAL SKETCH

Lihong Lao grew up in Shaoxing County, Zhejiang Province, China. She received her Bachelor and Master of Science degrees in Polymer Science and Engineering from Zhejiang University in 2007 and 2010. Her master research was polymeric biomaterials for tissue engineering. She then spent four years working as a chemist researcher in Dow Chemical Company, Shanghai Center, China.

Eager to learn more deep fundamentals of chemistry and materials, she began the Ph.D. study in Materials Science and Engineering program at Cornell University in 2014. She did one-year research rotation in Prof. Robert F. Shepherd's lab on the project of synthetic hydrogel materials for simulating arterial plaque. Interested in the materials design for fibrous systems, she then transferred to Prof. Jintu Fan's lab in Fiber Science program, and started the dissertation research on developing new functional fibrous materials with thermal comfort properties. Prof. Robert F. Shepherd and Prof. Emmanuel P. Giannelis are her two other committee members.

During her Ph.D. pursuits, she gained a strong understanding of polymers, fibrous systems, nanomaterials and soft materials, and applied different surface chemistries for developing functional materials. She has published/submitted several peer-reviewed journal articles, and filed two provisional patent applications.

ACKNOWLEDGMENTS

This dissertation was completed under the supervision of Prof. Jintu Fan, and financially supported in part by TAL Apparel Limited through its founding membership fund for Cornell Institute of Fashion & Fiber Innovation (CIFFI) (Project No. 3298753), and by Prof Fan's Faculty Startup and Endowed Chair Professor Fund. The completion of this dissertation owns much to the assistance of many parties.

First of all, deepest gratitude and appreciation to my academic chair, Prof. Jintu Fan for all the patient guidance, support, recognition and freedom he gave me throughout my Ph.D. study. Without his expertise, knowledge and professional advice, this dissertation would not be possible.

Deep thanks are expressed to Prof. Emmanuel Giannelis and Robert Shepherd, for being such great committee members. Prof. Giannelis gave valuable advice to my research, as well as great support for allowing me to collaborate with his lab members. Prof. Shepherd guided me in my quest for the knowledge of soft materials and advised my research by inspiring different ideas.

Special thanks are expressed to my collaborators, Dr. Liling Fu and Dr. Genggeng Qi in Prof. Giannelis' Lab, for guiding me in my quest for more knowledge about nanofluids; and Dr. Dahua Shou in our group, for assisting me the mechanism understanding for the directional liquid transport work.

Sincere appreciations are expressed also to Prof. Margaret Frey for providing the plasma etcher for my research, Hedan Bai for assisting on scheme designs, Dr. Yuen Shing Wu, Dr. Xia Zeng, Dr. Minji Kim, and Dr. Larissa Shepherd for guiding me some experiments and instruments, Prof. Minglin Ma, Dr. Thomas J. Wallin and Shuo Li for providing their advice through the research, and Karen Steffy for all the help on the administrative aspect of my research.

This work made use of the Cornell Center for Materials Research Facilities supported by NSF MRSEC program (DMR-1719875). I would thank Philip Carubia, Don Werder and John L. Grazul for their assistance on materials testing. This work also made use of the Digital Design and Fabrication Studio at College of Human Ecology. I would also thank Charles V. Beach and Vincent Chicone for their assistance on laser cutting and fabrication of molds and masks. This work further made use of Center for Nanomaterials Engineering & Technology at Cornell University.

Last but not least, thanks also to my parents, sister, husband and friends for the love and encouragement throughout this period.

TABLE OF PUBLICATION

Peer-reviewed Journal Articles

1. **Lihong Lao**, Dahua Shou, Yuen Shing Wu, Jintu Fan. "Skin-like" Fabric for Personal Moisture Management. ***Submitted***, 2019.
2. **Lihong Lao**, Yuen Shing Wu, Jintu Fan. Artificial Leaf Stomata for Personal Thermal Regulation . ***Submitted***, 2019.
3. **Lihong Lao**, Genggeng Qi, Emmanuel P. Giannelis, Jintu Fan. Fluorocarbon-free Oleophobic Coatings for Fabric Application. ***In preparation***, 2019.
4. **Lihong Lao**, Liling Fu, Genggeng Qi, Emmanuel P. Giannelis, Jintu Fan. Superhydrophilic Wrinkle-free Cotton Fabrics via Plasma and Nanofluid Treatment. ***ACS Applied Materials & Interfaces***, 2017 (9), 38109–38116.
5. **Lihong Lao**, Sanlin S. Robinson, Bryan Peele, Huichan Zhao, Benjamin C. Mac Murray, James K. Min, Bobak Mosadegh, Simon Dunham, Robert F. Shepherd. Selective Mineralization of Tough Hydrogel Lumens for Simulating Arterial Plaque. ***Advanced Engineering Materials***, 2017 (19), 1600591. (Highlighted on *AdvancedScienceNews.com*.)

Patent Applications

1. **Lihong Lao**, Dahua Shou, Jintu Fan. Preparation of Hydrophobic/Oleophobic Fabrics with Directional Liquid Transport Property. ***US Provisional Patent***. 2018. No. 62/750,062.
2. **Lihong Lao**, Jintu Fan. Breathable Fabrics with Smart Pores to Mimic Leaf Stomata. ***US Provisional Patent***. 2018. No. 62/750,706.

TABLE OF CONTENTS

LIST OF FIGURES

LIST OF SUPPORTING FIGURES

LIST OF TABLE

CHAPTER 1

INTRODUCTION

Clothing is an essential human need, which ensures the normal course of human life and protects human health in different climatic and working conditions. The choice of clothing is based on many factors such as personal desires and different applications [1]. For example, for basic daily use, the wearers may need comfort, protection, good appearance and durability, whereas for an active sport, the wearer may require additional performance such as body fit, fast wicking, active cooling, quick dry, etc. Among all the different functions, comfort is a very critical property in almost every clothing application due to thermal management and health demand.

Comfort is defined as a pleasant state of physiological, psychological and physical aspects between the body and the environment [2]. Physiological comfort refers to the human body's ability to maintain life. It depends on factors such as the temperature of body and skin, tactile sensations, neural responses, lung function, body mechanical efficiency, blood pressure, visual or aural stimulation, taste or smell sensations, and skin hygiene. Psychological comfort refers to the mind's ability to keep itself functioning satisfactorily without external help and is influenced by such attributes as the presence or absence of other human beings, fear, stress, pleasure, embarrassment, or pain. Physical comfort refers to the effects of the external environment on the body's physiological and psychological equilibrium [3]. Each aspect is important, but generally, the comfort preference is more towards the physiological and physical feeling than it is for psychological fulfillment [4, 5].

Physiological comfort relates to the body's thermal regulation and coordinates between production and loss of body heat. It has three categories, tactile (sensorial) comfort, thermophysiological comfort, and garment fit, of which thermophysiological comfort is very significant when the wearer is interacting with an external thermal environment [3].

1.1 Thermal Comfort

Thermophysiological comfort, simply referred as thermal comfort, is a condition or feeling achieved when complex interaction between human sensations, clothing systems and the surrounding environment. It is defined by ASHRAE as that "condition of mind which expresses satisfaction with the thermal environment" (British Standard-BS EN ISO 7730) [6]. Thermal comfort cannot be reached when the body is too cold or too warm or when perspiration produced by the body cannot be freely evaporated and transported to the surrounding environment. The expression of thermal comfort depends on the thermal physiological conditions of the human body, which include heat transfer and mass transfer [7].

1.1.1 Heat transfer

The human body, being a homeotherm, tries to maintain the core temperature at 37 ± 0.5 ºC, and a typical skin temperature of 33-35 ºC [3]. There are four modes of heat transfer for temperature maintenance, which are conduction, convection, radiation and evaporation (Figure 1.1) [3, 8]. The first three modes are considered as dry heat transfer, and the last one is referred as wet heat transfer.

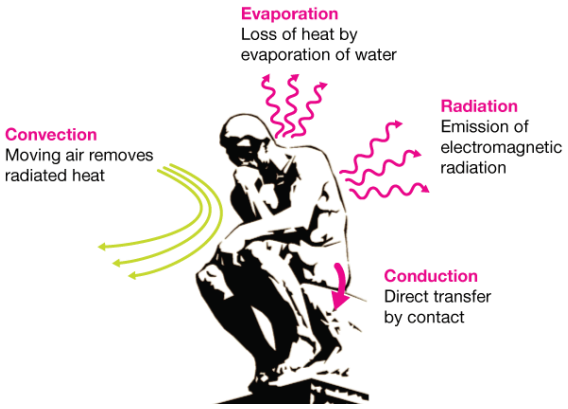

Figure 1.1 Four modes of heat transfer in a human body

In order to maintain the core temperature, the amount of the heat produced by the body and gained from the environment should be equal to the amount of heat loss. Therefore, the heat balance between the body and environment can be described by the following equation [3, 6] :

$$S = M - W - H_k - H_c - H_R - H_E - E_r \quad (\mathrm{W/m^2}) \tag{1.1}$$

where, S represents the rate of heat storage in body (under thermal equilibrium, $S = 0$), M is the rate of metabolic heat production, W is the external work, H_k, H_c, H_R, H_E are heat loss caused by conduction, convection, radiation, and evaporation, respectively, and E_r is the respiration heat loss.

If the rate of metabolic heat production is greater than the sum of all heat loss, the rate of heat storage S will be positive, which will cause the body temperature to rise. Conversely, if the S is negative, the body will lose heat and feel cool [9]. Conduction, convection and radiation are dominated by the temperature difference between skin surface and environment, while evaporation is transmission related to water vapor pressure between

them [7]. Under high activity or in a hot climate, 80% of energy is converted into heat. In such conditions, evaporation is the most important mode for heat loss. Amount of heat loss depends on the sweat evaporation rate, which further depends on the evaporative capacity of environment. Sweat rate can go up to as high as 2.5 L/h in hot and humid conditions due to additional convective and radiative heat loads [10]. If sweat cannot escape sufficiently fast through the clothing, there will be a build-up of moisture at the skin surface which will lead to uncomfortable sensations, such as dampness and clamminess [11].

1.1.2 Mass transfer

Clothing provides a microclimate between the body and the external environment, and acts as a barrier for heat and mass transfer in between (Figure 1.2). Mass transfer includes moisture transfer and gas flow. Moisture from clothing may be transported in vapor and liquid form. In case of vapor form, different mechanism like diffusion, sorption, absorption, convection and condensation are involved, whereas in case of liquid form, wetting and wicking are two mechanisms [7, 8].

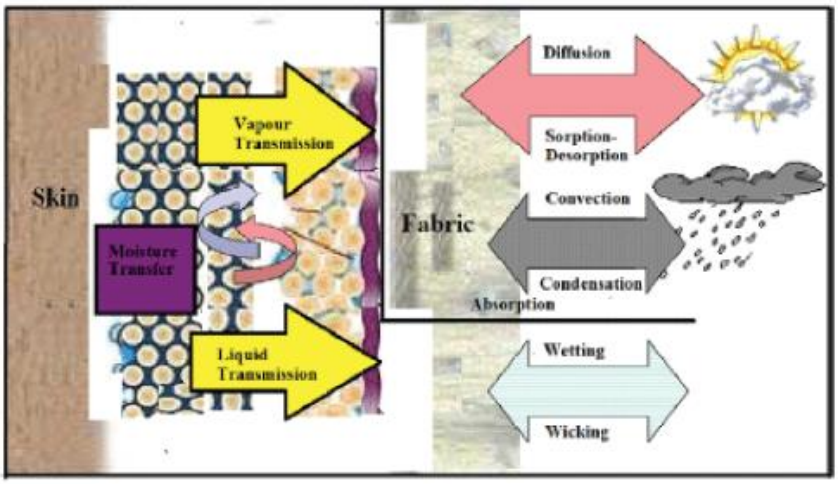

Figure 1.2 Moisture transfer through clothing systems

Wetting: Wetting is the initial process involved in fluid spreading on a material. During the wetting, the solid-air interface is replaced with solid-liquid interface (Figure 1.3) [3].

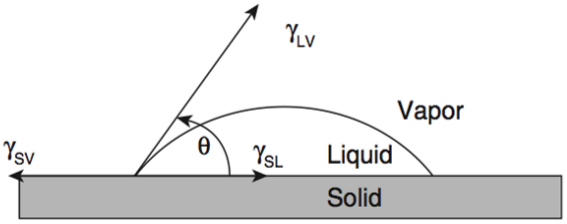

Figure 1.3 Different forces on a water droplet on a solid surface

The forces in equilibrium at the solid-liquid boundary is commonly expressed by the following Young-Dupre equation [12]:

$$cos\,\theta = \frac{\gamma_{SV}-\gamma_{SL}}{\gamma_{LV}} \tag{1.2}$$

where, γ represents the tension at the interface between the various combinations of solid (S), liquid (L) and vapor (V), and θ is the contact angle between the liquid and the surface of solid.

Wicking: wicking is due to solid-liquid molecular attraction at the surface of the solid materials, which is determined by the surface tension and effective capillary pathways and pore distribution [13]. In sweating conditions, wicking is the most effective process to maintain wearer's comfort feeling. When sweat (liquid) coming from the skin is spread through the fabrics, it reaches the spaces between the fibers and produces a capillary pressure (Figure 1.4) [3, 7].

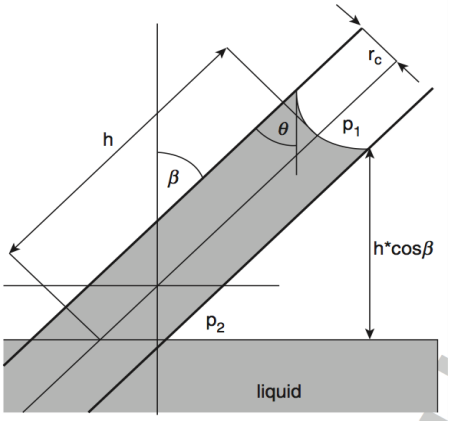

Figure 1.4 Liquid flow in a capillary (wicking)

Due to the meniscus curvature in the narrow confines of the pores, the liquid is dragged out by the capillary pressure, which is given by the Laplace equation [3]:

$$p_1 = \frac{2\gamma_{LV}Cos\theta}{r_c} \tag{1.3}$$

where, p_1 represents the capillary pressure developed in a capillary tube of radius r_c. A difference in the capillary pressure in the pores causes the liquid to spread in the media, and the ability to sustain the capillary flow is referred as wickability [14]. The wicking distance of the liquid can be approximately given by the Washburn-Lukas equation [15]:

$$L = \sqrt{\frac{r_c t \gamma_{LV} Cos\theta}{2\eta}} \tag{1.4}$$

where, L is penetration distance in time t, and η is the viscosity of the liquid. The amount of liquid that wicks through the channel is directly proportional to the pressure gradient. Besides, the moisture evaporation happens at the same time, which offers a dry feeling also.

Apart from moisture transfer, gas flow (e.g. air permeability) is also a very important parameter for evaluating the thermal comfort of the clothing systems. Air permeability is a property of how easily air can penetrate a fabric. It is extremely important for active wearers, as it will directly affect the breathability, and to some degree, the moisture management of a clothing system [16].

The theory of air flow through a porous media is based on Darcy's law, which relates the velocity of a flowing fluid through a porous column proportionally to the pressure difference and inversely proportional to the length of the column [17]. It was found larger pores contribute the most to air permeability, as the flow rate of air relates with the fourth power of the pore radius. Darcy's law can be summarized by the below equation:

$$Q = \frac{kA\Delta p}{\mu h} \tag{1.5}$$

where, Q is the flow rate in volume per time (cc/s), k is the permeability constant (Darcy), A is the area of the test sample (mm^2), h is the thickness of the sample (mm), μ the viscosity of the fluid (cP, 0.185 for air) and Δp is the differential pressure across the sample (psi).

In some cases, the thickness of fabric sample is surprisingly difficult to measure, which leads to a common source of error. In such circumstances, the inverse of permeability, gas flow resistance, is often used in its place. Resistance can be calculated by dividing the thickness h by the permeability constant k.

1.2 Evaluation of Thermal Comfort

Thermal comfort can be evaluated by both subjective and objective methods. In the subjective evaluation, the subjects (players) are asked to wear the garment under study, and each subject rates the comfort sensation like clammy, clingy, sticky, damp, heavy, etc. In the objective evaluation, various methods and equipment have been used.

1.2.1 Evaluation of heat transfer

Thermal conductivity and thermal insulation are the two main properties for measuring heat transfer through the clothing systems.

Thermal conductivity: Thermal conductivity is a fundamental property of the heat transfer through the clothing. For fibrous materials, still air inside is the most important contribution for thermal conductivity, as it has the lowest thermal conductivity value compared to all fibers ($\lambda_{air} = 0.025$) [18].

Thermal insulation: Thermal insulation can be expressed by the thermal resistance of the fabrics, and is inversely proportional to the effective thermal conductivity. In a dry fabric, it depends more heavily on fabric thickness than on fabric construction and fiber conductivity [19].

The thermal insulation properties of the clothing system can be measured using either the guarded hot plate or sweating thermal manikins.

1.2.1.1 Guarded hot plate

The guarded hot plate simulates the sweating skin, an isothermal hot body that is insulated on all sides and energy required to maintain the hot body at a constant temperature is measured (Figure 1.5) [3, 7]. This method also determines the moisture vapor resistance of the fabric by measuring the evaporative heat loss in the steady state conditions (see Section 1.2.2.1.2). The technique has been employed in four modern internationally accepted standards, viz. ASTM standard D1518 (2000), BS 4745 (1974), ASTM F1868 (2002), and ISO 11092 (2014) [3, 7].

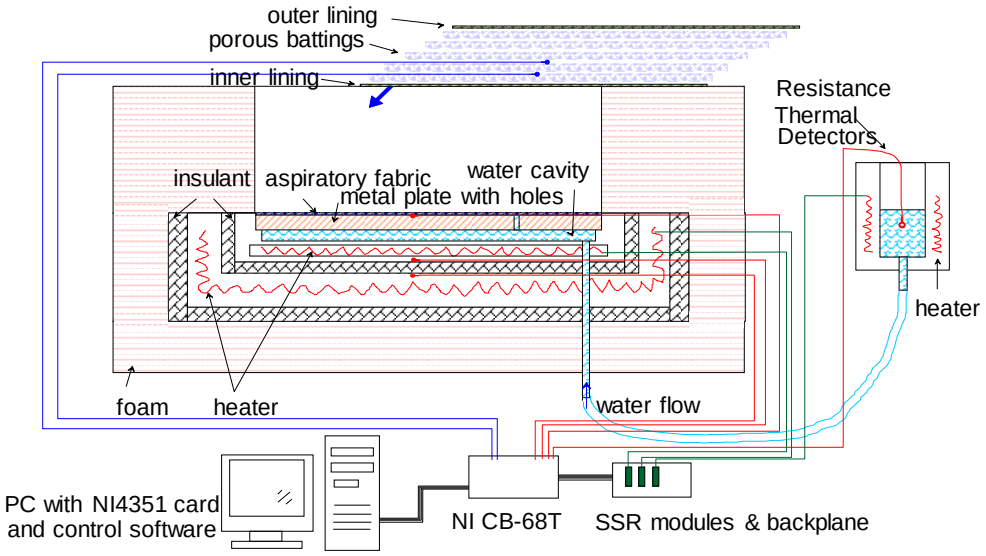

Figure 1.5 Schematic of a guarded hot plate

1.2.1.2 Thermal manikin

Thermal manikin is an instrument for determining the thermal properties of clothing systems. It has two types, viz. dry manikin and sweating manikin. The former one is used

to measure dry heat flow [20], whereas the sweating manikin simulates the perspiring human body, of which "Walter" developed in our group is a typical one (Figure 1.6) [21].

Figure 1.6 Sweating thermal manikin-"Walter"

The skin of sweating fabric manikin-"Walter" is made of permeable waterproof fabrics which is filled with water to create a soft body similar to the human. The core temperature of the body is controlled at 37 ^{o}C by using heaters within the trunk. By testing on the sweating thermal manikin, the thermal insulation of the clothing systems can be determined by [21]: .

$$I_t = \frac{A_s(\overline{T_s} - T_a)}{H} \tag{1.6}$$

where, I_t represents the total thermal insulation of the clothing system plus air layer, A_s is the surface area of the manikin, $\overline{T_s}$ is the mean skin temperature, T_a is the mean ambient temperature, and H is the total dry heat loss from the manikin.

Independently-controlled thermal zones can be created at different locations of the sweating manikin to measure the heat transfer and moisture transmission from different parts of the body [21].

1.2.2 Evaluation of mass transfer

As mentioned in Section 1.1.2, mass transfers through clothing systems either by vapor or liquid moisture forms, or through air flow. There are various methods for measuring different transfer properties.

1.2.2.1 Measurement of vapor transmission

Water vapor permeability is a major property for measuring the vapor transmission behavior of the clothing systems. In different methods, different terms have been used to express this property. The most common terms and the related measurements are listed below.

1.2.2.1.1 Moisture vapor transmission rate

Moisture vapor transmission rate, or water vapor transmission rate (WVTR) is the rate of water vapor transmission perpendicularly through a known area of a fabric within a controlled condition. For measuring this, a upright cup method (ASTM E96, or BS 7209, Figure 1.7) is commonly used [22, 23], where a cup containing distilled water is covered by a test fabric, and placed in a controlled environment of 20 ^{o}C and 65% relative humidity.

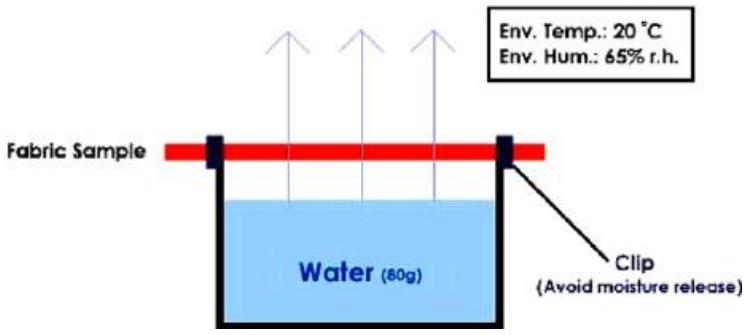

Figure 1.7 Schematic of cup method to measure moisture transmission rate

WVTR is expressed as by:

$$WVTR = \frac{24M}{At} \quad (\text{g/m}^2\text{/day}) \tag{1.7}$$

where, M represents the loss in mass (g), A is the internal area of the cup (m^2) and t is the time interval (h). A is calculated using the following relationship:

$$A = \left(\frac{\pi d^2}{4}\right) \times 10^{-6} \quad (\text{m}^2) \tag{1.8}$$

where, d is the internal diameter of cup (mm).

The moisture transmission rate can also be measured by the Moisture Transmission Tester (Figure 1.8) developed by Ludlow Corp [24], which offers a faster and more simplified method than the ASTM E96 Cup Method. The test fabric is clamped between two halves of a cell, where the low half of the cell containing distilled water and the upper half dried by desiccant at the beginning of the test. The cell is placed in a controlled chamber of 20 ^{o}C and 65% relative humidity. Water vapor from the lower half of the cell (wet side) is transmitted through the sample to the upper half (dry side), and the humidity change is

detected by a humidity sensor in the upper half of the cell. The humidity change is recorded every 3 min, when humidity rises from 50% to 60%.

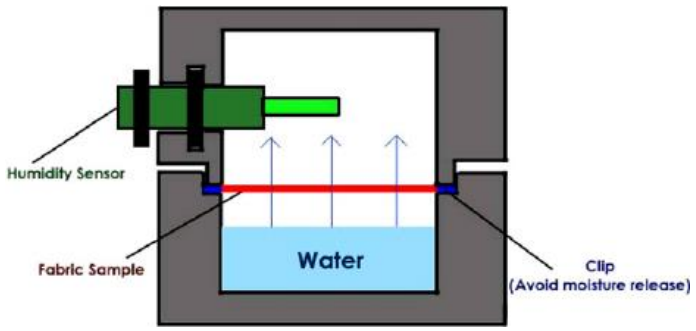

Figure 1.8 Schematic of moisture transmission tester to measure moisture transmission rate

The moisture transmission rate (T) is calculated by:

$$T = (269 \times 10^{-7}) \left(\frac{\Delta\%RH \times 1440}{t}\right)(H) \quad (\text{g/m}^2\text{/day}) \tag{1.9}$$

where, $\Delta\%RH$ is the average of humidity difference between the lower and upper halves of the cell, t is the time between successive readings (t = 3 min), and H is the water content in the air at the cell temperature (H = 45.74 g/m^3).

1.2.2.1.2 Moisture vapor resistance

Moisture vapor resistance (R_e) can be measured by the guarded sweating hot plate (Figure 1.5) as described in ISO 11092 (2014) and ASTM F1868 [3]. By measuring the evaporative heat loss, the total moisture vapor resistance of the test fabric on the plate and the surface air layer, can be determined by:

$$R_e = \frac{A(P_{ss} - P_{sa}H_a)}{H_e} \tag{1.10}$$

where, R_e is the total moisture vapor resistance, A is the sample covering area (A =0.0444 m^2), P_{ss} is the saturated vapor pressure at the skin temperature (controlled at 35 ^oC), P_{sa} is the saturated vapor pressure at the ambient temperature, H_a is the ambient relative humidity (%) and H_e is the evaporative heat loss. To obtain the intrinsic moisture vapor resistance of the fabric, it is recommended to plot the measured R_e values against the numbers of fabric layers (e.g. five), and use linear regression to calculate the slope for the line as the resistance of a single layer of the fabric.

The moisture vapor resistance can also be measured by the sweating manikin (Figure 1.6) as reported by Fan and coworkers [21]. Similar to Equation (1.10), the total moisture vapor resistance can be determined by:

$$R_e = \frac{A(P_{ss} - P_{sa}H_a)}{H_e} - R_{es} \tag{1.11}$$

where, R_e is the total moisture vapor resistance, A is the surface area of the manikin, P_{ss} is the saturate vapor pressure at the skin temperature, P_{sa} is the statured vapor pressure at the ambient temperature, H_a is the ambient relative humidity (%), H_e is the evaporative heat loss, R_{es} is the moisture vapor resistance of the fabric skin which is calibrated in advance (R_{es} = 8.6 m^2 Pa/W). H_e is calculated from the measurement of evaporative water loss, H_e = λQ, where λ is the heat of evaporation of water at the skin temperature (λ = 0.67 W h/g at 34°C), and Q is the rate of evaporative water loss per hour.

1.2.2.1.3 Moisture permeability index

Moisture permeability index (I_m), is a dimensionless parameter, which measures the relative efficiency of the moisture transmission, as described in ISO 9920 (2007) [3]. It can be calculated from the thermal insulation (R_t) in m^2 °C/W and moisture vapor resistance (R_e) in m^2 Pa/W, i.e.

$$I_m = 60.6 \times \frac{R_t}{R_e} \tag{1.12}$$

Alternatively, the moisture permeability index can also be defined based on the WVTR Cup Method (ASTM E96) (Figure 1.7) using the following equation:

$$I_m = [\frac{(WVTR)_f}{(WVTR)_r}] \times 100 \quad (\%) \tag{1.13}$$

where, $(WVTR)_f$ is the mean WVTR of the three test fabrics, and $(WVTR)_r$ is the mean WVTR of the three reference fabrics.

It should be noted that results of the same property obtained from the different available methods are not always comparable due to the different testing conditions.

1.2.2.2 Measurement of liquid water transport

Liquid water transport properties are important for clothing systems, especially when wearers are in high physical activity, or under hot and humid conditions [25, 26]. In these conditions, the ideal fabric should not only absorb liquid rapidly but also transport it out promptly to avoid the discomfort of the fabric sticking to the skin. As mentioned in Section

1.1.2, liquid water transport through the fabric takes place in two processes, i.e. wetting followed by the sequential wicking.

1.2.2.2.1 Wettability

Wettability of a material can be determined by measuring the contact angle between the liquid and the materials by an image processing method [27] . This principle has been used in many techniques like drop analyser tester and automated contact angle tester. A typical contact angle meter is shown Figure 1.9. Usually, the tester can measure both static wetting angle and dynamic wetting angle. The dynamic contact angle is used as a boundary for modelling problems in capillary hydrodynamics. It differs from the static advancing or receding values, even at low velocities.

Figure 1.9 Contact angle meter (model: Attension® Theta Lite)

1.2.2.2.2 Wicking

After wetting the fabric, the liquid reaches the spaces between the fibers and a capillary pressure is developed which forces the liquid to wick along the capillary. Wicking can be

evaluated either from infinite (unlimited) reservoir or from finite (limited) reservoir [12] . The wicking forms from an infinite reservoir include longitudinal wicking, in-plane wicking and transplanar (or transverse) wicking, whereas spot test is another form of wicking from finite reservoir [28].

Longitudinal wicking test: A strip of the test fabric is suspended vertically with its lower end immersed in a reservoir of distilled water, to which a dye may be added for tracking the movement of water (Figure 1.10). The height water has reached is measured after a fixed time. There are two standards for this measurement, viz. BS 3424 (1996) Method 21 and DIN 53924 (1978) [3]. The first one specifies a very long time period (24 h) and is intended for coated fabrics with very slow wicking ability, whereas the latter one specifies a much shorter time of 5 min maximum, and therefore is more relevant to rapidly wicking fabrics.

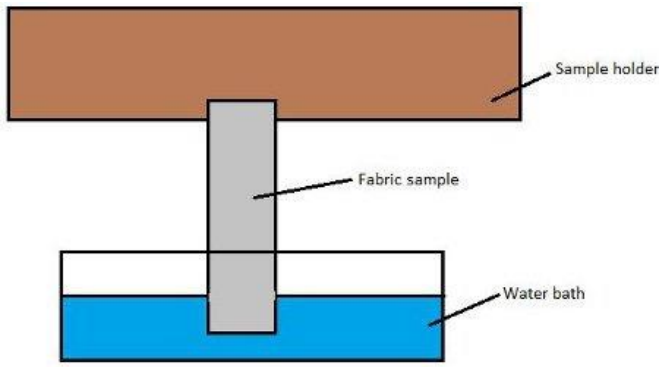

Figure 1.10 Schematic of longitudinal wicking test

Transplanar wicking test: Transplanar wicking transports the liquid through the fabric so as to minimize the wetness sensation. Figure 1.11a illustrates a schematic diagram of the transplanar water transport tester (TWTT) [29]. In the test, a test fabric is placed on a metal plate on top of a water container. A heater is fixed underneath to maintain a constant

temperature of the water. As water is absorbed by or transported through the fabric, water is continuously supplied to the water container through siphon action because it is connected with the left upper reservoir in which water is pumped from the lower reservoir . Since the water level in the testing block is kept constant at that of the upper reservoir, the rate of water absorbed or transported through the fabric can be measured by weighing the total weight of the upper and lower reservoirs and the associated attachments using an electronic balance. The affiliated computer records the amount of water wicked (AWW, g/g) and wicking time (WT, s), and can convert them to surface-water transport rate (SWTR, g/g/s) [7]. Apart from these measurements, this instrument is able to get a new absorption parameter named "maximum water absorption" [30]. A picture of the actual instrument is shown in Figure 1.11b [29].

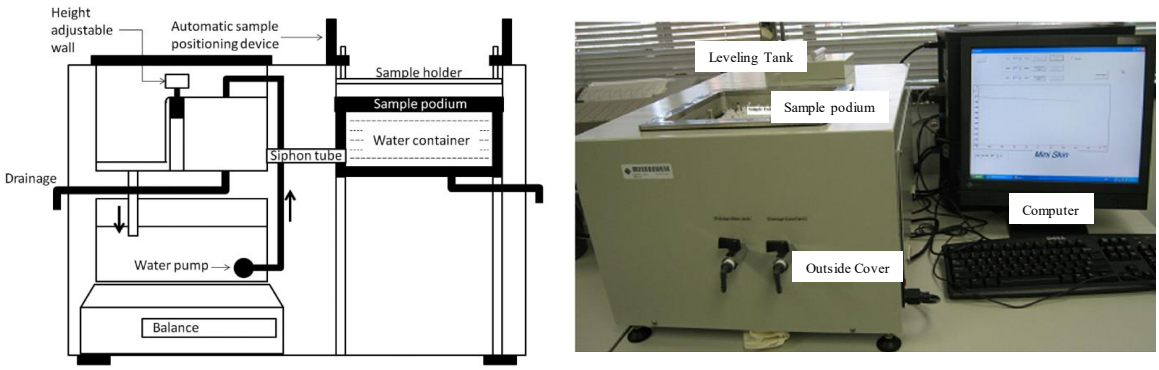

(a) (b)

Figure 1.11 Transplanar water transport tester. (a) Schematic and (b) a picture of a tester.

In-plane wicking test: In-plane wicking is the liquid spreading area in a fabric which facilitates the evaporation of sweat within the fabric. The behavior can be assessed either visually [14, 31], concurrently measured from the transplanar wicking test [29] , or by

measuring the electrical conductivity concentrically around the spot where water is dropped on a test fabric [31, 32], as described in the below spot test.

Spot test: This test can be conducted on an instrument called Moisture Management Tester (MMT) under AATCC 195 method (Figure 1.12a) [33, 34]. The MMT evaluates liquid absorption properties based on the measurement of the change in electrical resistance on a test fabric [34]. A specimen of the test fabric is horizontally placed between an upper and lower sensor having concentric pins (Figure 1.12b). A drop of liquid is delivered from a certain height onto the upper surface (skin side) of the test specimen. As the liquid is transported through the specimen, changes in electrical resistance are recorded. By converting to the liquid content, the instrument gives various moisture management indices, including the accumulated liquid absorption of the upper and lower surfaces of the fabric, maximum difference of the water content between the upper and lower fabric surfaces, initial liquid absorption speeds and spreading rates of water at the upper and lower surface.

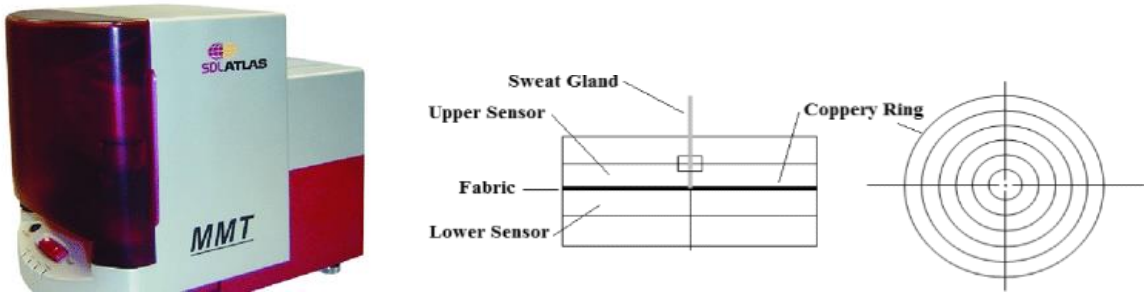

(a) (b)

Figure 1.12 Moisture management tester. (a) A picture of a tester (model: M290, SDL Atlas). (b) Schematic of tester sensors.

1.2.2.3 Evaluation of air permeability

Air permeability is a measure of air flow passing through a given area of a fabric. The measurement can be classified into two types. In one type, the pressure difference between two surfaces of a test fabric is fixed, and measurement is based on the air flow through the material; In another type, the rate of air flow through the fabric is adjusted to a fixed value, and the pressure difference developed across the fabric in order to maintain this air flow is then measured [35]. In the apparel industry, it is more common to use the first method to measure the air flow and thereby calculate the air permeability of a fibrous system.

ASTM D 737-96 and BS 9237 are two standard methods for measuring air permeability [35]. According to these methods, the air flow through a given area of a fabric is measured at a constant pressure drop across the fabric. The fabric is clamped into the air inlet of the tester, and through the use of a pump, the air pressure is made different on different sides of the fabric (Figure 1.13a). Air flows from the side with higher air pressure, through the fabric, to the other side with a lower air pressure. The rate of air flow at this point is measured using a flow meter, and the air permeability is determined. The KES-F8 Air Permeability Tester is a typical instrument for the test (Figure 1.13b). The test can also be done on a gas permeability module on a Capillary Flow Porometer (Figure 1.13c).

(a) (b) (c)

Figure 1.13 Air permeability testers. (a) Schematic of air permeability test. (b, c) Pictures of the actual testers with (b) KES-F8 Air Permeability Tester and (c) Capillary Flow Porometer (Porous Materials Inc., USA), respectively.

1.3 Factors of Thermal Comfort

Thermal comfort of the clothing systems is affected by many factors, of which fibers, yarns and fabrics are the main contributors. Other parameters including skin heat transfer, external heat flux exposure and air gap present between fabric and skin, are also influencing the performance. All these different parameters are inter-related and dependence of thermal comfort of the fabrics on these parameters can be complex.

1.3.1 Fiber parameters

Fiber bulk density: Generally, the greater the bulk density of the fibers, the worse the thermal insulation (warmth), due to the replacement of air by fibers having a greater heat conductivity. However, a too low bulk density of the fibers is also not good, as the radiant heat from the skin can pass through the garment, reducing the thermal insulation [3].

Fiber wettability: Hydrophilic fibers like cotton and viscose tend to have very good wettability [36, 37]. A combination of polyethylene terephthalate (PET) fiber with

hydrophilic thermoregulating viscose Outlast® achieves better wicking ability but poorer drying capability [38].

Water absorption: An increase of the water content will decrease the thermal insulation, as it decreases the air gap between the fibers [3]. The water within the fabrics can absorb the body heat through evaporation, which may cause the "after chill" effect to the wearers, especially after heavy exercise [39].

Fiber cross-sectional shape: Fiber cross-sectional shape plays an important role in moisture and liquid transfer of a fabric. Tetrachannel and hexachannel cross sections offer more surface area for liquid to transport and gives better wicking properties and faster drying [38]. Polyester fibers with trilobal and triangular cross-sections are also reported to improve liquid moisture transmission as compared to normal circular shaped fibers [40]. Five-leaf cross-sectional shapes showed enhanced wicking ability of fabric as compared to circular fibers due to higher capillary forces generated by larger specific surface area [41]. Overall, the fibers having higher filament shape factors improve the moisture management, but the fabrics can have less permeability to air and moisture vapors [42].

Hollow fiber: Hollow fiber helps to trap still air within the fabric, therefore will improve the thermal insulation of the fabrics [3]. Dupont's Dacron 88 is an example. It is a hollow polyester fiber developed for insulation of clothing and backpacking applications [43].

Fiber blend: Core-shell fibers with polyester in core and polyester/cotton in the shell showed a better absorption ability due to the hydrophilicity of cotton and better diffusion

rate of the PET filaments [44]. Soybean protein fiber and cotton blended T-shirt had superior wicking than cotton T-shirts [45].

1.3.2 Yarn parameters

Yarn twist and linear density: With an increase in twist coefficient and linear density, air permeability and vapor transmission are improved, but the absorption are reduced because of a longer wetting time of fabric [46] and the thermal insulation is decreased as well [47]. The wicking height is reported to initially ascend until the maximum height is reached, and then descend [41].Better wicking takes place when more yarns are bundled together [3].

Yarn cross-sectional shape: Polyester fabrics with a four or six channeled yarn structure were developed by Invista, under the trade name of Coolmax® (Figure 1.14a) [8] . Because of the special cross-sectional shapes, the yarns increase surface area that can pull the moisture away from the skin and keeps the wearer cool and dry. The company further combined the channeled surface with a hollow core and developed a new product of Thermolite® (Figure 1.14b), which enables the moisture wicking from the skin when wearer is hot as well as providing warmth for added comfort in colder days [8].

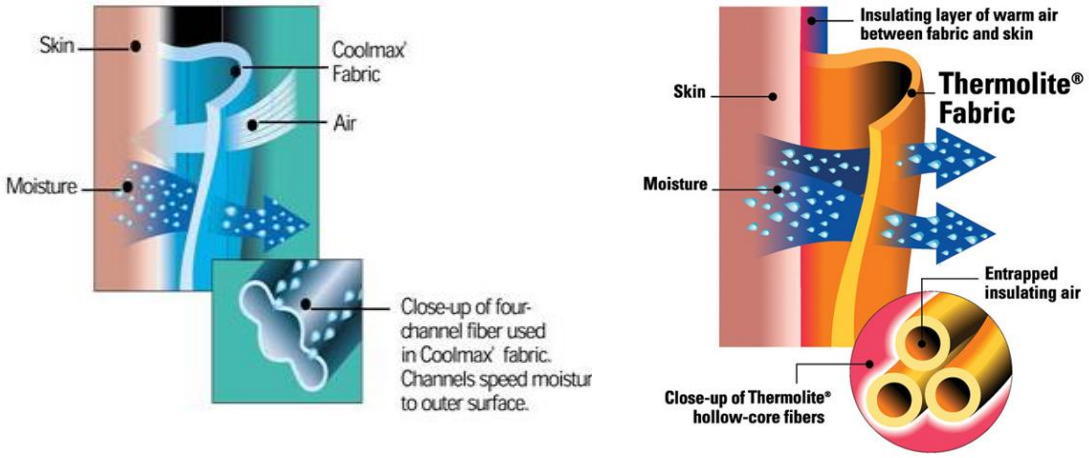

(a) (b)

Figure 1.14 Schematic of different cross-sectional yarns developed by Invista. (a) Coolmax® fabric. (b) Thermolite® fabric.

Filament drawing: High degree of filament drawing can reduce the wicking height, as the drawing reduces the twist coefficient. Under the same twist level, the wicking height of low-stretch yarns is larger than that of the parallel-drawn yarn [41].

Microdenier polyester yarn: Fabric knitted with microdenier polyester yarn showed better moisture vapor transmission, faster heat transfer and cooler feeling as compared to spun polyester, polyester/cotton and 100% cotton yarns [8].

1.3.3 Fabric parameters

Fabric thickness: It is the most important factor governing thermal insulation. There is a linear relationship between thermal insulation and the fabric thickness [3]. Dense and thick fabrics also tend to have a greater resistance to moisture transmission [36].

Fabric weight: A slight increase in thermal insulation value is observed with an increase in the weight of fabric [3]. Also, the greater the fabric weight, the faster the intrinsic absorption, as observed for similar knitted fabric structures [36].

Pore size and porosity: The smaller pore sizes produce higher capillary pressure and thus enhance the liquid spreading and wicking [48, 49]. Furthermore, inter-fiber pores should have proper dimensions to produce sufficient capillary pressure and inter-connective pathways to transport the liquid, and to have sufficient overall porosity to retain the liquid.

Structural variation: It has been reported that the structural heterogeneities in terms of spatial variations in area density, irregularities in fiber orientation, variations in fiber composition, and variations in needle punching for nonwoven fabrics, will result in the water transport properties being different in different directions [50]. The fiber orientation can also influence the in-plane fluid flow and wicking property of a fabric [51]. Texturizing can produce loops, curls or crimps to smooth fibers so as to create a fuzzy or natural appearance and impart more air spaces within their structure [43], therefore the thermal insulation of the fabrics will improve.

Fabric construction: Structure of knitted fabrics and weave type of woven fabrics play crucial role in comfort performance of the clothing systems. Majumdar et al. [52] compared three fabric structures and found that the thermal resistances are the least and air permeability the highest for plain knitted fabrics followed by rib and interlock knitted fabrics. For woven fabrics, the twill weave type has higher thermal insulation and air permeability than the plain weave fabrics [47]. The effect of fabric construction on the water absorption was investigated by Kim et al. [36] who tested a variety of knitted and

woven fabrics, and found the intrinsic absorption of a non-pile woven fabric is higher than that of a double-sided pile fabric, because of the greater surface contact it generates.

Multilayer construction: The thermal insulation of a fabric can improve significantly if covered with a fine closely woven outer fabric or air impermeable surface [3]. Benisek et al. [53] found that a cloth construction with a high density woven fabric as outer layer and a bulky knitted fabric as inner layer offers better thermal protection. In the 1970s, W. L. Gore and Associates introduced Gore-Tex® fabric, which had a high standard of water resistance combined with a high level of breathability, and is designed to be a lightweight, waterproof material for all-weather use [54]. Gore-Tex® fabric is a multilayer construction, composed of a soft inner liner, a resistant outer shell, a middle thin film of stretched polytetrafluoroethylene (PTFE) and two protection interlayers (Figure 1.15). The PTFE polymer film is claimed to contain 1.4 billion tiny holes per square centimeter, which can repel liquid water while allowing water vapor to pass through. Besides, Yao et al. [33] tried to develop different types of multilayer fabrics so as to achieve good moisture management properties, viz. to facilitate the transport of vapor or liquid to the outer layer so as to keep the skin dry.

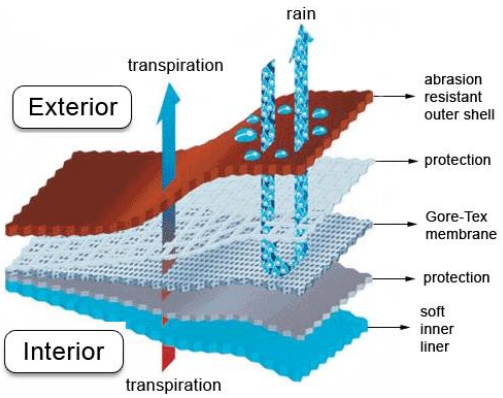

Figure 1.15 Schematic of a composite Gore-Tex fabric for outdoor clothing

Cover factor: Cover factor is also an important attribute influencing the moisture management of a fabric. For example, a knitted fabric with higher cover factor takes more time to wet, resulting in lower overall moisture management capacity [55].

1.3.4 Surface treatment and finishing

Surface treatment and finishing can modify the comfort properties of the fabrics. For example, plasma surface treatment has been used to improve the wettability and rewettability of textile materials [56], as well as the wicking property [57]. Hydrophilic finishing can also improve water absorption [58], e.g. hydrophilic softener applied to a wrinkle-free treated garment improved the water absorption rate [59], and polyester groups introduced on a membrane to impart hydrophilicity on Sympatex polyester film (Akzo Nobel) [60]. Polyurethane coating has been widely used to prepare microporous films and coatings to endow low-temperature flexibility, high abrasion resistance and soft handle, such as Entrant (Toray Industries), Porelle (Porvair), Permatex (J.B. Broadley) and Tarka (Acordis) [60, 61]. Other chemical approaches are also employed in the finishing process. For instance, by polymerization of acrylic acid on the surface of a polyester fabric, the moisture management has been enhanced [62]. Polyester fabric with incorporated activated carbon particles showed improved moisture comfort due to absorption of sweat impulses by the carbon [63]. The presence of a microporous membrane or a laminating substrate in a double fabric construction increases the vapor pressure build-up and a prolonged inner fabric temperature [64]. The different moisture management finishing can also influence the thermal conductivity and thermal absorptivity [65].

1.3.5 Other parameters

The microclimate around the body, such as skin temperature, humidity, air and wind motion, will also influence the thermal comfort of clothing systems. The values of these parameters depend on the amount of heat produced by the body and the heat exchange with the environment [60].

Air gaps: Air is a good insulator as compared to other fabric materials. Air gaps between the body and the fabrics and skin provide additional thermal protection. It was found the larger the air gap, the greater the thermal insulation; but the thermal resistance starts to decrease beyond a gap of about 7.5 to 10 mm, because of convection effects. Still air trapped within fibrous materials will also enhance the thermal insulation of the clothing systems [3].

Wind velocity: Increased wind velocity will reduce the thermal insulation of a fabric compared to that in still air. On the other hand, strong wind will make the fabric less resistant to the vapor and air flow, therefore the moisture transmission and air permeability increase [3] .

Surrounding temperature: Fabric temperature is expected to increase when it is exposed to high surrounding temperature, as encountered by firefighters or some industrial and military workers. Such high temperatures will change the molecular arrangement of the fibers resulting in fabric shrinkage, thereby reducing the air gap within the clothing system; Consequently, thermal insulation decreases [66]. Harold et al. [67] also observed that thermal conductivity increases linearly with an increase in both fabric mean temperature

and its surrounding pressure. Additionally, they found that thermal conductivity decreased with an increase in the molecular weight of the surrounding gas.

1.4 Recent Trends in Thermal Comfort Improvement

Generally, clothing systems with a good thermal comfort property will have positive attributes, including breathability, good water vapor/liquid transmission property and optimum heat regulation [7]. Other performance such as easy care, durability, and smart designs will endow additional values for developing high functional clothing systems.

1.4.1 Temperature responsive membranes

Temperature responsive membranes are those responding with the temperature stimulus that could be incorporated into clothing systems for thermoregulation. Usually these materials have both hydrophilic and hydrophobic phases, and undergo abrupt changes in electrostatic and hydrophobic interactions in an aqueous solution at a critical temperature [68]. Poly(N-isopropylacrylamide) (PNIPAAm) is the most representative thermo-responsive polymer. It can switch hydrophilic and hydrophobic state by varying the temperature below or above the lower critical solution temperature (LCST) of ~32 ^{o}C (Figure 1.16) [69]. By fabricating a porous membrane with thermo-responsive PNIPAAm, Kim et al. [70, 71] and Park et al. [72] found the pores can open under temperatures higher than LCST, and thus increase the water vapor transmission rate.

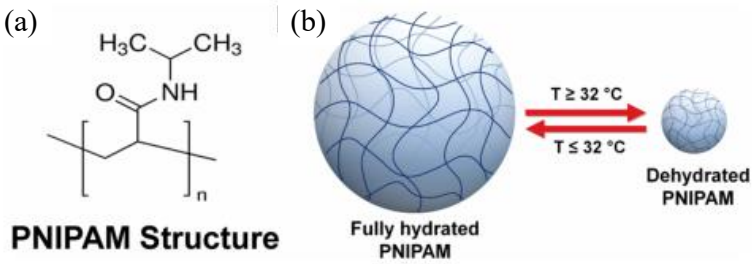

Figure 1.16 Poly(N-isopropylacrylamide) (PNIPAAm) structure and phase transition under different temperatures. (a) Chemical structure of PNIPAAm. (b) Scheme to show the volume phase transition of cross-linked PNIPAM hydrogel. Below the LCST (32 ^{o}C), the hydrogel is in a swollen hydrated state. Above the LCST, the hydrogel is in a compact and dehydrated state.

Another category of thermo-responsive membrane is based on shape memory materials. These materials can change their moisture transmission at the transition temperature, such as glass transition temperature or melting point of crystalline segments. For instance, when melting takes place, the motion of the soft-segment molecular chains leads to an increase in free volume and thus more free paths to allow the water vapor to pass through more easily [73]. The crystal melting of a shape memory polyurethane film is also demonstrated to increase the water vapor permeability when the temperature ranges from 10 to 50 °C, and the relative change of amorphous area increases with the rise of temperature as well [74]. A nickel-titanium alloy is another example of shape memory materials, which expand at a certain temperature, resulting in increased air gap between the layers (Figure 1.17) [75, 76]. Air being a good insulator, the expanded space will result in less heat transfer to the body and thus better thermal protection, as demonstrated by the alloy integrated multilayer fabrics, an actual prototype of thermal protective clothing.

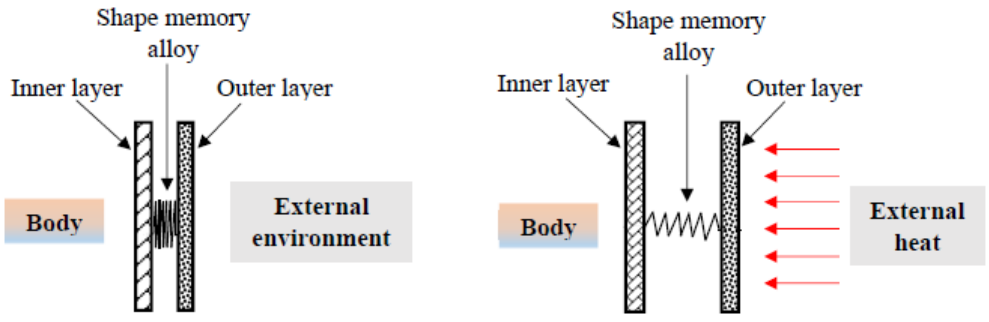

(a) (b)

Figure 1.17 Effect of shape memory alloy on thermal protective clothing. (a) Shape memory alloy in original state during normal conditions. (b) Shape memory alloy in expanded state during heat exposure.

Phase change materials (PCM) is a third type of temperature responsive materials. It is a substance that melts or solidifies at a certain temperature, therefore is capable of storing and releasing large amounts of energy. Heat is absorbed or released when the material changes from solid to liquid and vice versa. Various PCM materials, such as hydrated inorganic salts, linear long chain hydrocarbons, polyethylene glycol, and paraffin wax (octadecane, nonadecane, hexadecane, etc.) can be encapsulated in textile materials [60], of which paraffin waxes is the most preferred materials due to the non-corrosiveness, chemical and thermal stability, and low under cooling [77]. Paraffin waxe is made of linear long chain hydrocarbons. The melting temperature and crystallization points vary depending on the number of carbon atoms. Octadecane is particularly suitable for clothing because its melting point is ~28.2 ^{o}C, which absorbs a large amount of heat and releases that heat in a slush state, e.g. below the mean skin temperature of 33.3 ^{o}C [78]. The temperature range can be controlled through a mixture of different types of paraffin waxes based on the different requirement. Shim et al. [79] used paraffin mixture that contains 40% octadecane and 60% hexadecane as the PCM in thermoregulatory clothing. Because of

different phase change temperatures (28.3 °C and 18.3 °C for octadecane and hexadecane, respectively), the PCM enables the suit to provide both cooling and heating effects depending on the environment temperatures. However, paraffin based PCMs are generally not suitable for firefighters because of the high flammability [80].

Outlast® fabric (Outlast® Technologies LLC), originally developed for the National Aeronautics and Space Administration (NASA), is another example utilizing a PCM named Thermocules™, microcapsules that absorb, store and release heat for optimal thermal comfort. The Thermocules™ are encapsulated into fibers and fabrics with a diameter of only a few micrometers (Figure 1.18a) [60]. When the skin gets hot, they absorb the heat as they change from a solid to a liquid state; and as the skin cools, they release the heat as they return to a solid state (Figure 1.18b). Therefore, the fabric can continually regulate the skin's microclimate, and act as a transient thermal barrier by protecting the wearer from a cold or hot environment [78].

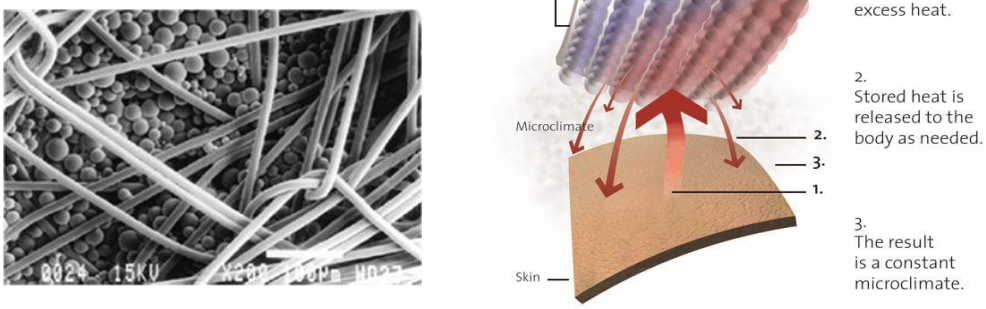

(a) (b)

Figure 1.18 Outlast® phase change fabric. (a) Thermocules™ microcapsules in an Outlast® fabric (scar bar 100 µm). (b) Functioning principle of the Outlast® fabric.

1.4.2 Moisture responsive membranes

Moisture responsive membranes are those that respond with a moisture or humidity stimulus. Researchers in Massachusetts Institute of Technology (MIT) media lab designed a moisture responsive workout suit with ventilating flaps that open and close in response to an athlete's body heat and sweat (Figure 1.19a) [81]. These flaps, which range from thumbnail- to finger-sized, are made of heterogeneous biohybrid films that are composed of humidity-inert fabric substrate (Latex) lined with a layer of live microbial cells, named Natto cells, which can shrink and swell in response to the changes in humidity (Figure 1.19b). Such actuating behavior of the cells drives the flaps to open when an athlete is severely sweating, and pulls them closed when the body has cooled down.

(a)

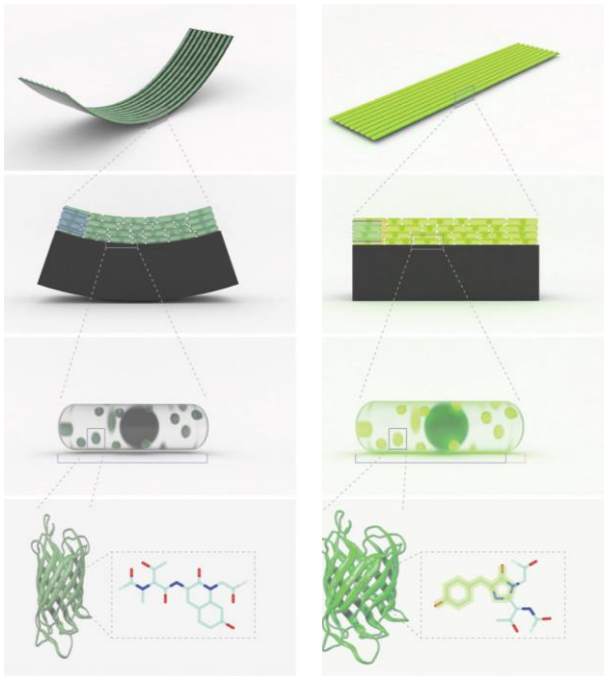

(b)

Figure 1.19 A moisture responsive biologic fabric integrated to a workout suit. (a) Images of garment prototype with the moisture responsive biologic fabric before exercise with flat ventilation flaps (left) and after exercise with curved ventilation flaps (right). (b) An illustration showing the reversible transformation of the biohybrid film incorporated with Natto cells. The film bends at low humidity levels with shrunk cells (left) and becomes flat and glows at high humidity levels (right).

Using similar dual-layer and flap concepts, Mu et al. [82] attached a commercial perfluorosulfonic acid ionomer (PFSA) film on an inert substrate of polyethylene glycol terephthalate (PET) film, and integrated it into a commercial sports shirt to facilitate the personal heat and humidity management (Figure 1.20a). The PFSA matrix with semilunar patterns is able to curl in an outward direction in response to the vapor stimuli. The fabric patented with the PFSA flaps exhibited a higher WVTR (237 g/m^2/h) than the standard polyester fabric (145 g/m^2/h) (Figure 1.20b). A wearing test reveals that the PFSA actuator-based shirts cooled down the skin temperature by 1.3 ^{o}C compared with a typical commercially available sportswear after a man running for 3 km (Figure 1.20c).

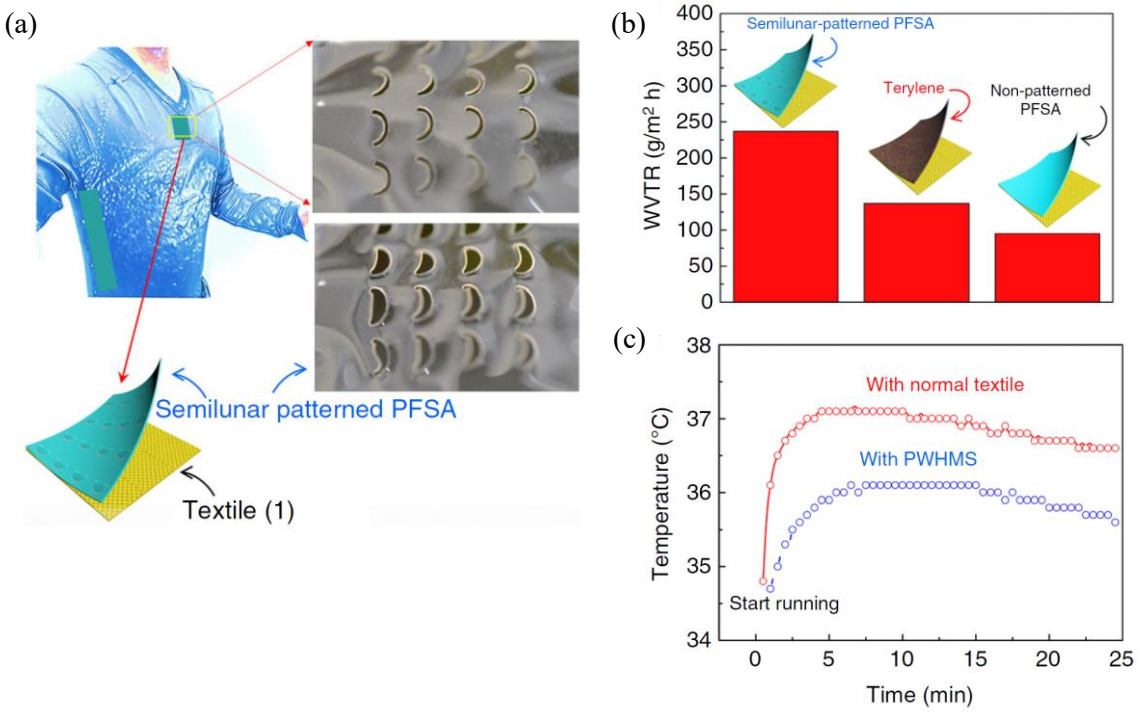

Figure 1.20 A perfluorosulfonic acid ionomer (PFSA) matrix with semilunar patterns integrated into commercial sports shirt to develop clothing for personal humidity and heat management. (a) Schematic of a sports shirt with the patterned PFSA film which is able to curl in an outward direction under high humidity. (b) Water vapor transmission rate test of three type of PFSA films with semilunar patterns shirt, standard polyester fabric sports shirt, and PFSA film (without any pattern)-based shirt. (c) Plots of the time-dependent skin temperature of a man running 3 km wearing different shirts.

1.4.3 Infrared reflective films

Infrared thermal radiation from clothing systems may contribute more than 50 % of the total body heat loss in a relatively cold environment [83]. Hence, regulation of infrared thermal radiation can be applied for thermoregulation.

Hsu et al. [84] developed a metallic nanowire-coated cotton textile that aimed to warm up human body through increasing the reflection of body infrared radiation by 40% (Figure 1.21). The network of the metallic nanowires (silver nanowires, AgNW) has void space of ~200 nm, smaller than the infrared reflective (IR) wavelength, and thus can allow the IR radiation to be reflected back toward the body (Figure 1.21a). Therefore the heat loss can be minimized, viz. 21% more thermal insulation, whereas the moisture vapor transmission will not be blocked through the fabric, viz. only 2% decrease (Figure 1.21b).

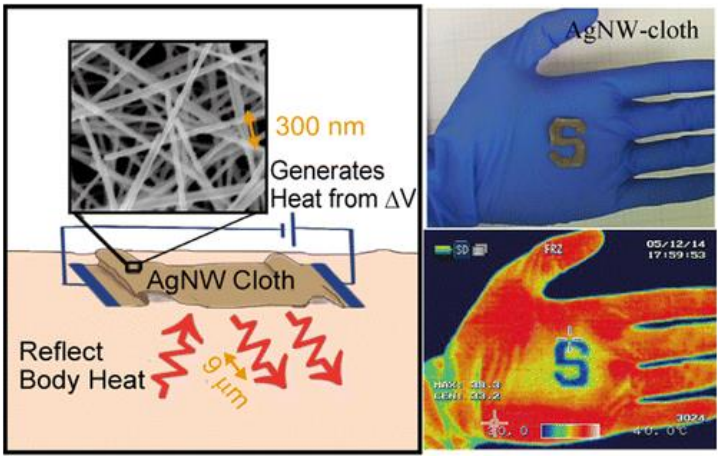

(a) (b)

Figure 1.21 Nanowire cloth with thermal radiation insulation and active heating. (a) Concept illustration. (b) Regular photos (top) and thermal images (bottom) of the AgNW-cloth, respectively.

Hsu et. al [85] later developed a radiative cooling fabric using a commercial available nanoporous polyethylene (nanoPE) film with 50% pore volume. With a pore size of 50~1000 nm, the nanoPE film is transparent to the mid-infrared radiation (7~14 μm) but opaque to the visible light, leading to an increased IR radiation dissipation and a passive cooling effect. To enhance the water vapor permeability and the wicking ability of the material, the nanoPE film was punched with microholes, and then coated with hydrophilic agent polydopamine (PDA), and further sandwiched by a cotton mesh. It was found the skin covered with the nanoPE textile could have a surface temperature 2.7 ^{o}C lower than that covered with a normal cotton. However, the cooling effect of the fabric highly depends on the difference between skin temperature and environment temperature. Wearers in a hot environment, e.g. > 30 ^{o}C, may not be able to benefit from radiative cooling significantly.

1.4.4 Directional liquid transport fabrics

Although conventional hydrophilic fabrics such as cotton and viscose can absorb sweat, they tend to retain the sweat and make the skin uncomfortable due to the wet and cold feelings under hot and humid conditions, or after exercises. Clothing systems having directional liquid transport properties are thus highly desirable to expedite the transmission of liquid sweat, thus making the skin dry, but blocking external liquids. Directional liquid transport fibrous materials or membranes have been widely explored recently. Basically, they can be achieved either by creating lyophobic-to-lyophilic gradient across the thickness, or stacking two layers of materials with opposite wettability to form a Janus membrane (Figure 1.22) [86, 87]. Liquid tends to flow from the lyophobic (e.g. hydrophobic or oleophobic) side to the lyophobilic (e.g. hydrophilic or oleophilic) side of the fibrous

materials as a result of differential capillary pressure. The movement of liquid can be an automatic process without extra energy.

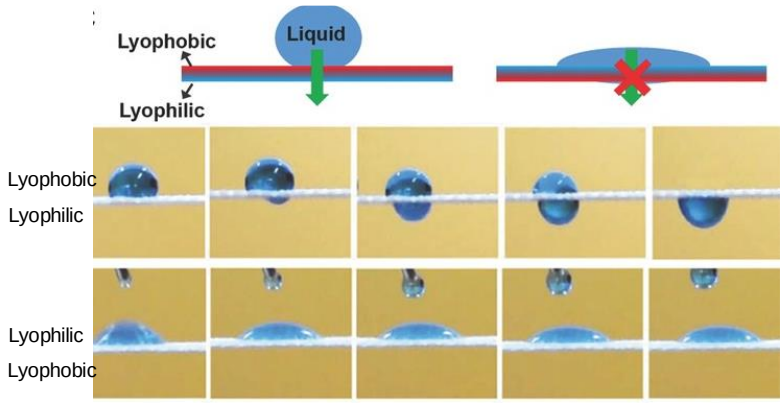

Figure 1.22 Directional liquid transport in a porous material. Liquid is able to transport from the lyophobic side to the lyophilic side, but not vice versa.

To realize the performance of wettability gradient or Janus membrane, various approaches have been reported. For instance, a multi-layer fabric was constructed with a thick inner moisture permeable hydrophobic fabric layer, a thin intermediate hydrophilic fabric layer and a second thick outer hydrophilic fabric layer so that liquid sweat tended to wick from the inner hydrophobic layer to the outer hydrophilic layer [88]. Photo-sensitive superhydrophobic coating was applied on cotton or polyester fabrics followed by ultra-violet (UV) illumination on one-side to induce hydrophilicity gradient [89-91]. Electrospun hydrophobic/hydrophilic or oleophobic/oleophilic dual-layer nanofibrous membranes are widely explored for the water and oil transport applications, respectively [92, 93]. Different hydrophobic materials were coated on one side of the membranes via electro-spraying or vapor diffusion to generate Janus membranes [94-97]. Combining both the multilayer and wettability gradient strategies, a trilayer fibrous membrane with progressive wettability by introducing a transfer layer was recently reported [98], which

demonstrated the continuous directional water transport and prevention of water penetration in the reverse direction.

The mechanism of liquid directional transport was investigated through an electrospun Janus hydrophobic/hydrophilic membrane [92]. It was proposed that hydrostatic pressure (HP) is the driving force of the directional flow. As shown in Figure 1.23, the spherical water droplet on the hydrophobic side generated a HP at the liquid-air interface. When the HP is large enough, it overcomes the water transport barrier force (hydrophobic force, HF) caused by the capillary pressure of the hydrophobic side, thus allowing water transport to the hydrophilic matrix; in the meantime, the capillary force (CF) within the hydrophilic layer assists water spread (Figure 1.22a). On the contrary, when water is dropped onto the hydrophilic side, it easily gets absorbed, resulting in a negligible HP on the hydrophobic layer and therefore the water is blocked from the penetration (Figure 1.22b).

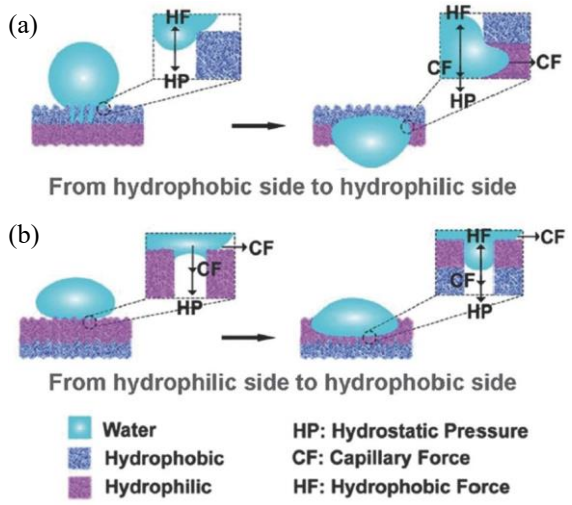

Figure 1.23 A mechanism to explain the directional water transport in a hydrophobic/hydrophilic multi-layer fibrous system. (a) Water droplet placed on the hydrophobic side having HP > HF at liquid–air interface can reach the hydrophilic layer, where the CF will enable water to spread within the hydrophilic layer. (b) Water droplet placed on the hydrophilic side having a negligible HP cannot overcome the HF of the hydrophobic layer, therefore can only spread within the hydrophilic layer under the CF.

1.4.5 Biomimetic fabrics

Biomimetics is the replicating or mimicking of biological mechanisms found in nature. Several attempts have been made for designing biomimetic fabrics. Biomimetics of plant structures have been employed in our group to fabricate either woven or knitted fabrics which improve the absorption and directional transport properties [99, 100]. In a woven structure, a tree structured network was formed, where the bottom layer is a 4/4 matt bottom layer with four yarns bundled together, the middle layer is the split of the "four-yarn stem" into two "two-yarn branches", and the top layer is a plain weave, in which the yarns are separate so as to achieve a higher surface area to volume ratio (Figure 1.24a) [99] . In a knitted structure, large loops are formed at the back side and smaller loops at the face side (Figure 1.24b) [100]. The loops in the back side are formed by two yarns grouped together on every other needle, but the loops at the face side are formed by a single yarn on every needle, creating in a greater exposed surface area at the face than that at the back side. Therefore, the face sides can promote surface evaporation, whereas the back side with the bundle of two yarns facilitates the initial liquid absorption and transport from the back to the face side, resulting in a process similar to the "cohesion-tension mechanism" in plants. More recently, Wang et al. [101] reported a trilayered electrospun fibrous membrane with multi-branched macro-, micron-, and sub-micron-sized pores plus a sprayed fluorinated polyurethane layer with low surface energy (Figure 1.24c). Such porous Murray membranes endowed with interconnected multiscale capillary channels can have excellent moisture wicking and directional water-transport performance, and therefore have potential to provide thermal comfort during the sweating activities.

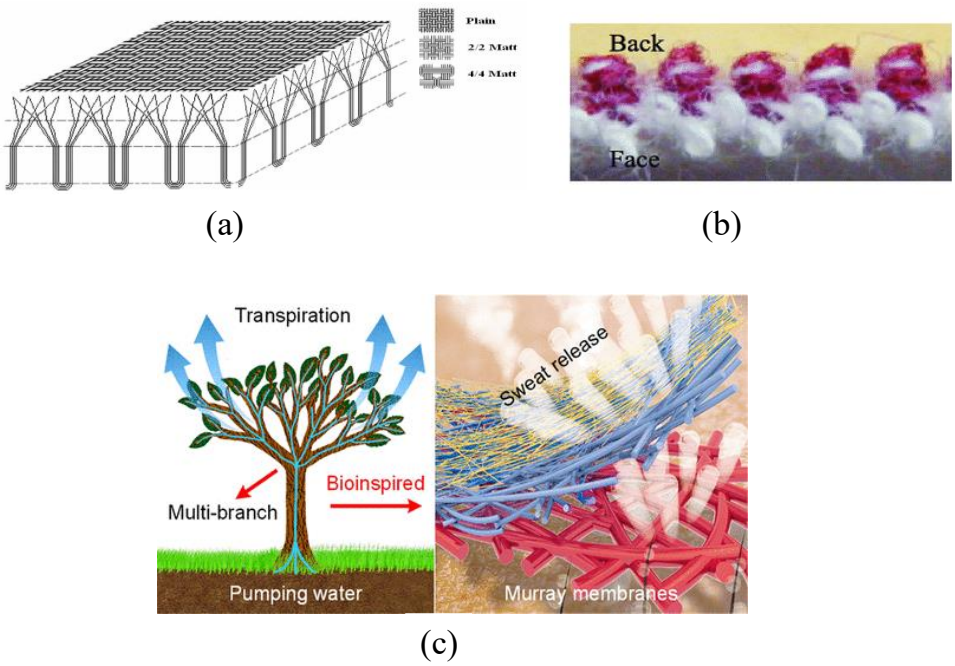

Figure 1.24 Biomimetic plant branching structured fabrics. Plant branching structures in (a) a woven fabric, (b) a knitted fabric and (c) an electrospun nonwoven fabric, respectively.

Another biomimetic principle is based on leaf stomata. A stomata is a pore in the epidermis of plant leaves which facilitate the gas exchange and water vapor transmission. The stomata open and close in response to changing environment, such as light intensity, humidity, and carbon dioxide concentration (Figure 1.25a) [60, 102, 103]. Akzo Nobel marketed a stomata analogic product under the trade name of Stomatex® [104]. It is a neoprene fabric along with foam insulation which has a series of convex domes. These domes function in a similar way to the leaf transpiration, and provide a controlled release of water vapor to make the clothing comfortable (Figure 1.25b) [60]. Stomatex® is claimed to respond to the level of activity by pumping faster as more heat is produced during active sports, returning to a more passive state when the body is cooled down. Yet, the triggering of the pores is based on body motion [104], therefore is not actually environment responsive.

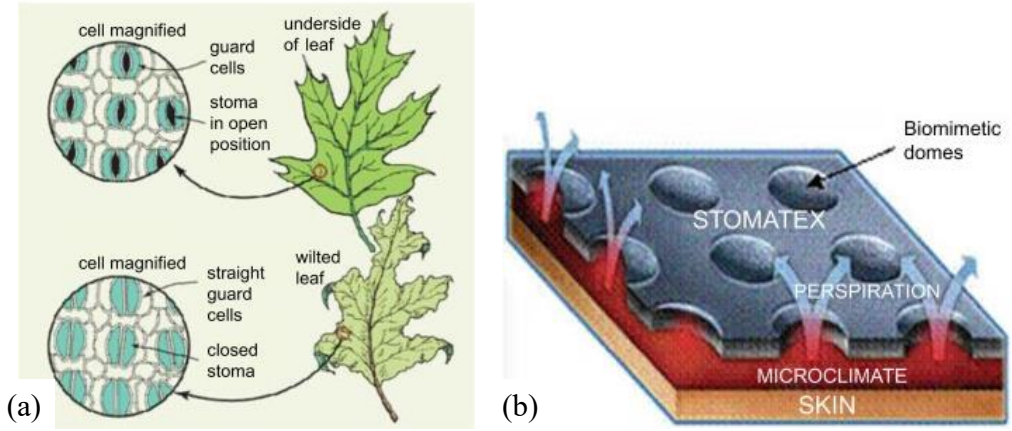

Figure 1.25 Biomimetics of leaf stomata in fabrics. (a) Function of leaf stomata in plants. (b) Akzo Nobel's Stomatex® biomimetic fabric.

1.4.6 Active thermoregulation

It has been observed that in spite of rapid developments in new materials and fabric designs for clothing thermal comfort, it is not sufficient to provide protection in high heat flux or cold environment. This led to the search for active thermoregulation which can provide extra protection to the wearers by supplying heat or cold sources to the clothing system via an external energy input. Active thermoregulation can be either active heating or active cooling, depending on wearer's different need to keep the balance in body microclimate.

Active heating can be realized by electrical heating, chemical heating, and fluid heating. Electrical heating is the most straight-forward approach, which uses a battery as an energy source. Batcheller et al. [105] incorporated flexible electrical copper wires into a stretchable and breathable fabric. Under monitoring by a microprocessor, the heating wires were capable of providing a warm feeling according to the change in the skin temperature, without causing an uncomfortable hot sensation. The design can be further improved by a microcomputer-based temperature control system which controlled the heat rate for

different body parts based on various requirement of different areas [106]. Chemical heating is an economical approach to generate heat without using a battery. Chan et al. [107] used granular mixtures of magnesium and iron particles as heat generators and developed a light weight heating system for shallow water divers. When magnesium reacts with sea water in the presence of cathode, the system generates the heat with a power density of 0.31 W/g, which can keep the diver warm for 3 hours at a water temperature of 10 ^{o}C. Fluid heating is another way to produce heat, in which liquid or gas is used for heat distribution and exchange. Nesher et al. [108] developed a water circulating warming garment called "Allon thermoregulation" (Figure 1.26), and used it to alleviate hypothermia during coronary artery bypass graft surgery. Water was circulated by a pump between two layers of the garment and transfer controlled heat throughout the operation. By continuous monitoring a patient's skin temperature, body temperature can be controlled during the surgery. Sessler et al. [109] injected warm air into a disposable plastic/paper quilt-like blanket and used it to provide warm microenvironment around the patient. It was found after 135 minutes of anesthesia, patients warmed by forced-air blanket had a core temperature 1 ^{o}C higher than that of patients with a normal reflective insulation. The fluid heating usually requires a tubing system, which may increase the garment stiffness and restrict the mobility of the wearers.

Figure 1.26 A water circulating warming garment “Allon thermoregulation”. It is specially designed to fit around the neck, torso, and limbs to provide warming without interfering with the surgical field.

Active cooling is used to release the heat from the clothing system and prevent heat-related injuries in extreme hot environment. Active cooling can be realized by liquid or air cooling. Similar to a liquid heating system, in a liquid cooling garment, cold liquid is circulated through the garment in contact with the skin via a micro-pump. After absorbing the heat, the liquid becomes hot initially, but it can be cooled back with the help of a liquid reservoir filled with ice-packs. The life cycle of the garment will increase by increasing the amount of ice-pack but it increases the weight of the clothing system as well, therefore these parameters should be optimized [110]. Liquid cooling garments were famously applied on Apollo flights to keep astronaut’s temperature to a normal range [111]. 40 plastic tubes with cooling water were sewn inside a suit of stretchable underwear with nylon slip layers between the tubes and skin. The cooling system is able to provide a maximum cooling power of 500 kcal/h, which is superior compared with the average work load of 200-300 kcal/h for the lunar surface activities. Apart from the circulating cooling, cooling can also be triggered by the evaporation of water. Yang et al. [112] developed a vacuum cooling

pad which contains a water bag and a desiccant (LiCl) component separated from each other (Figure 1.27). When the system was evacuated by a vacuum pump, the water was evaporated and generated a cooling capacity of 373.1 W/m^2 in an environment of 37 ^oC and 50% relative humidity. Compared with the circulating, evaporative cooling endows a lighter weight to the whole system, but continuously consumes the water therefore have a short lifecycle. In terms of air cooling, Weber et al. [113] developed a lightweight garment composed of an air impermeable outer layer and a permeable inner layer, which allows the air to contact with the skin without escaping out; however the vapor impermeable design will bring discomfort to the body. Chinevere et al. [114] studied an air-cooling ventilation system which consists of a three-dimensional (3D) spacer liner and impermeable outer layer. The 3D spacer liner was designed to create more space for air ventilation and control the air distribution. It was found the ventilation system reduces the physiology strain of wearers in a hot and humid environment (35 ^oC, 75% RH), and prolong the tolerance time by 20 min. In a hot dry environment (40 °C, 20% RH), the ventilation system can also significantly reduce the core temperature due to the sufficient evaporative capacity. Lu et al. [115] developed a hybrid cooling system based on phase change materials (Glauber's salt with a melting temperature of 21 ^oC) and air ventilation fans. The sweating manikin test showed that, in a hot wet condition (35°C, 75%RH), the hybrid cooling garment is able to prove a cooling power of 108 W with a duration more than 3 hours, compared with 66 W and 6 min for the system with only the PCM.

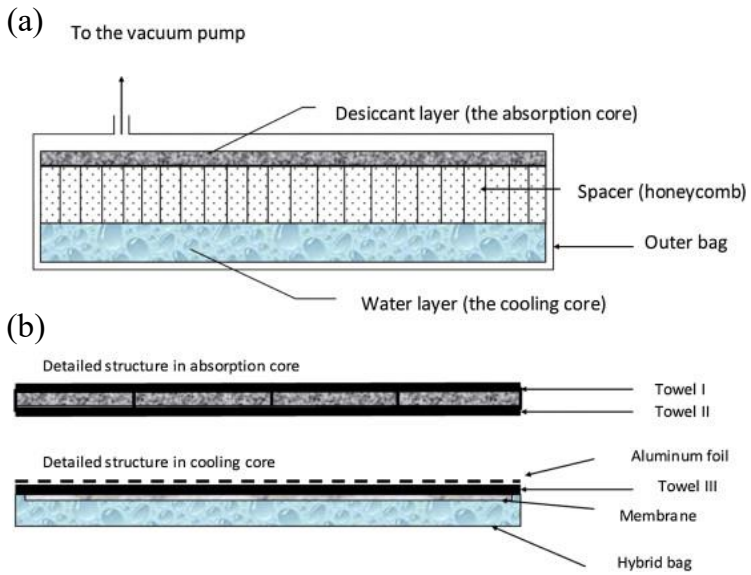

Figure 1.27 Schematic of cross-sectional view of a vacuum desiccant cooling pad. (a) The vacuum cooling pad which contains a water bag and a desiccant component. (b) Its absorption core and cooling core.

In addition, active heating and cooling can be realized on the same clothing system by careful design. Zhao et al. [116] developed a lightweight thermoregulatory undergarment with both active cooling and heating capability without interfering with the wearer's outer appearance (Figure 1.28). The dual mode was realized through a portable thermoelectric energy conversion unit (TECU), which can convert electrical energy to cooling or heating powers. The pumped air passing through the unit can get cooled or heated and distributed to different areas of human body by a branched soft tubing network within the undergarment. The system can provide 18.4 W and 66.8 W of cooling during non-sweating and sweating (246.9 g/h, at 22 ^{o}C and 65% RH) conditions, respectively. Subjective tests showed that the wearers can feel two points change in both cooling and heating mode when the room temperature set-points were set at 26 ^{o}C and 19 ^{o}C, respectively.

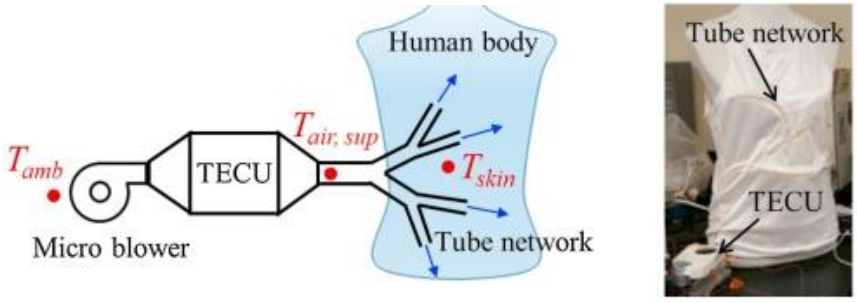

(a) (b)

Figure 1.28 Personal thermal management using portable thermoelectrics for building energy saving. (a) Schematic and (b) prototype of a thermoregulatory clothing with tree-like tube network connected to the portable thermoelectric energy conversion unit (TECU) and knitted into the clothing.

1.5 Challenges

Despite many attempts in developing thermally comfortable clothing systems, there are still many challenges that need to be addressed for providing better heat or moisture transfer properties for different applications.

The first challenge lies in the conflict between multiple functions on the same clothing system. For example, for the multilayer design of the moisture responsive garment developed by MIT media lab, although they endow good ventilation and cooling performance, the fabrics become thick and less stretchable, and the bending actuations of the flaps are through-plane, therefore may affect the wearers' mobility, tactile comfort as well as the appearance of the clothing. For different chemically treated fabrics, they may be able to achieve desired wettability, wicking, moisture vapor or liquid transfer properties, their durability or lifecycle after repeated laundering is still a concern. Active heating or cooling clothing systems can provide enhanced thermoregulation, however they may have to compromise in terms of increased weight, reduced breathability and flexibility; at the

same time, safety is a concern when the wearers have to carry an energy source and triggering agents such as battery and ice within the clothing systems.

The second challenge is to develop a “skin-like” smart fibrous system. Although existing directional liquid transport materials exhibit faster liquid flow from the lyophobic side (e.g. skin side) to the lyophilic side (e.g. environment side) than flow in the reverse direction, the liquid tends to spread and absorb in the lyophilic side. When it becomes saturated, the capillary flow from the lyophobic side to the lyophilic side slows down and directional flow may be eventually stopped. The saturation of liquid on the lyophilic side will increase the discomfort due to increased weight. Besides, the lyophilic side inherently does not repel external liquid. Nevertheless, fibrous materials that mimics the skin of mammals, which allows directional liquid flow and simultaneously repels external liquid contaminants have yet to be developed.

The third challenge is to achieve unique functions using biomimetics. Although branched or leaf stomata structures have been generated on fibrous systems by mimicking the plant, their performance in liquid absorption and transport is still not sufficient. For example, transpiration of the water through the plant involves water uptake by the root hair, water suction through the plant tissues, and water release as vapor forms by the leaves; The leaf stomata regulates the pore behaviors by the two guard cells, which swell under light and humid (wet) conditions, creating an open pore to draw water in, whereas shrink under dark and dry conditions, closing the pore to prevent the water loss. These mechanisms should be carefully understood in order to be applied in artificial material designs for the analogous performance.

1.6 Dissertation Scope and Organization

Clothing systems with excellent thermal comfort are an important issue for general consumers, technical textiles, sportswear and activity wear. This dissertation focuses on improving the moisture vapor and liquid transmission properties for different fibrous systems. The application of my results is not limited to the clothing systems, but can also be expanded into other applications such as separation/filtration membranes, medical care products, flexible microfluidic devices.

Chapter 1 introduces the background, challenge and scope of the study. It reviews the current literature including the different types of thermal comfort, evaluation methods, contributing factors and recent trends in improving the thermal comfort performance.

Chapter 2 reports a study to improve the wettability of a wrinkle-free cotton fabric, with the goal of solving the dilemma of achieving both wrinkle-free property and superhydrophilicity on a cotton fabric in a conventional wrinkle-free finishing process. A plasma pre-treatment and a specially engineered silica-based nanofluid were used as surface finishing on the wrinkle-free fabric. The finishing parameters were investigated and optimized. The durability of the fabrics in terms of wettability improvement and wrinkle-free maintenance were evaluated by aging, laundering and abrasion tests.

Chapter 3 reports the development of a “skin-like” directional water transport fabric which enables water flow in one direction, but repels water absorption/penetration in the opposite direction. The study was targeted to fill the existing gap of achieving the water repellency on a directional flow fabric. The exceptional property of the fabric was achieved by

creating gradient wettability channels through the thickness of a predominantly hydrophobic fabric via selective plasma treatment with patterned masks. The directional water transport property and the water repellency was evaluated via various experiments including contact angle test, water dripping test, water flux test and shower test. Theoretical modelling was also conducted to explain the mechanism of the phenomenon, and correlate it with the microstructures and wettability.

Chapter 4 reports the development of the biomimicry of the leaf stomata to create smart pores on a fabric for improving the breathability. The design principle was based on the guard cells' structure and function, where a special hydrogel system composed of a highly crosslinked inner layer and a less crosslinked outer layer was patterned on the slit ("pore") of the fabric. The opening and closing of the artificial stomata (viz. moisture responsiveness) were observed visually and under optical microscopy. The breathability under different conditions was tested via water vapor transmission and air permeability.

Chapter 5 summarizes the conclusion and significance of the studies. Limitations of the study and suggestions for further studies are also included.

REFERENCES

[1] E. Kamalha, Y.C. Zeng, J.I. Mwasiagi, S. Kyatuheire, The comfort dimension; a review of perception in clothing, *J Sens Stud* **28**(6) (2013) 423-444.

[2] K. Slater, The assessment of comfort, *J Text I* **77**(3) (1986) 157-171.

[3] J. Fan, Physiological comfort of fabrics and garments, *Woodhead Publ Text* (96) (2009) 201-250.

[4] S. Kaplan, A. Okur, The meaning and importance of clothing comfort: A case study for Turkey, *J Sens Stud* **23**(5) (2008) 688-706.

[5] S. Kaplan, A. Okur, Determination of coolness and dampness sensations created by fabrics by forearm test and fabric measurements, *J Sens Stud* **24**(4) (2009) 479-497.

[6] P.O. Fanger, J. Hojbjerre, J.O. Thomsen, Thermal comfort conditions in the morning and in the evening, *Int J Biometeorol* **18**(1) (1974) 16-22.

[7] D, Bhatia, U. Malhotra, Thermophysiological wear comfort of clothing: an overview, *J Textile Sci Eng* **6** (2016) 250.

[8] M. Manshahia, A. Das, High active sportswear - A critical review, *Indian J Fibre Text* **39**(4) (2014) 441-449.

[9] G. Havenith, Heat balance when wearing protective clothing, *Ann Occup Hyg* **43**(5) (1999) 289-296.

[10] S.M. Shirreffs, L.F. Aragon-Vargas, M. Chamorro, R.J. Maughan, L. Serratosa, J.J. Zachwieja, The sweating response of elite professional soccer players to training in the heat, *Int J Sports Med* **26**(2) (2005) 90-95.

[11] C.J. Veitch, G.R.S. Naylor, The mechanics of fiber buckling in relation to fabric-evoked prickle, *Wool Tech Sheep Bree* **40**(1) (1992) 31-34.

[12] E. Kissa, Wetting and wicking, *Text Res J* **66**(10) (1996) 660-668.

[13] Y. Li, Q.Y. Zhu, Simultaneous heat and moisture transfer with moisture sorption, condensation, and capillary liquid diffusion in porous textiles, *Text Res J* **73**(6) (2003) 515-524.

[14] P.R. Harnett, P.N. Mehta, A survey and comparison of laboratory test methods for measuring wicking, *Text Res J* **54**(7) (1984) 471-478.

[15] Y.K. Kamath, S.B. Hornby, H.D. Weigmann, M.F. Wilde, Wicking of spin finishes and related liquids into continuous filament yarns, *Text Res J* **64**(1) (1994) 33-40.

[16] J. McCann, D. Bryson, Textile-led design for the active ageing population, *Elsevier* 2014.

[17] M.R. Carter, E.G. Gregorich, Soil sampling and methods of analysis, *Lewis Publishers* 1993.

[18] N. Oglakcioglu, P. Celik, T.B. Ute, A. Marmarali, H. Kadoglu, Thermal comfort properties of angora rabbit/cotton fiber blended knitted fabrics, *Text Res J* **79**(10) (2009) 888-894.

[19] A.K. Haghi, Moisture permeation of clothing - A factor governing thermal equilibrium and comfort, *J Therm Anal Calorim* **76**(3) (2004) 1035-1055.

[20] N. Suprun, Dynamics of moisture vapour and liquid water transfer through composite textile structures, *Magic World of Textiles, Book of Proceedings* (2002) 411-414.

[21] J.T. Fan, Y.S. Chen, Measurement of clothing thermal insulation and moisture vapour resistance using a novel perspiring fabric thermal manikin, *Meas Sci Technol* **13**(7) (2002) 1115-1123.

[22] ASTM E96 / E96M-16, Standard test methods for water vapor transmission of materials, *ASTM* (2005).

[23] BS 7209, Specification for water vapour permeable apparel fabrics, *British Standard* (1990).

[24] F.Y. Kar, Effect of heat and moisture transfer properties of T-shirts on comfort sensations, *M Phil. Thesis*, The Hong Kong Polytechnic University (2007) 59–60.

[25] P. Zhang, Y. Watanabe, S.H. Kim, H. Tokura, R.H. Gong, Thermoregulatory responses to different moisture-transfer rates of clothing materials during exercise, *J Text I* **92**(4) (2001) 372-378.

[26] S.J. Park, H. Tokura, M. Sobajima, Effects of moisture absorption of clothing on pitching speed of amateur baseball players in hot environmental conditions, *Text Res J* **76**(5) (2006) 383-387.

[27] T.H. Grindstaff, A simple apparatus and technique for contact-angle measurements on small-denier single fibers, *Text Res J* **39**(10) (1969) 958–962.

[28] A. Patnaik, R. S. Rengasamy, V. K. Kothari, A. Ghosh, Wetting and wicking in fibrous materials, *Text Prog* **38**(1) (2006) 1.

[29] M. Sarkar, J.T. Fan, X.M. Qian, Transplanar water transport tester for fabrics, *Meas Sci Technol* **18**(5) (2007) 1465-1471.

[30] Q. Chen, K.P.M. Tang, P.B. Ma, G.M. Jiang, Evaluation of water absorption and transport properties of weft knitted polyester fabrics by spontaneous uptake water transport tester and conventional test methods, *Fiber Polym* **17**(8) (2016) 1287-1295.

[31] R.M. Rossi, R. Stampfli, A. Psikuta, I. Rechsteiner, P.A. Bruhwiler, Transplanar and in-plane wicking effects in sock materials under pressure, *Text Res J* **81**(15) (2011) 1549-1558.

[32] C. Keiser, C. Becker, R.M. Rossi, Moisture transport and absorption in multilayer protective clothing fabrics, *Text Res J* **78**(7) (2008) 604-613.

[33] B.G. Yao, Y. Li, J.Y. Hu, Performance of moisture management tester for characterizing the dynamic liquid moisture transport properties of textile materials, *Textile Bioengineering and Informatics Symposium Proceedings, Vols 1 and 2* (2008) 724-730.

[34] J.Y. Hu, Y. Li, K.W. Yeung, A.S.W. Wong, W.L. Xu, Moisture management tester: A method to characterize fabric liquid moisture management properties, *Text Res J* **75**(1) (2005) 57-62.

[35] Y. Li, A.S.W. Wong, Application of clothing biosensory engineering, *Woodhead Text Ser* (51) (2006) 301-310.

[36] S.H. Kim, J.H. Lee, D.Y. Lim, H.Y. Jeon, Dependence of sorption properties of fibrous assemblies on their fabrication and material characteristics, *Text Res J* **73**(5) (2003) 455-460.

[37] J.H. Lee, S.H. Kim, K.J. Lee, D.Y. Lim, H.Y. Jeon, Determining the absorption properties of split-type microfiber fabrics by measuring the change in color depth, *Text Res J* **74**(3) (2004) 271-278.

[38] R. Fangueiro, A. Filgueiras, F. Soutinho, M.D. Xie, Wicking behavior and drying capability of functional knitted fabrics, *Text Res J* **80**(15) (2010) 1522-1530.

[39] Y.S. Chen, J.T. Fan, W. Zhang, Clothing thermal insulation during sweating, *Text Res J* **73**(2) (2003) 152-157.

[40] B. Das, A. Das, V.K. Kothari, R. Fanguiero, M. de Araujo, Effect of fibre diameter and cross-sectional shape on moisture transmission through fabrics, *Fiber Polym* **9**(2) (2008) 225-231.

[41] N. Wang, A.X. Zha, J.X. Wang, Study on the wicking property of polyester filament yarns, *Fiber Polym* **9**(1) (2008) 97-100.

[42] M. Manshahia, A. Das, Thermophysiological comfort characteristics of plated knitted fabrics, *J Text I* **105**(5) (2014) 509-519.

[43] S.M. Watkins, Clothing: the portable environment, 2nd ed., *Iowa State University Press*, Ames, 1995.

[44] C.L. Su, J.X. Fang, X.H. Chen, W.Y. Wu, Moisture absorption and release of profiled polyester and cotton composite knitted fabrics, *Text Res J* **77**(10) (2007) 764-769.

[45] X.Q. Dai, R. Imamura, G.L. Liu, F.P. Zhou, Effect of moisture transport on microclimate under T-shirts, *Eur J Appl Physiol* **104**(2) (2008) 337-40.

[46] M. Manshahia, A. Das, Thermo-physiological comfort of compression athletic wear, *Indian J Fibre Text* **39**(2) (2014) 139-146.

[47] N. Ozdil, A. Marmarali, S.D. Kretzschmar, Effect of yarn properties on thermal comfort of knitted fabrics, *Int J Therm Sci* **46**(12) (2007) 1318-1322.

[48] Y.L. Hsieh, Liquid Transport in Fabric Structures, *Text Res J* **65**(5) (1995) 299-307.

[49] R.M. Crow, R.J. Osczevski, The interaction of water with fabrics, *Text Res J* **68**(4) (1998) 280-288.

[50] S.M. Montgomery, B. Miller, L. Rebenfeld, Spatial-distribution of local permeabilities in fibrous networks, *Text Res J* **62**(3) (1992) 151-161.

[51] N. Mao, S.J. Russell, Directional permeability in homogeneous nonwoven structures Part I: The relationship between directional permeability and fibre orientation, *J Text I* **91**(2) (2000) 235-243.

[52] A. Majumdar, S. Mukhopadhyay, R. Yadav, Thermal properties of knitted fabrics made from cotton and regenerated bamboo cellulosic fibres, *Int J Therm Sci* **49**(10) (2010) 2042-2048.

[53] L. Benisek, G.K. Edmondson, W.A. Phillips, Protective clothing - evaluation of wool and other fabrics, *Text Res J* **49**(4) (1979) 212–221.

[54] D. J. Gohlke, J. C. Tanner, Gore-Tex® waterproof breathable laminates, *J Coated Fabrics* **6**(1) (1976) 28-38.

[55] W. Wardiningsih, O. Troynikov, Influence of cover factor on liquid moisture transport performance of bamboo knitted fabrics, *J Text I* **103**(1) (2012) 89-98.

[56] P. Spence, L. Wadsworth, T. Chihani, Plasma surface treatment for improved wettability and rewettability, *Proc Inda-Tec* **97**(1997) 8–10.

[57] K.K. Wong, X.M. Tao, C.W.M. Yuen, K.W. Yeung, Wicking properties of linen treated with low temperature plasma, *Text Res J* **71**(1) (2001) 49-56.

[58] M.S. Ibrahim, K.M. El Salmawi, S.M. Ibrahim, Electron-beam modification of textile fabrics for hydrophilic finishing, *Appl Surf Sci* **241**(3-4) (2005) 309-320.

[59] L. Lau, J.T. Fan, T. Siu, L.Y.C. Siu, Comfort sensations of polo shirts with and without wrinkle-free treatment, *Text Res J* **72**(11) (2002) 949-953.

[60] S. Kanjana, B. Ambika, Nalankilli G, Breathable garments with thermo– physiological wear comfort - a review, *Curr Trends Fashion Technol Textile Eng* **3**(1) (2018) 1-6.

[61] M.B. Sampath, M. Senthilkumar, Effect of moisture management finish on comfort characteristics of microdenier polyester knitted fabrics, *J Ind Text* **39**(2) (2009) 163-173.

[62] M. Okubo, M. Tahara, Y. Aburatani, T. Kuroki, T. Hibino, Preparation of PTFE film with adhesive surface treated by atmospheric-pressure nonthermal plasma graft polymerization, *Ieee T Ind Appl* **46**(5) (2010) 1715-1721.

[63] R. Splendore, F. Dotti, B. Cravello, A. Ferri, Thermo-physiological comfort of a PES fabric with incorporated activated carbon Part I: preliminary physical analysis, *Int J Cloth Sci Tech* **22**(5) (2010) 333-342.

[64] J.O. Kim, Dynamic moisture vapor transfer through textiles Part III: Effect of film characteristics on microclimate moisture and temperature changes, *Text Res J* **69**(3) (1999) 193-202.

[65] M.B. Sampath, S. Mani, G. Nalankilli, Effect of filament fineness on comfort characteristics of moisture management finished polyester knitted fabrics, *J Ind Text* **41**(2) (2011) 160-173.

[66] M. Wang, X.H. Li, J. Li, B.G. Xu, A new approach to quantify the thermal shrinkage of fire protective clothing after flash fire exposure, *Text Res J* **86**(6) (2016) 580-592.

[67] J.H. Harold, F.F. George, The thermal conductivity of a multilayer sample of underwear material under a variety of experimental conditions, *Text Res J* **34**(1964) 401–410..

[68] D.S. Bag, K.U.B. Rao, Smart polymers and their applications, *J Polym Mater* **23**(3) (2006) 225-248.

[69] T.Y. Wu, A.B. Zrimsek, S.V. Bykov, R.S. Jakubek, S.A. Asher, Hydrophobic collapse initiates the poly(n-isopropylacrylamide) volume phase transition reaction coordinate, *J Phys Chem B* **122**(11) (2018) 3008-3014.

[70] H. Kim, S.J. Lee, Stomata-inspired membrane produced through photopolymerization patterning, *Adv Funct Mater* **25**(28) (2015) 4496-4505.

[71] H. Kim, S.J. Lee, Fabrication of triple-parted stomata-inspired membrane with stimulus-responsive functions, *Sci Rep-Uk* **6** (2016) 21258.

[72] Y. Park, M.P. Gutierrez, L.P. Lee, Reversible self-actuated thermo-responsive pore membrane, *Sci Rep-Uk* **6** (2016) 39402.

[73] X.M. Ding, J.L. Hu, X.M. Tao, C.R. Hu, Preparation of temperature-sensitive polyurethanes for smart textiles, *Text Res J* **76**(5) (2006) 406-413.

[74] X.M. Ding, J.L. Hu, X.A. Tao, Effect of crystal melting on water vapor permeability of shape-memory polyurethane film, *Text Res J* **74**(1) (2004) 39-43.

[75] D. Congalton, Shape memory alloys for use in thermally activated clothing systems, *Appl Mech Eng, Vol 4, Special Issue: "Icer '99",* (1999) 423-428.

[76] B.W. Hendrickson, The impact of a variable air gap on the thermal performance of firefighter protective clothing, *M.S. Thesis*, University of Maryland (2011).

[77] D. Arjun, J. Hayavadana, Thermal energy storage materials (PCMS) for textile applications, *J Text App Tech Man* **8**(4) (2004) 1-11.

[78] S. Mondal, Phase change materials for smart textiles - An overview, *Appl Therm Eng* **28**(11-12) (2008) 1536-1550.

[79] H. Shim, E.A. McCullough, B.W. Jones, Using phase change materials in clothing, *Text Res J* **71**(6) (2001) 495-502.

[80] M.M. Yazdi, M. Sheikhzadeh, Personal cooling garments: a review, *J Text I* **105**(12) (2014) 1231-1250.

[81] W. Wang, L.N. Yao, C.Y. Cheng, T. Zhang, H. Atsumi, L.D. Wang, G.Y. Wang, O. Anilionyte, H. Steiner, J.F. Ou, K. Zhou, C. Wawrousek, K. Petrecca, A.M. Belcher, R. Karnik, X.H. Zhao, D.I.C. Wang, H. Ishii, Harnessing the hygroscopic and biofluorescent behaviors of genetically tractable microbial cells to design biohybrid wearables, *Sci Adv* **3**(5) (2017).

[82] J.K. Mu, G. Wang, H.P. Yan, H.Y. Li, X.M. Wang, E.L. Gao, C.Y. Hou, A.T.C. Pham, L.J. Wu, Q.H. Zhang, Y.G. Li, Z.P. Xu, Y. Guo, E. Reichmanis, H.Z. Wang, M.F. Zhu, Molecular-channel driven actuator with considerations for multiple configurations and color switching, *Nat Commun* **9** (2018) 590.

[83] J.D. Hardy, The physical laws of heat loss from the human body, *Proc Natl Acad Sci U S A* **23**(12) (1937) 631-7.

[84] P.C. Hsu, X.G. Liu, C. Liu, X. Xie, H.R. Lee, A.J. Welch, T. Zhao, Y. Cui, Personal thermal management by metallic nanowire-coated textile, *Nano Lett* **15**(1) (2015) 365-371.

[85] P.C. Hsu, A.Y. Song, P.B. Catrysse, C. Liu, Y.C. Peng, J. Xie, S.H. Fan, Y. Cui, Radiative human body cooling by nanoporous polyethylene textile, *Science* **353**(6303) (2016) 1019-1023.

[86] Y. Zhao, H. X. Wang, H. Zhou, T. Lin, Directional fluid transport in thin porous materials and its functional applications, *Small* **13**(4) (2017).

[87] J.Q. Li, Y.X. Song, H.X. Zheng, S.L. Feng, W.H. Xu, Z.K. Wang, Designing biomimetic liquid diodes, *Soft Matter* **15**(9) (2019) 1902-1915.

[88] L.M. Herbert, L.B. Daniel, Multi-layer moisture management fabric and garments incorporating a moisture management panel, *patent* US5306536A (1993).

[89] H.X. Wang, J. Ding, L.M. Dai, X.G. Wang, T. Lin, Directional water-transfer through fabrics induced by asymmetric wettability, *J Mater Chem* **20**(37) (2010) 7938-7940.

[90] Y.Y. Kong, Y.Y. Liu, J.H. Xin, Fabrics with self-adaptive wettability controlled by "light-and-dark", *J Mater Chem* **21**(44) (2011) 17978-17987.

[91] H. Zhou, H. Wang, H. Niu, T. Lin, Superphobicity/philicity Janus fabrics with switchable, spontaneous, directional transport ability to water and oil fluids, *Sci Rep* **3** (2013) 2964.

[92] J. Wu, N. Wang, L. Wang, H. Dong, Y. Zhao, L. Jiang, Unidirectional water-penetration composite fibrous film via electrospinning, *Soft Matter* **8**(22) (2012) 5996-5999.

[93] H.X. Wang, H. Zhou, H.T. Niu, J. Zhang, Y. Du, T. Lin, Dual-layer superamphiphobic/superhydrophobic-oleophilic nanofibrous membranes with unidirectional oil-transport ability and strengthened oil-water separation performance, *Adv Mater Interfaces* **2**(4) (2015).

[94] C. Zeng, H.X. Wang, H. Zhou, T. Lin, Directional water transport fabrics with durable ultra-high one-way transport capacity, *Adv Mater Interfaces* **3**(14) (2016).

[95] H. Liu, J.Y. Huang, F.Y. Li, Z. Chen, K.Q. Zhang, S.S. Al-Deyab, Y.K. Lai, Multifunctional superamphiphobic fabrics with asymmetric wettability for one-way fluid transport and templated patterning, *Cellulose* **24**(2) (2017) 1129-1141.

[96] H.J. Wang, W.Y. Wang, H. Wang, X. Jin, J.L. Li, Z.T. Zhu, One-way water transport fabrics with hydrophobic rough surface formed in one-step electrospray, *Mater Lett* **215** (2018) 110-113.

[97] X.L. Tian, H. Jin, J. Sainio, R.H.A. Ras, O. Ikkala, Droplet and fluid gating by biomimetic janus membranes, *Adv Funct Mater* **24**(38) (2014) 6023-6028.

[98] D.Y. Miao, Z. Huang, X.F. Wang, J.Y. Yu, B. Ding, Continuous, spontaneous, and directional water transport in the trilayered fibrous membranes for functional moisture wicking textiles, *Small* **14**(32) (2018).

[99] J.T. Fan, M.K. Sarkar, Y.C. Szeto, X.M. Tao, Plant structured textile fabrics, *Mater Lett* **61**(2) (2007) 561-565.

[100] Q. Chen, J.T. Fan, M. Sarkar, G.M. Jiang, Biomimetics of plant structure in knitted fabrics to improve the liquid water transport properties, *Text Res J* **80**(6) (2010) 568-576.

[101] X. Wang, Z. Huang, D. Miao, J. Zhao, J. Yu, B. Ding, Biomimetic fibrous murray membranes with ultrafast water transport and evaporation for smart moisture-wicking fabrics, *ACS Nano* **13**(2) (2019) 1060-1070.

[102] O.L. Lange, R. Losch, E.D. Schulze, L. Kappen, Responses of stomata to changes in humidity, *Planta* **100**(1) (1971) 76-86.

[103] M.R.G. Roelfsema, R. Hedrich, In the light of stomatal opening: new insights into 'the Watergate', *New Phytol* **167**(3) (2005) 665-691.

[104] Stomatex® Technology, *http://www.stomatex.com/faqs.htm#what*

[105] B.D. Batcheller, K.L. Brekkestran, R.L. Minch, Electrically heated garment, *Patent* US5032705A (1991).

[106] L.B. Kelvin, A.T. Kamyab, N.N. Nguyen, B.D Batcheller, Electronic control system and method for cold weather garment, *Patent* US5105067A (1989).

[107] C.Y.L. Chan, D.R. Burton, Local heating source for shallow water divers, *J Power Sources* **6**(3) (1981) 291–304.

[108] N. Nesher, T. Wolf, I. Kushnir, M. David, G. Bolotin, R. Sharony, R. Pizov, G. Uretzky, Novel thermoregulation system for enhancing cardiac function and hemodynamics during coronary artery bypass graft surgery, *Ann Thorac Surg* **72**(3) (2001) S1069-76.

[109] D.I. Sessler, A. Moayeri, Skin-surface warming - heat-flux and central temperature, *Anesthesiology* **73**(2) (1990) 218-224.

[110] T.H. Guo, B.F. Shang, B. Duan, X.B. Luo, Design and testing of a liquid cooled garment for hot environments, *J Therm Biol* **49-50** (2015) 47-54.

[111] J.M. Waligora, E.L. Michel, Application of conductive cooling for working men in a thermally isolated environment, *Aerosp Med* **39**(5) (1968) 485-7.

[112] Y.F. Yang, J. Stapleton, B.T. Diagne, G.P. Kenny, C.Q. Lan, Man-portable personal cooling garment based on vacuum desiccant cooling, *Appl Therm Eng* **47** (2012) 18-24.

[113] S. Weber, Air cooling garment for medical personnel, *Patent* US5970519A (1999).

[114] T.D. Chinevere, B.S. Cadarette, D.A. Goodman, B.R. Ely, S.N. Cheuvront, M.N. Sawka, Efficacy of body ventilation system for reducing strain in warm and hot climates, *Eur J Appl Physiol* **103**(3) (2008) 307-314.

[115] Y.H. Lu, F.R. Wei, D.D. Lai, W. Shi, F.M. Wang, C.S. Gao, G.W. Song, A novel personal cooling system (PCS) incorporated with phase change materials (PCMs) and

ventilation fans: An investigation on its cooling efficiency, *J Therm Biol* **52** (2015) 137-146.

[116] D.L. Zhao, X. Lu, T.Z. Fan, Y.S. Wu, L. Lou, Q.W. Wang, J.T. Fan, R.G. Yang, Personal thermal management using portable thermoelectrics for potential building energy saving, *Appl Energ* **218** (2018) 282-291.

CHAPTER 2

SUPERHYDROPHILIC WRINKLE-FREE COTTON FABRICS VIA PLASMA AND NANOFLUID TREATMENT*

Abstract

We demonstrate in this study, a wrinkle-free, superhydrophilic cotton fabric (contact angle ~ 0 ^{o}) by uniformly attaching specially engineered nanoparticles to plasma pre-treated cotton fabric. Because of their highly charged nature, the nanoparticles are firmly anchored on the fabric via electrostatic interactions, as confirmed by microscopy and chemical analyses. The durability of wetting behavior and wrinkle-free property of the nanoparticle-coated fabrics was evaluated via aging, laundering and abrasion tests. The strongly attached coatings are stable enough to maintain their superhydrophilic nature even after 60 days of aging at room temperature, 50 laundering cycles and 25,000 abrasion cycles. Moreover, the nanoparticle-coated superhydrophilic fabrics exhibit great wrinkle-recovery property, tensile strength as well as abrasion resistance performance up to 25,000 abrasion cycles.

* **Lihong Lao**, Liling Fu, Genggeng Qi, Emmanuel P. Giannelis, Jintu Fan. Superhydrophilic Wrinkle-free Cotton Fabrics via Plasma and Nanofluid Treatment. ***ACS Applied Materials & Interfaces***, 2017 (9), 38109–38116.

2.1 Introduction

For more than two decades in the apparel industry, there has been consistently high demand of wrinkle-free cotton garments for easy care and comfort. The untreated cotton fabrics are easy to produce wrinkles due to the weak hydrogen bonds in their crystalline and amorphous structures, when an external distortion force is applied or during laundering [1]. Wrinkle-free finishing has therefore been developed and widely applied to cotton fabrics. Conventional wrinkle-free finishing is based on the crosslinking reaction between molecular chains of cellulose using formaldehyde derivatives, e.g. dimethyloldihydroxyethyleneurea (DMDHEU) [1]. The crosslinking reaction eliminates the hydroxyl (-OH) groups in cotton, which increases wrinkle-resistance and shape retention. However, the finishing reduces the hydrophilicity of the fabric due to the reduction of -OH groups. Consequently, the moisture sorption capacity and wicking properties are reduced, resulting in a deterioration in the comfort of cotton fabric [2, 3]. Therefore, recovering the hydrophilicity of wrinkle-free finished cotton has very significant practical value.

One of the major approaches manipulating the hydrophilicity of fabrics is surface modification using nanoparticles, including titanium dioxide (TiO_2) nanoparticles [4, 5], silica nanoparticles [6, 7], and nanoparticle mixtures such as silica/TiO_2 nanoparticles [8], and silica/silver nanoparticles [9]. Recently, surface-functionalized nanoparticle fluids with tunable rheological behavior were developed by the Giannelis' group [10-13] and found applications in a number of areas such as water treatment and battery separator applications. Surface modification of silica or other metal oxide nanoparticles [10-13] with

appropriate organosilanes forms hairy nanoparticles with a permanent charge. These hybrid nanoparticles in the neat state (i.e. in the absence of any solvent) represent a unique class of solvent-free fluids that are distinguished from conventional colloidal suspensions. The charged silica nanoparticles have been successfully grafted on several water purification membranes to improve their surface wetting characteristics. For example, charged silica nanoparticles have been used to coat polyvinylidene fluoride (PVDF) ultrafiltration and forward osmosis polyamide membranes, which successfully improved the hydrophilicity of the membranes and decreased the tendency of the membranes to fouling [14, 15].

Previous studies have shown that oxidative, nonthermal plasma treatment is an effective approach to improve the hydrophilicity of fabrics [16-19], by creating -COOH, -CO, and other functional surface groups [20]. Moreover, the effective pore size may increase due to plasma etching, reducing the capillary pressure and thus increasing the hydrophilicity [21, 22]. However, the durability of hydrophilicity introduced solely by plasma treatment is a concern. A reversal of the surface wetting has been observed upon aging due to a decrease of plasma-induced hydrophilic surface groups [18, 23]. As demonstrated in this study, the reversal of the surface wetting of wrinkle-free fabrics can be prevented by attaching engineered hydrophilic nanoparticles (NPs) to the plasma pre-treated fabric (Figure 2.1). Because of their charged nature, the nanoparticles are firmly anchored on the fabric via strong electrostatic interactions leading to a stable and robust coating. By tuning the treatment conditions, highly durable superhydrophilic fabrics can be prepared while maintaining their wrinkle-free performance without adversely affecting fabric handle.

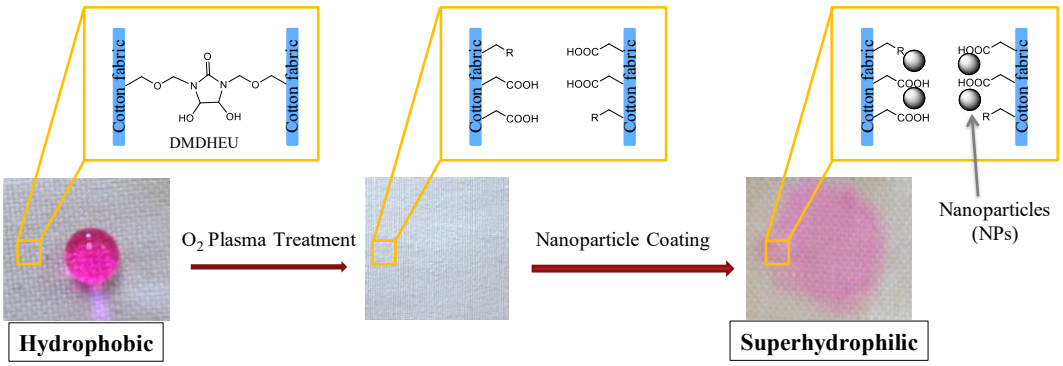

Figure 2.1 Synthesis of superhydrophilic wrinkle-free cotton fabrics and the corresponding water contact angles before and after

2.2 Experimental Section

2.2.1 Preparation of charged silica nanoparticles

The preparation of the charged colloidal silica nanoparticles was reported previously [14, 15]. Colloidal silica, Ludox HS-30 (30 wt% water suspension), with a mean diameter of 16 nm was purchased from Sigma Aldrich. 3 g of the colloidal silica was diluted with deionized (DI) water (30 mL) and sonicated for 30 min. 3.2 g of N-trimethoxysilylpropyl-N,N,N-trimethylammonium chloride (50 wt %, Gelest) was diluted with 20 g of water and then added to the dispersion under rigorous stirring. The dispersion was adjusted to pH~5 using 0.1 N HCl and stirred at 70 ^{o}C for 24 hours to complete the reaction. Subsequently, the suspension was dialyzed (3.5k MWCO, Pierce) against deionized water for 48 hours to remove any unreacted reactants. A schematic of the synthesis and the final molecular structure of the positively charged colloidal silica nanoparticles is shown in Figure 2.2.

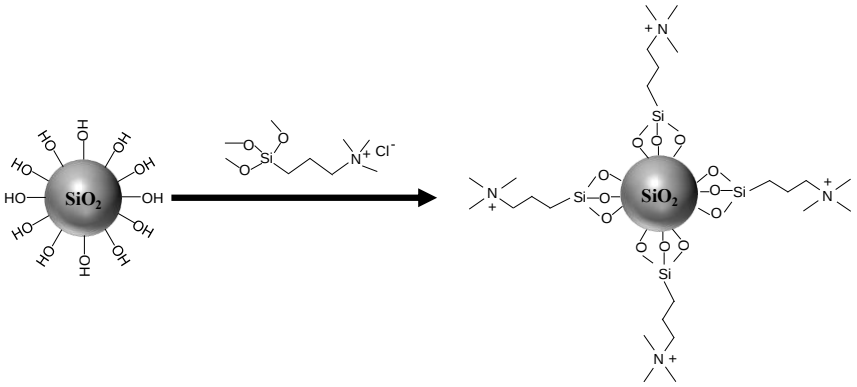

Figure 2.2 Synthesis of positively charged silica nanoparticles

2.2.2 Preparation of silica nanoparticle-coated superhydrophilic fabrics

DMDHEU treated wrinkle-free cotton fabrics were supplied by TAL Apparel Limited. A cleaned wrinkle-free fabric sample (~1.0 × 1.0 inch) was firstly treated by an O_2 gas plasma etcher (PE100RIE, Plasma Etch Inc.), under a flow rate of 50 cc/min and power of 100 W or 300 W for a certain time. The plasma pre-treated fabric was then soaked into 2 ml of the silica nanoparticle suspension overnight at room temperature, followed by 3 times of rinsing with 5 ml of deionized (DI) water. The as-prepared NP-coated fabric sample was fully dried in the oven at 80 ^{o}C for 15 min.

2.2.3 Characterization

Contact angle measurement: Contact angles (CA) of the fabrics was measured via the sessile drop method using a Video Contact Angle (VCA) System (AST Products, Billerica, MA) equipped with the software (VCA Optima XE). A 2 µL water droplet was placed on the fabric surface and stabilized for 0.6 s before the measurement. Four, randomly selected spots were tested on each specimen and the results from at least three similar specimens were averaged for each fabric sample.

Morphology analysis: Scanning electron microscopy (SEM, Tescan Mira3 FESEM) was used to study the microstructure of the wrinkle-free fabric before and after nanoparticle treatment. The samples were coated with a thin layer of gold palladium before observation. Energy-dispersive X-ray spectroscopy (EDS) was used for elemental analysis.

Chemical analysis: Fourier transform infrared (FTIR) spectrometer (Nicolet Magna-IR® 560) was used to characterize the chemical composition of the fabric before and after plasma and nanoparticle treatments. The spectra were recorded in attenuated total reflection (ATR) mode with a scan range of 4000-400 cm^{-1} and a resolution of 2 cm^{-1} up to 64 scans.

Thermal analysis: A thermogravimetric analyzer (TGA 500, TA Instruments) was used to determine the amount of silica nanoparticles deposited on the treated fabric. 5-10 mg of each sample was placed in an alumina ceramics crucible and thermally heated from 30 to 990 ^{o}C in a nitrogen gas medium with a heating rate of 10 ^{o}C/min. The weight percentage of silica nanoparticles was estimated by calculating the difference between the remaining weight of pristine wrinkle-free fabric and NP-coated fabric.

Evaluation of wrinkle-free performance: The wrinkle recovery angle (WRA) measurement (AATCC Test Method 66-2014) was used to analyze the wrinkle-free performance of the fabrics before and after the nanoparticle treatment using an SDL Atlas Crease Recovery Tester. Six specimens (40 × 15 mm) in both the warp and weft directions were measured for each sample. Each specimen was folded in the length direction and horizontally placed in the loading device with a fixed loading pressure (1.019 kg) for 5 min. The recovery angle was measured after placing one end of the sample in the tester holder for another 5 min.

All the samples were placed in a standard atmosphere (65 ± 2% relative humidity, and a temperature of 20 ± 2 ^{o}C) for at least 24 hours prior to testing.

Evaluation of mechanical behavior: Tensile tests of the wrinkle-free fabrics before and after plasma pre-treatment and NP coating were carried out on a uniaxial load test machine (Model #5566, Instron, USA) according to ASTM D5034-09 standards, and fracture stress (σ_f), fracture strain (ε_f) and Young's modulus (E) were determined. Four specimens (40 × 15 mm) in both warp and weft directions were measured for each fabric sample. The thickness of each sample was measured using a vernier caliper at five different locations. The average thickness of wrinkle-free fabric, plasma pre-treated fabric and NP-coated fabric was found to be 0.22 mm, 0.22 mm, 0.23 mm, respectively. The gauge length was set to 25 mm and the cross-head speed was 300 mm/min. Each test was stopped until the load was recovered to 90% of the peak load. All the samples were placed in a standard atmosphere (65 ± 2% relative humidity, and a temperature of 20 ± 2 ^{o}C) for at least 24 hours prior to testing.

Evaluation of laundering durability: The washing fastness of the treated fabrics was evaluated according to AATCC Test Method 124-1996 with certain modifications. Each laundering cycle consists of one washing and two rinsing steps as follows: the NP-coated fabric sample (1 × 1 inch) was washed with 5 ml of 0.25 wt% of a commercial detergent (Tide®, Procter & Gamble) at room temperature for 5 min. Subsequently, the sample was rinsed with DI water at room temperature for 5 min. During the washing and rinsing steps, mechanical agitation was applied using a New Brunswick Innova 2000 Platform Shaker.

Finally, the sample was completely dried at 80 ^{o}C in an oven for 10 min before the next laundering cycle.

Evaluation of abrasion resistance: Abrasion resistance of fabrics is generally one of several factors contributing to wear performance or durability. Abrasion resistance was evaluated according to ASTM D 4966 using SDL Atlas Martindale Abrasion Tester. Three specimens were measured for each sample. The specimens were cut into a circle with 1.5 inches in diameter, weighed and loaded into the tester holders using a polyurethane backing. A fixed weight was loaded to give a pressure of 1.31 ± 0.03 psi (9 ± 0.2 kPa) on each specimen. The machine was then set to run for up to 25,000 cycles at 47.5 rpm. All the samples were placed in a standard atmosphere (65 ± 2% relative humidity, and a temperature of 20 ± 2 ^{o}C) for at least 24 hours prior to testing.

The experimental data were analyzed using ANOVA. The significance level was set at $p<0.05$. Results were reported as mean ± standard deviation.

2.3 Results and Discussion

2.3.1 Wetting behavior of the NP-coated fabrics

We used contact angle measurements to investigate the wetting behavior of the wrinkle-free cotton fabrics before and after silica nanoparticle deposition. We studied samples exposed to a series of plasma pre-treatments using different plasma power levels (100 W and 300 W) and plasma duration times (1 min, 3 min, 5 min and 9 min) (Table 2.1, and Figure S2.1). The wrinkle-free cotton fabric showed a contact angle of 139 ^{o} (Figure 2.1 and Figure S2.2a, also notated as ^{a} in Table 2.1) while that of the neat cotton fabric is 0 ^{o}.

The increased hydrophobicity is caused by the crosslinking of cotton molecules with the wrinkle-free agents, DMDHEU [2, 3].

A series of experiments were designed to investigate the influence of plasma treatment parameters (plasma duration time and power level) as well as the synergistic effects between nanoparticle coating and plasma pre-treatment. Plasma pre-treatment is necessary to secure the immobilization of the nanoparticle coating. Nanoparticle coated fabric without the plasma pre-treatment exhibited a high CA, ~ 110 ^{o} (Table 2.1), probably due to the lack of available functional groups for the charged silica NPs to adhere [24]. Higher hydrophilicity of the fabrics was observed with increasing plasma treatment time and power level. The fabric became superhydrophilic (CA 0-10 ^{o}, notated as ++ in Table 2.1) after being treated under 300 W for 5 min and less hydrophilic (CA 10-90 ^{o}, notated as + in Table 2.1) under 100 W for 5 min. A longer treatment for 9 min brought superhydrophilicity under both plasma powers, but part of the fabric turned slightly yellow (Figure S2.2d). Interestingly, the hydrophilicity of the fabrics treated only by plasma was usually transient. For example, after aging at room temperature (RT) for 7 days the contact angle of the sample treated under 300 W for 5 min increased to ~ 65 ^{o} and further increased to ~ 125 ^{o} after 10 days. This reversal of the surface wetting was consistent with prior studies [18, 23], which can be attributed to the reorientation of hydrophilic groups towards the bulk of the materials during the long-time air exposure [25]. Therefore, plasma treatment alone is not suitable to prepare wrinkle-free fabrics with durable superhydrophilicity. It should be noted that the combination of plasma pretreatment followed by deposition of charged silica nanoparticles greatly improves the durability of the superhydrophilicity. The fabrics pre-treated with plasma for 3 min under 300 W still

remained superhydrophilic after aging for 7 days. Considering the effect of treatment and process cost, we chose the fabric after plasma pre-treatment under 300 W for 5 min followed by silica nanoparticle deposition for further experiments.

Table 2.1 Wetting behavior of wrinkle-free fabrics under different treatment conditions

Day	Day 0				Day 7			
Plasma Power	100 W		300 W		100 W		300 W	
Treatment / Plasma Time	Plasma only	Plasma + NPs	Plasma only	Plasma + NPs	Plasma only	Plasma + NPs	Plasma only	Plasma + NPs
0 min			-[a]	-[b]			-	-
1 min	-	-	-	+	-	-	-	+
3 min	-	+	+	++	-	-	-	++
5 min	+	++	++	++	-	++	+	++
9 min	++	++	++	++	+	++	++	++

Note: The symbols -, + and ++ represent hydrophobic (contact angle 90–150 °), hydrophilic (contact angle 10-90 °) and superhydrophilic (contact angle 0–10 °) properties of the fabrics, respectively. [a] and [b] represent the pristine wrinkle-free fabrics (CA 139 °) and the wrinkle-free fabrics after directly depositing silica nanoparticles without plasma pre-treatment (CA 110 °), respectively.

2.3.2 Morphology and chemical analysis of the NP-coated fabrics

Figure 2.3 compares the morphology of the wrinkle-free fabrics before and after plasma treatment and nanoparticle coating. The pristine fabric showed a smooth fibrous surface (Figure 2.3a, d), a normal morphology of cotton fibers [21, 26]. The fabric treated by plasma (300 W, 5 min), however, transformed to a rough surface (Figure 2.3b). The higher magnification SEM image reveals the fiber surface has been etched by the higher-energy plasma, forming crack and void structures (Figure 2.3e), which was also observed

previously [20, 21, 24]. The roughness of the fibers increased after the silica nanoparticle deposition (Figure 2.3c, f). Energy dispersive X-ray analysis spectroscopy (EDS) confirmed the silica coating on the fiber surface, as indicated by the silicon (Si) peak and an increase of oxygen (O) intensity (Figure S2.3c). In addition, TGA shows a residue of 2.6% (Figure S2.4), which we attribute to the presence of the nanoparticles. The morphology of the NP-coated fabric (Figure 2.3c, f) was different from those of nanoparticle attachment on fabric surfaces reported previously [6, 27], probably due to the difference of deposited nanoparticles and the stronger interaction between the nanoparticles and the surface of the fabric in our system.

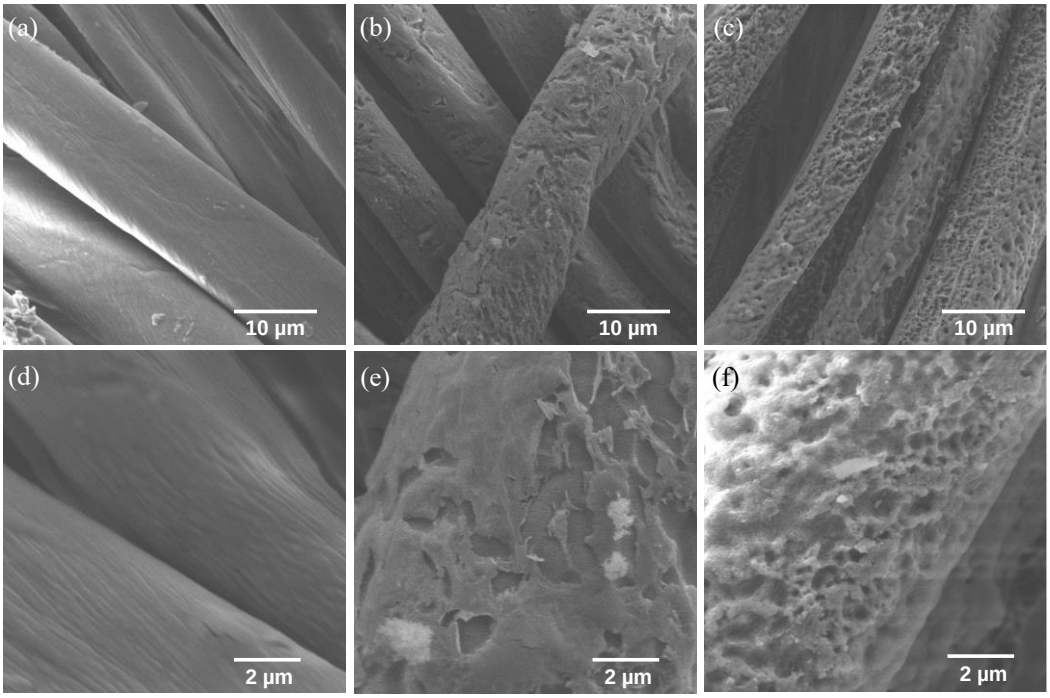

Figure 2.3 SEM morphologies of wrinkle-free fabric before and after plasma pre-treatment and silica nanoparticle coating. (a) Pristine wrinkle-free fabric, (b) wrinkle-free fabric after plasma treatment only (300 W, 5 min) and (c) wrinkle-free fabric after plasma pre-treatment (300 W, 5 min) followed by silica nanoparticle coating, respectively. (d-f) are high magnifications of (a-c), respectively.

The chemical nature of the NP-coated wrinkle-free fabrics were further characterized by FTIR spectra, as shown in Figure 2.4. All the samples before and after plasma and silica nanoparticle deposition possess a similar cotton (cellulose) IR spectrum. The broad absorptions between 3500-3000 cm^{-1} was attributed to the stretching of O–H group and those between 3000-2800 cm^{-1} was due to the C-H stretching [28, 29]. The bands at 1425 cm^{-1} and 1315 cm^{-1} were due to the symmetric C-H bending and C-C (and C-O) skeletal vibrations, respectively [28]. The absorption peaks at 1103 cm^{-1} and 1160 cm^{-1} were attributed to the overlapping of C-O-C skeletal vibration [30]. The bands at 1680 cm^{-1} and 1270 cm^{-1} correspond to the C=O and C-N groups in DMDHEU after the wrinkle-free finishing of the cotton fabric, respectively [26, 30]. The peak at 1496 cm^{-1} was C-O-C bending vibration resulting from the reaction of DMDHEU and cotton fiber [26, 30]. When the fabric was coated with silica nanoparticles, there was a noticeable intensity increase of the peaks at 1090 cm^{-1} and 786 cm^{-1}, the characteristic bands of Si-O-Si asymmetric and symmetric stretching vibrations, respectively [28, 29] although the former somehow overlapped with the peaks from C-O-C and -C-OH vibrations [26, 30]. This observation further confirms the presence of silica nanoparticles in the wrinkle-free cotton fabric and is consistent with the results discussed above. The FTIR spectrum of the fabric pre-treated by plasma (300 W, 5 min) did not show any difference compared with that of the pristine wrinkle-free fabric, probably because the amount of hydrophilic groups created by plasma treatment is too low and beyond the detection limit of FTIR.

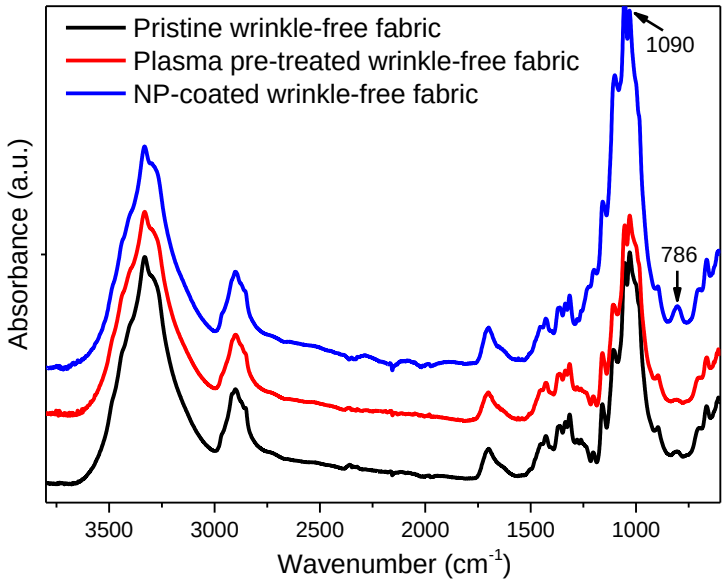

Figure 2.4 FTIR spectra of pristine, plasma pre-treated and silica nanoparticle-coated wrinkle-free fabrics. The arrows show the characteristic peaks associated with Si-O-Si stretching vibrations.

2.3.3 Wrinkle-free performance of the NP-coated fabrics

Wrinkle recovery angle (WRA) is an indication of the ability of a fabric to recover from incidental creasing, and thus is widely used to evaluate the wrinkle-free performance of a fabric [31]. The WRA of the fabrics before and after silica nanoparticle deposition was measured according to AATCC Test Method 66-2014. An original neat cotton fabric before wrinkle-free treatment was used as the control. As shown in Figure 2.5, the wrinkle-free cotton fabric exhibited both high warp and weft wrinkle recovery angles (127 ^{o} and 123 ^{o}, respectively) that almost double those of the original cotton samples (68 ^{o} and 68 ^{o}, respectively) (significance level p<0.05). A minor loss of wrinkle recovery angles was observed after plasma treatment under 300 W for 5 min, namely a 16% (107 ^{o}) and 8% (113 ^{o}) decrease in the warp and weft direction, respectively. After silica nanoparticle

coating, the WRA of the fabric further decreased slightly to 101 ^{o} in both warp and weft directions (p<0.05). These findings were different from prior studies, where WRA has increased both after plasma pre-treatment and further coating of wrinkle-resistant agent (TiO_2 nanoparticles) compared with untreated cotton fabrics [1, 24, 32]. The researchers attributed the WRA increase to the reduced inter-fiber friction and restricted molecular movement, caused by plasma induced rough surfaces and the presence of nanoparticles inside the fibers, respectively. Nonetheless, they also found a decrease in WRA with the increasing concentration of TiO_2 nanoparticles, which interfered the crosslinking of cellulose molecules [1, 32]. In our case, we postulate the slight loss of WRA was due to the damage on the fiber surface created by the high-energy etching (Figure 2.3b, e) and the increased inter-yarn and inter-fiber friction caused by the relatively high loading of the silica nanoparticles (Figure 2.3c, f and Figure S2.4) [33]. Nevertheless, the WRA values of NP-coated wrinkle-free cotton fabric are still significantly higher than those of pristine cotton fabric. The sum of the WRA values of NP coated wrinkle-free cotton fabric in warp and weft directions was 202 ^{o}, indicating a good wrinkle-free property, which was comparable or even better than the cotton fabrics after wrinkle-resistant finishing, e.g. DMDHEU/nano-TiO_2, 1,2,3,4-butanetetracarboxylic acid (BTCA)/nano-TiO_2, BTCA/sodium hypophosphite (SHP)/nano-TiO_2, in the prior reports [1, 24, 32]. The results demonstrated that the NP-coated cotton fabric can achieve superhydrophilicity while maintain great wrinkle-free performance.

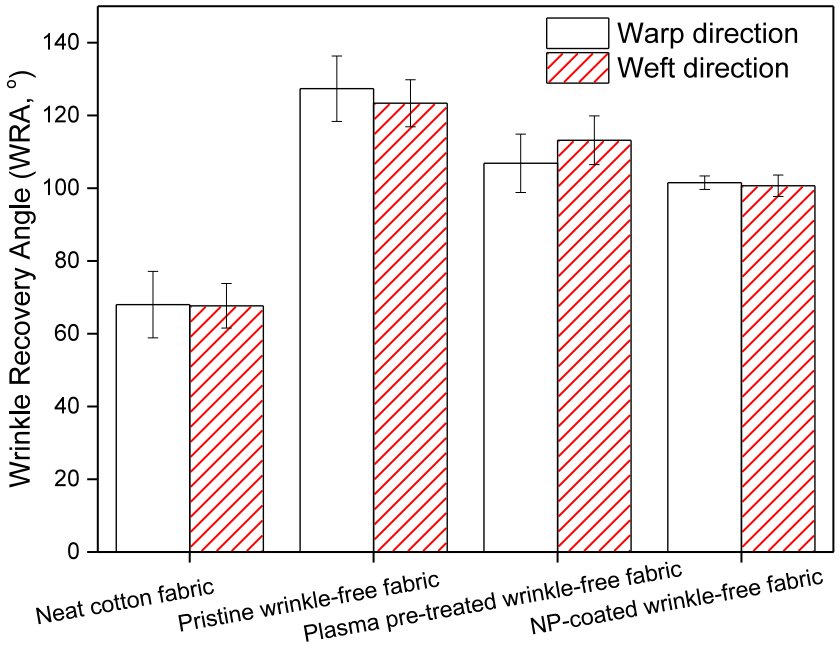

Figure 2.5 Wrinkle recovery angles (WRA) of original neat cotton fabric, pristine wrinkle-free fabric, wrinkle-free fabric after plasma pre-treatment (300 W, 5 min), and wrinkle-free fabric after plasma pre-treatment (300 W, 5 min) followed by NPs coating.

2.3.4 Mechanical properties of the NP-coated fabrics

The mechanical properties of the NP-coated fabrics were evaluated via uniaxial tensile test. Figure 2.6a shows representative stress-strain curves of the fabrics before and after plasma and nanoparticle treatment, and Figure 2.6b-d summarized their fracture stress (σ_f), fracture strain (ε_f) and Young's modulus (E, at 1.9% strain), respectively. For all three different fabrics, the facture stresses and Young's moduli were higher along warp directions (Figure 2.6a, A-C), and the fracture strains were larger along weft directions (Figure 2.6a, A'-C'). Compared with the pristine wrinkle-free fabric ($\sigma_{f\,(warp)}$ ~ 51.9 MPa, $\varepsilon_{f\,(warp)}$ ~ 8.8%; $\sigma_{f\,(weft)}$ ~ 20.4 MPa, $\varepsilon_{f\,(weft)}$ ~ 15.8%), significant increase of the facture stress was observed for the fabrics both after plasma pre-treatment and NP coating, especially in the warp direction

(p<0.05), namely $\sigma_{f\,(warp)}$ ~ 67.5 MPa, $\sigma_{f\,(warp)}$ ~ 69.8 MPa, respectively (Figure 2.6b); while the facture strains for the NP-coated fabric slightly increased in the warp direction (p>0.05), and decreased in the weft direction (p<0.05) (Figure 2.6c). The modulus of the NP-coated wrinkle-free fabric in the warp direction (E ~ 57.0 MPa) was comparable with that of the pristine wrinkle-free fabric (E ~ 64.7 MPs) (p>0.05), though the value of the plasma pre-treated wrinkle-free fabric decreased (E ~ 48.6 MPa) (p<0.05); the moduli in the weft directions were similar among all the fabric samples, and were significantly lower than those in warp directions (p<0.05) (Figure 2.6d). The increasing trend of the strength for the plasma pre-treated samples was similar as those reported in previous studies, and was attributed to the greater cohesive force caused by the increased inter-yarn and inter-fiber fiber friction with the etched surface (Figure 2.3b, e) [34-36] . The further increase of the strength for the silica NP-coated samples might be contributed to the fact that nanoparticles can provide additional resistance to fiber slippery [37], which was also observed in a nano-TiO_2 incorporated cotton fabric after a certain TiO_2 loading [38]. Overall, the results showed neither the plasma pre-treatment nor the silica nanoparticle coating has any detrimental effect on the mechanical properties of the fabrics, instead they even endowed a higher tensile strength.

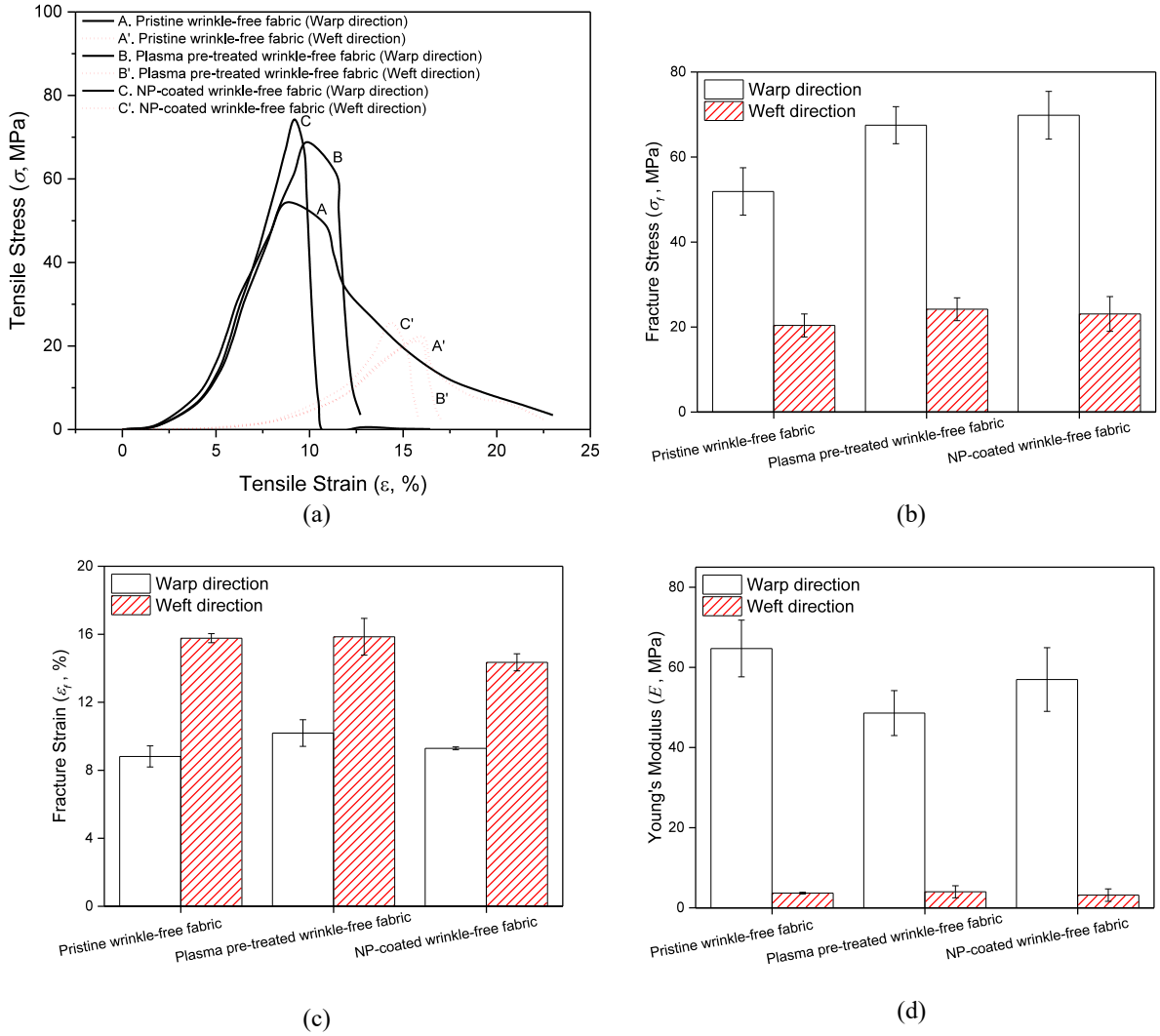

Figure 2.6 Tensile properties of wrinkle-free fabric before and after plasma pre-treatment and silica nanoparticle coating. (a) Typical stress-strain curves for pristine wrinkle-free fabric, plasma pre-treated (300 W, 5 min) wrinkle-free fabric, and NP-coated wrinkle-free fabric, in both warp and weft directions. (b-d) Fracture stress (σ_f), fracture strain (ε_f) and Young's Modulus (E, at 1.9% strain) for the three fabrics, respectively, in both warp and weft directions.

2.3.5 Durability of the NP-coated fabrics

The durability of the NP-coated fabrics was evaluated in terms of wetting behavior and wrinkle-free property after aging, laundering and abrasion. As shown in Table 2.2 (and Figure S2.5), the NP-coated fabrics retained superhydrophilicity after 60 days of aging at

RT or heating at 80 ºC for 4 hours, while the fabrics treated by plasma alone reversed to hydrophobic. The samples remained superhydrophilic after 50 laundering cycles and up to 25,000 abrasion cycles, respectively.

Table 2.2 Durability of wetting behaviors of NP-coated wrinkle-free fabrics (plasma pre-treated under 300 W for 5 min) via aging, laundering and abrasion tests.

Durability tests	Experiment condition	Fabric sample	
		Plasma only (300 W, 5 min)	Plasma + NPs
Aging	80 ºC, 4 hours	-	++
	RT, 60 days	-	++
Laundering	19 cycles	N/A	++
	50 cycles	N/A	++
Abrasion	1,000 cycles	N/A	++
	2,000 cycles	N/A	++
	25, 000 cycles	N/A	++

Note: The symbols - and ++ represent hydrophobic (contact angle 90–150 °) and superhydrophilic (contact angle 0–10 °) properties of the fabrics, respectively.

In addition, as shown in Figure 2.7, the NP-coated wrinkle-free treated fabric after 25,000 abrasion cycles had an average WRA value (e.g. average of WRA value in warp and weft direction) of 121 º, which is even slightly higher than that before the abrasion test (p>0.05) (Figure 2.5). On the other hand, the WRA of the pristine wrinkle-free fabric and neat cotton fabric decreased to 103 º (p<0.05) and 68 º (p>0.05), respectively.

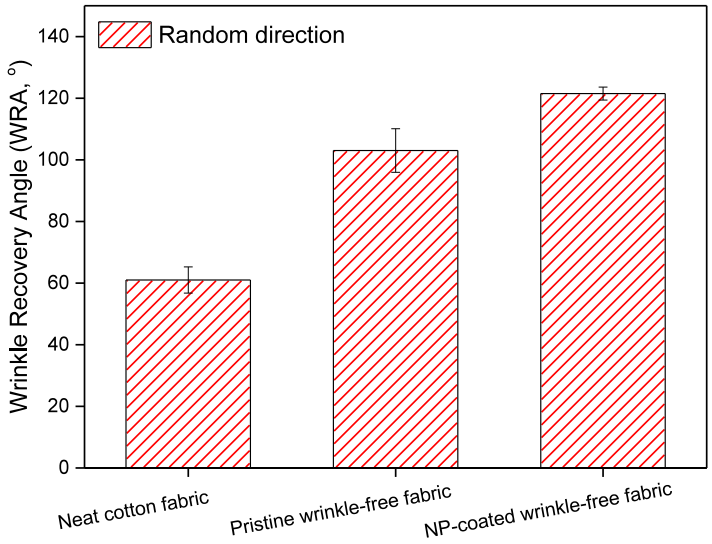

Figure 2.7 Durability of wrinkle-free performance of NP-coated fabric (plasma pre-treated under 300 W for 5 min) via 25,000 cycles' abrasion tests.

When the fiber morphology was examined after the abrasion test (Figure 2.8), it was found that there were more breakages of fibers for both pristine wrinkle-free fabric (Figure 2.8a-c) and NP-coated fabric (Figure 2.8d-f), with increasing abrasion cycles. Regardless, the surface of the fibers in the NP-coated fabrics was still much rougher (Figure 2.8d-f) compared with the control samples (Figure 2.8a-c), which was an indicator of continuous presence of nanoparticles. TGA also confirmed the presence of silica nanoparticles residue of 2.5% on the fabric after 25,000 abrasion cycles (Figure S2.6), which was almost the same as that before abrasion (Figure S2.4). These results indicate the robustness of the nanoparticle coating on the fabrics because of the strong electrostatic interactions [14], resulting in a good durability of both superhydrophilicity and wrinkle-free properties.

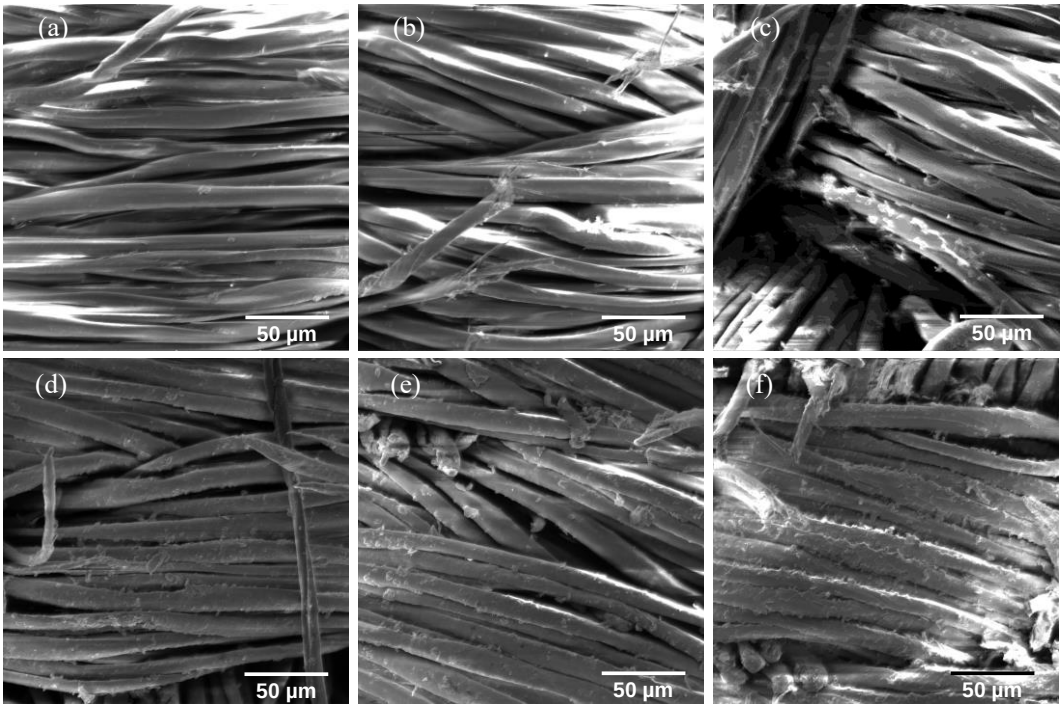

Figure 2.8 SEM morphologies of different fabrics after 1,000-25,000 cycles' abrasion tests. (a-c) Pristine wrinkle-free fabric and (d-f) NP-coated wrinkle-free fabric (plasma pre-treated under 300 W for 5 min) after abrasion for (a, d) 1,000 cycles, (b, e) 2,000 cycles and (c, f) 25,000 cycles, respectively.

Combining the WRA (Figure 2.7) and the surface morphology (Figure 2.8) after abrasion, we speculated that the slight reduction of the wrinkle recovery performance of the pristine wrinkle-free fabric and pristine cotton fabric may be caused by the damage imparted on the fabric surface during the abrasion process (Figure 2.8c), while the slight increase of wrinkle recovery performance of NP-coated fabric may be caused by the consolidation of internal fabric structure during the abrasion process (Figure 2.8f). In general, it can be concluded that the wrinkle recovery performance of NP-coated wrinkle-free treated fabric are stable even after prolonged abrasion cycles.

2.4 Conclusion

A new approach to endow hydrophilicity to wrinkle-free cotton fabrics is reported. Conventional wrinkle-free treatment of cotton fabrics tends to make the fabrics hydrophobic, resulting in the deterioration of comfort associated with moisture sorption and wicking properties. Although wrinkle-free fabrics can be made hydrophilic through plasma treatment alone, their hydrophilicity is not stable and they revert to hydrophobic behavior after aging. In this work, we have developed a process for achieving durable superhydrophilicity on wrinkle-free cotton fabrics through a combination of plasma treatment followed by attachment of charged silica nanoparticles. SEM images show silica nanoparticle coating roughened the surface of the wrinkle-free fabrics. Chemical analyses also confirmed the presence of nanoparticles on the fabrics. The nanoparticle-treated fabrics retain their superhydrophilicity after 60 days of aging at RT, 50 laundering cycles and 25,000 abrasion cycles. Finally, the nanoparticle-coated fabrics also exhibit a good wrinkle-free performance, tensile strength and abrasion resistance after 25,000 abrasion cycles.

2.5 Supporting Information

Wetting behavior of the NP-coated fabrics

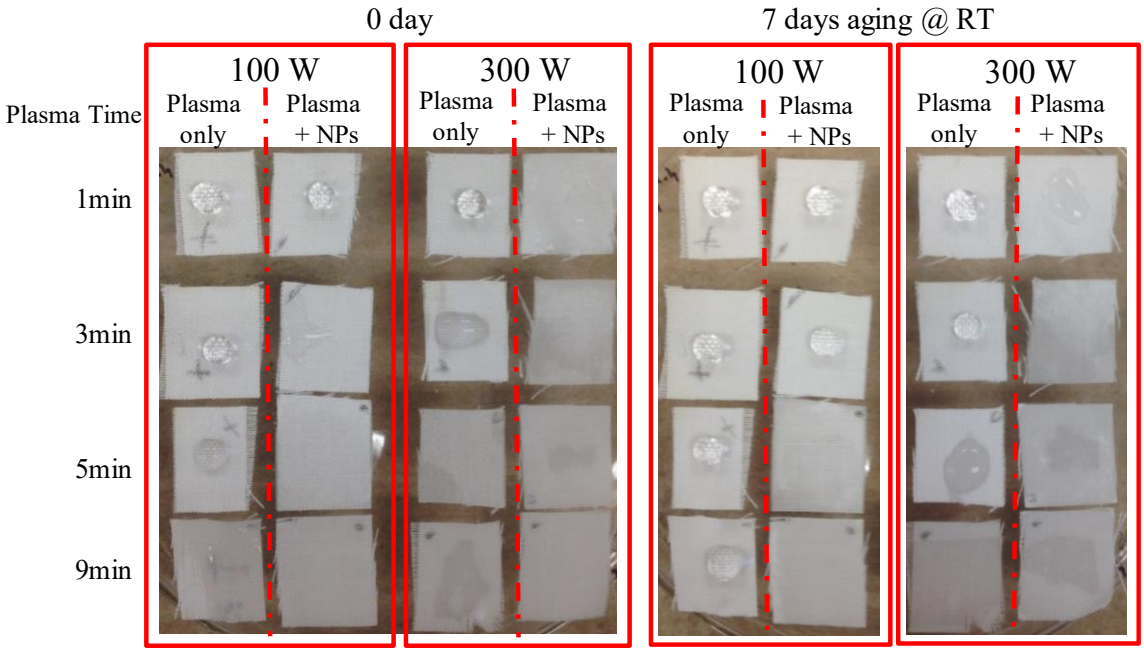

Figure S2.1 Images of water droplets on the wrinkle-free fabrics to show the hydrophilicities under different treatment conditions.

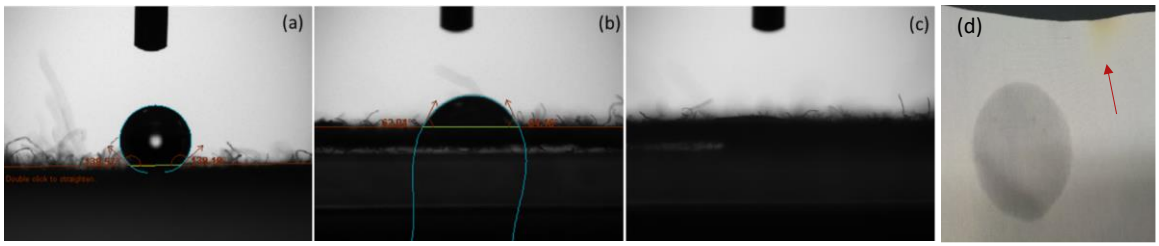

Figure S2.2 Contact angle test of wrinkle-free fabrics before and after plasma pre-treatment and silica nanoparticle coating. (a-c) Contact angle of a water droplet on (a) pristine hydrophobic wrinkle-free fabric (CA= 138.8 °), (b) a hydrophilic wrinkle-free fabric after plasma treatment only (300 W, 3 min) (CA= 63.1 °), and (c) a superhydrophilic wrinkle-free fabric after plasma pretreatment (300 W, 3 min) followed by silica nanoparticle coating (CA= 0 °), respectively. (d) An image of a water droplet on a superhydrophilic wrinkle-free fabric after plasma treatment only (300 W, 9 min), with an arrow showing the yellowing of the fabric.

Chemical analysis of the NP-coated fabrics

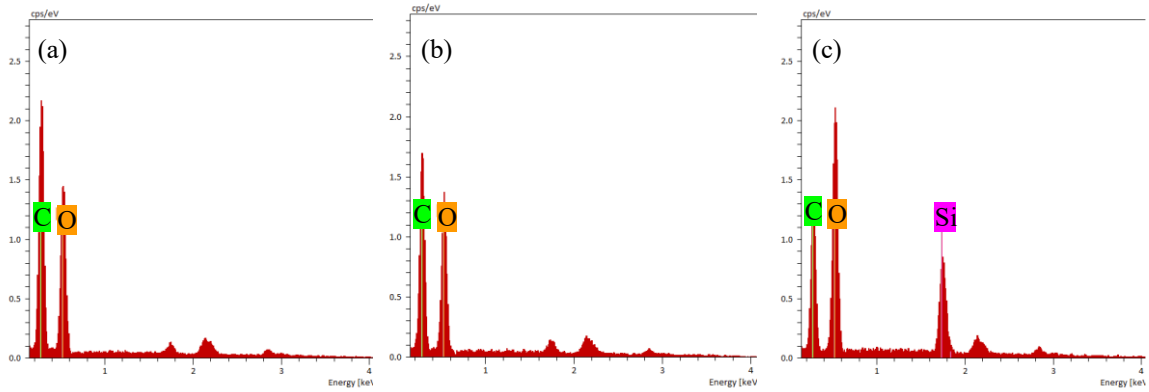

Figure S2.3 Energy-dispersive X-ray spectrum (EDS) of wrinkle-free fabrics before and after plasma pre-treatment and silica nanoparticle coating. (a) Pristine wrinkle-free fabric, (b) wrinkle-free fabric after plasma treatment only (300 W, 5 min) and (c) wrinkle-free fabric after plasma pretreatment followed by silica nanoparticle coating, respectively.

Thermal analysis of the NP-coated fabrics

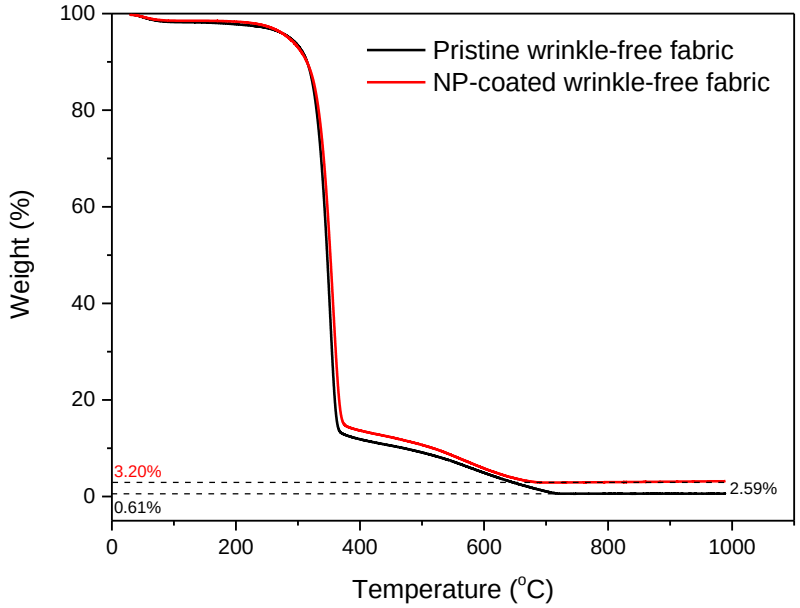

Figure S2.4 Thermogravimetric analysis (TGA) spectra of pristine wrinkle-free fabric and silica nanoparticle-coated wrinkle-free fabric.

Durability of the NP-coated fabrics

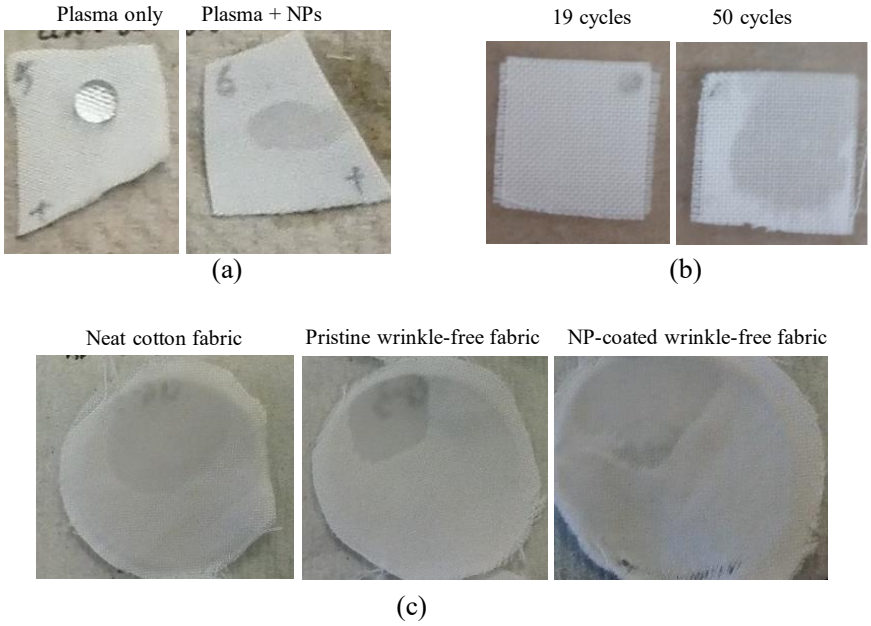

Figure S2.5 Water droplets on the fabrics to show durability of wetting behaviors of NP-coated wrinkle-free fabrics (plasma pretreated under 300 W for 5 min) via aging, laundering and abrasion tests. (a) 60 days of RT aging test: (left) wrinkle-free fabric after plasma treatment only and (right) wrinkle-free fabric after plasma pretreatment followed by NPs-coating, respectively.(b) Laundering test: NP-coated wrinkle-free fabric after (left) 19 cycles' and (right) 50 cycles' laundering, respectively. (c) Abrasion test after 25,000 cycles: (left) original neat cotton fabric, (middle) pristine wrinkle-free fabric and (right) NP-coated wrinkle-free fabric, respectively.

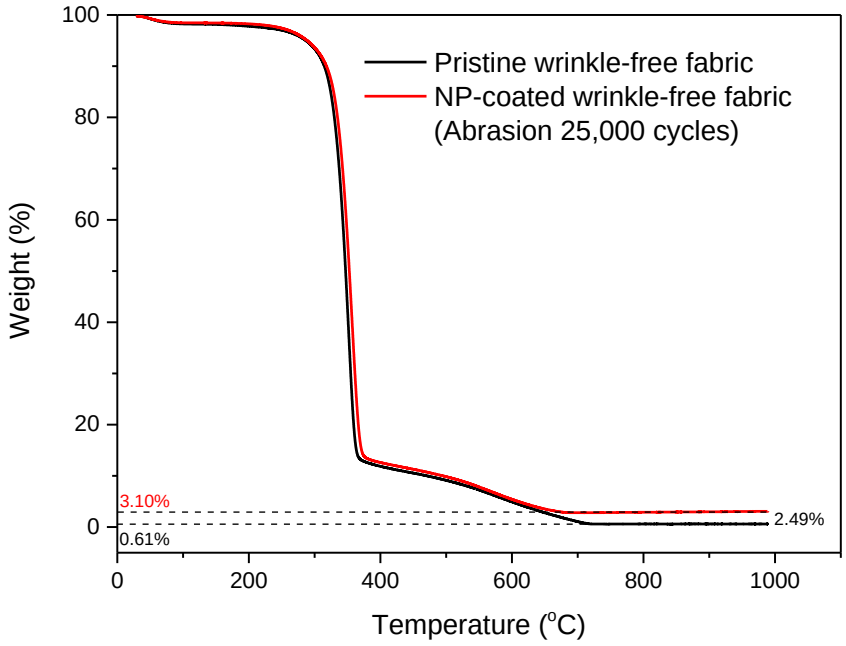

Figure S2.6 TGA spectra of pristine wrinkle-free fabric and NP-coated wrinkle-free fabrics after 25,000 abrasion cycles.

REFERENCES

[1] Y.L. Lam, C.W. Kan, C.W.M. Yuen, Wrinkle-resistant finishing with dimethyloldihydroxyethyleneurea (DMDHEU) - the effect of co-catalyst, *Text Res J* **81**(14) (2011) 1419-1426.

[2] W. Simpson, G. Crawshaw, Wool: Science and technology, *Elsevier* 2002.

[3] T. Hongu, M. Takigami, G. Phillips, New millennium fibers, *Elsevier* 2005.

[4] R. Wang, K. Hashimoto, A. Fujishima, M. Chikuni, E. Kojima, A. Kitamura, M. Shimohigoshi, T. Watanabe, Light-induced amphiphilic surfaces, *Nature* **388** (1997) 431-432.

[5] M. Montazer, E. Pakdel, M.B. Moghadam, The role of nano colloid of TiO2 and butane tetra carboxylic acid on the alkali solubility and hydrophilicity of proteinous fibers, *Colloids Surf A Physicochem Eng Asp* **375**(1) (2011) 1-11.

[6] D. Chen, L. Tan, H. Liu, J. Hu, Y. Li, F. Tang, Fabricating superhydrophilic wool fabrics, *Langmuir* **26**(7) (2009) 4675-4679.

[7] W.S. Tung, W.A. Daoud, Effect of wettability and silicone surface modification on the self‐cleaning functionalization of wool, *J Appl Polym Sci* **112**(1) (2009) 235-243.

[8] K. Guan, Relationship between photocatalytic activity, hydrophilicity and self-cleaning effect of TiO_2/SiO_2 films, *Surf Coat Technol* **191**(2) (2005) 155-160.

[9] B. Tang, J. Wang, S. Xu, T. Afrin, J. Tao, W. Xu, L. Sun, X. Wang, Function improvement of wool fabric based on surface assembly of silica and silver nanoparticles, *Chem Eng J* **185** (2012) 366-373.

[10] R. Rodriguez, R. Herrera, L.A. Archer, E.P. Giannelis, Nanoscale ionic materials, *Adv Mater* **20**(22) (2008) 4353-4358.

[11] A.B. Bourlinos, R. Herrera, N. Chalkias, D.D. Jiang, Q. Zhang, L.A. Archer, E.P. Giannelis, Surface ‐ functionalized nanoparticles with liquid ‐ like behavior, *Adv Mater* **17**(2) (2005) 234-237.

[12] N.J. Fernandes, J. Akbarzadeh, H. Peterlik, E.P. Giannelis, Synthesis and properties of highly dispersed ionic silica–poly (ethylene oxide) nanohybrids, *ACS Nano* **7**(2) (2013) 1265-1271.

[13] R. Rodriguez, R. Herrera, A.B. Bourlinos, R. Li, A. Amassian, L.A. Archer, E.P. Giannelis, The synthesis and properties of nanoscale ionic materials, *Appl Organomet Chem* **24**(8) (2010) 581-589.

[14] S. Liang, Y. Kang, A. Tiraferri, E.P. Giannelis, X. Huang, M. Elimelech, Highly hydrophilic polyvinylidene fluoride (PVDF) ultrafiltration membranes via postfabrication grafting of surface-tailored silica nanoparticles, *ACS Appl Mater Interfaces* **5**(14) (2013) 6694-6703.

[15] A. Tiraferri, Y. Kang, E.P. Giannelis, M. Elimelech, Superhydrophilic thin-film composite forward osmosis membranes for organic fouling control: fouling behavior and antifouling mechanisms, *Environ Sci Technol* **46**(20) (2012) 11135-11144.

[16] C.-w. Kan, C.-w.M. Yuen, Plasma technology in wool, *Text Progr* **39**(3) (2007) 121-187.

[17] R. Morent, N. De Geyter, J. Verschuren, K. De Clerck, P. Kiekens, C. Leys, Non-thermal plasma treatment of textiles, *Surf Coat Technol* **202**(14) (2008) 3427-3449.

[18] C. Canal, R. Molina, E. Bertran, A. Navarro, P. Erra, Effects of low temperature plasma on wool and wool/nylon blend dyed fabrics, *Fiber Polym* **9**(3) (2008) 293-300.

[19] A. Bozzi, T. Yuranova, J. Kiwi, Self-cleaning of wool-polyamide and polyester textiles by TiO 2-rutile modification under daylight irradiation at ambient temperature, *J Photochem Photobiol A Chem* **172**(1) (2005) 27-34.

[20] K.N. Pandiyaraj, V. Selvarajan, Non-thermal plasma treatment for hydrophilicity improvement of grey cotton fabrics, *J Mater Process Tech* **199**(1-3) (2008) 130-139.

[21] S. Inbakumar, R. Morent, N. De Geyter, T. Desmet, A. Anukaliani, P. Dubruel, C. Leys, Chemical and physical analysis of cotton fabrics plasma-treated with a low pressure DC glow discharge, *Cellulose* **17**(2) (2010) 417-426.

[22] K. Wong, X. Tao, C. Yuen, K. Yeung, Wicking properties of linen treated with low temperature plasma, *Text Res J* **71**(1) (2001) 49-56.

[23] C. Canal, R. Molina, E. Bertran, P. Erra, Study on the influence of scouring on the wettability of keratin fibers before plasma treatment, *Fiber Polym* **9**(4) (2008) 444-449.

[24] Y.L. Lam, C.W. Kan, C.W.M. Yuen, Effect of plasma pretreatment on the wrinkle-resistance properties of cotton fibers treated with a 1,2,3,4-butanetetracarboxylic acid sodium hypophosulfite system with titanium dioxide as a cocatalyst, *J Appl Polym Sci* **120**(3) (2011) 1403-1410.

[25] J. Nakamatsu, L.F. Delgado-Aparicio, R. Da Silva, F. Soberon, Ageing of plasma-treated poly(tetrafluoroethylene) surfaces, *J Adhes Sci Technol* **13**(7) (1999) 753-761.

[26] S.H. Hsieh, C.H. Huang, S.P. Chiu, Effects of chitosan addition to DMEU-processed cotton fabrics for adsorbing metallic ions in waste water, *J Appl Polym Sci* **101**(6) (2006) 4440-4445.

[27] G.Y. Bae, B.G. Min, Y.G. Jeong, S.C. Lee, J.H. Jang, G.H. Koo, Superhydrophobicity of cotton fabrics treated with silica nanoparticles and water-repellent agent, *J Colloid Interface Sci* **337**(1) (2009) 170-175.

[28] B.H. Patel, S.B. Chaudhari, P.N. Patel, Nano silica loaded cotton fabric; characterization and mechanical yesting, *Res J Engineering Sci* **3**(4) (2014) 19-24.

[29] A. Beganskienė, V. Sirutkaitis, M. Kurtinaitienė, R. Juškėnas, A. Kareiva, FTIR, TEM and NMR investigations of stöber silica nanoparticles, *Mat Sci (Medziagotyra)* **10**(4) (2004) 287-290.

[30] K.S. Huang, K.L. Yang, S.J. Lin, W.T. Lian, Antiwrinkle treatment of cotton fabric with a mixed sol of TEOS-TTB/DMDHEU, *J Appl Polym Sci* **106**(4) (2007) 2559-2564.

[31] X.Q. Qiu, C.Q. Yang, Wrinkle recovery angle and wrinkle recovery appearance rating for durable press finished cotton fabrics, *AATCC Rev* **5**(12) (2005) 34-38.

[32] Y.L. Lam, C.W. Kan, C.W.M. Yuen, Effect of concentration of titanium dioxide acting as catalyst or co-catalyst on the wrinkle-resistant finishing of cotton fabric, *Fiber Polym* **11**(4) (2010) 551-558.

[33] M.P. Gashti, F. Alimohammadi, A. Shamei, Preparation of water-repellent cellulose fibers using a polycarboxylic acid/hydrophobic silica nanocomposite coating, *Surf Coat Tech* **206**(14) (2012) 3208-3215.

[34] Y.L. Lam, C.W. Kan, C.W.M. Yuen, C.H. Au, Fabric objective measurement of the plasma-treated cotton fabric subjected to wrinkle-resistant finishing with BTCA and TiO_2 system, *Fiber Polym* **12**(5) (2011) 626-634.

[35] C.W. Kan, Y.L. Lam, Low stress mechanical properties of plasma-treated cotton fabric subjected to zinc oxide-anti-microbial treatment, *Materials* **6**(1) (2013) 314-333.

[36] P.K. Panda, M. Jassal, A.K. Agrawal, In situ atmospheric pressure plasma treatment of cotton with monocarboxylic acids to impart crease-resistant functionality, *Cellulose* **23**(1) (2016) 993-1002.

[37] L.H. Lao, Y. Zhu, Y.Y. Zhang, Z.Y. Gao, F. Zhou, L.K. Chen, H.W. Ouyang, C.Y. Gao, Mineralization of collagen-coated electrospun poly(lactide-co-glycolide) nanofibrous mesh to enhance growth and differentiation of osteoblasts and bone marrow mesenchymal stem cells, *Adv Eng Mater* **14**(4) (2012) B123-B137.

[38] T. Karthik, R. Rathinamoorthy, R. Murugan, Enhancement of wrinkle recovery angle of cotton fabric using citric acid cross-linking agent with nano-TiO_2 as a co-catalyst, *J Ind Text* **42**(2) (2012) 99-117.

CHAPTER 3

"SKIN-LIKE" FABRICS WITH BOTH DIRECTIONAL WATER TRANSPORT AND WATER REPELLENT PROPERTIES[*]

Abstract

Recently, directional water transport is widely investigated in the application of functional fabrics for sweat-wicking and quick dry purpose. Conventional directional water transport tends to occur on asymmetric multilayer-assembled fabrics or fabrics with gradient wettability, where water is able to transport only from a hydrophobic layer (e.g. next-to-skin side) to hydrophilic layer (e.g. external surface); however, the liquid transport rate slows down and the fabric becomes heavy and clingy once the outer layer is saturated. In addition, these fabrics cannot repel the external liquid. We demonstrate in this study, for the first time, a "skin-like" directional water transport fabric which enables continuous one-way liquid flow through spatially distributed channels acting like "sweating glands", yet repels external liquid contaminants. The water transmission rate can be 15 times greater than that of best commercial breathable fabrics. The exceptional property of the fabric is achieved by creating gradient wettability channels across a predominantly superhydrophobic fabric via selective plasma treatment with patterned masks. The directional water transport property was confirmed via various experiments including

[*] **Lihong Lao**, Dahua Shou, Yuen Shing Wu, Jintu Fan. "Skin-like" Fabric for Personal Moisture Management. ***Submitted***. 2019.

contact angle test, water dripping test, water flux test and shower test. The flow directionality is explained by the Gibbs pinning criterion. In additional to functional clothing, this concept can be extended to develop materials for oil–water separation, wound dressings, geotechnical engineering, flexible microfluidics and fuel cell membranes.

3.1 Introduction

Personal moisture management is essential to thermal comfort and performance. Moisture management fabrics that promote wicking of sweat away from skin are commercially available [1, 2], but such fabrics are not repellent to external liquid water. On the other hand, commercially available breathable fabrics, although water repellent, can only allow a moisture vapor transmission rate up to ~460 $g/m^2/h$ [3, 4], which is far less than the sweating rate of an average person under moderate exercise (~1000 $g/m^2/h$) [5].

Directional liquid transport, which is also referred as "one-way" liquid transport, is a phenomenon that liquid moves in a specific direction[6]. It has been widely found in the nature on insects and plants. Examples include beetle's back[7, 8], spider silk [9] and cactus branch [10], where their surfaces have special structures and wettability, which lead to different surface energy and capillary pressure for one-way water collection. Besides the natural creatures, the directional liquid transport property is also very promising for various applications such as functional clothing [11, 12], oil-water separation [13, 14], wound dressings [15, 16], geotechnical engineering [17, 18], flexible microfluidics [19, 20], fuel cell membranes [21], etc.

Recently, different porous materials (e.g. fabrics) capable of directionally transporting liquid from one side of the material to the other, yet not capable of repelling liquid absorption or penetration from the other side have been reported. They may be grouped into two categories. One is to create lyophilicity (e.g. hydrophilicity or oleophilicity) gradient through the fabric thickness, another one is to assemble two layers of materials with different lyophilicity as an asymmetric construct [6, 22]. In both cases, liquid tends to transport from lyophobic (e.g. hydrophobic or oleophobic) side to lyophobilic (e.g. hydrophilic or oleophilic) side of the fibrous materials, but is blocked in the reverse direction. For instance, for the first category, Wang et al. [23], Kong et al. [24] and Zhou et al. [25] separately applied photo-sensitive superhydrophobic coating on cotton or polyester fabrics followed by ultra-violet (UV) illumination on one-side to induce hydrophilicity gradient to enable directional water transport abilities through the fabric thickness. Zhang et al. [26] prepared hydrophilic-to-hydrophobic gradient dynamers via phase separation and used them as asymmetric membranes for directional water transport. For the second category, Wu et al. [27] and Wang et al. [28] used electrospinning to form hydrophobic/hydrophilic and oleophobic/oleophilic dual-layer nanofibrous membrane with directional water and oil transport properties, respectively. Tian et al. [29] used vapor diffusion method to deposit fluoroalkyl silane on one side of cotton fabric to form hydrophilic/hydrophobic Janus-type membrane with directional water droplet gating behavior. Sun et al. [30] used three-step plasma polymerization to create asymmetric wettability on bifacial fabrics to develop directional water transport ability. Zeng et al. [22], Liu et al. [31] and Wang et al. [32] created different wettability across the fabric thickness by electro-spraying hydrophobic coating on a hydrophilic fabric. Si et al.[33] treated

hydrophobic membranes by floating one side on a hydrophilic solution to form Janus membranes with directional water penetration ability. Hou et al. [34] recently reported an anisotropic Janus membrane with nanoneedle and electrospun nanofiber interpenetrating structures for achieving unidirectional liquid penetration “diode” performance. Combining both multilayer and wettability gradient strategies, Miao et al. [11] fabricated a trilayer fibrous membrane with progressive wettability by introducing a transfer layer to ensure continuous directional water transport and prevention of water penetration in the reverse direction.

The other strategy of creating directional flow across the fabric thickness is to create gradient/differential sizes of interconnected pores across the thickness. Our group [35-37] developed a type of branching fabric structure, in which yarns are bundled together on one side and separated on the other, leading to an interconnected branching pore network with larger pores on one side and smaller pores on the other. It was demonstrated that liquid water flows faster from the larger pore side to the smaller pore side than in the opposite direction. In a recently published work [38], it was further shown that, if the pore size expansion angle is sufficiently large, flow from the smaller pore size to the larger pore size can be stopped, leading to an all hydrophilic (or lyophilic) fabric diode with directional flow characteristic. The mechanisms of directional capillary flow [39, 40] and the optimum design parameters [41-44] in terms of porosity, pore diameter distribution across the gradient porous media, thickness and porosity ratios for the two-layer fibrous media for maximum flow asymmetricity have been investigated theoretically in our lab. Experimentally, Wang et al. [12] also recently reported a synergistic assembly strategy to create fiber-based porous Murray membranes combining a multibranching porous structure

and surface energy gradient to enable directional water transport and quick-dry performance.

Although, in these existing directional liquid transport (or fluid diode) materials, liquid, e.g. water, is able to directionally transport from hydrophobic side to the hydrophilic side, but not vice versa, liquid tends to spread and be absorbed on the hydrophilic side. Consequently, the directional water transport will be stopped when the hydrophilic side is fully saturated, and the saturation of water on the hydrophilic side may also increase discomfort due to increased weight. Furthermore, the hydrophilic external side of the fabric makes it non-preventive to external water, stain or liquid pathogen.

Here, we present a conceptually novel design strategy by mimicking the master of sweat regulation—human skin. Human skin is an ideal directional liquid flow material as it excretes liquid sweat and protect the body from external liquid contaminants (Figure 3.1a) [45, 46]. In this study, for the first time, we developed a "skin-like" directional liquid transport fabric, which allows continuous one-way water flow and repels external liquid (Figure 3.1b). This is achieved by endowing gradient wettability in distributed porous channels on a predominantly hydrophobic fabric. We used a hydrophilic cotton fabric as a starting material, and pre-treated it with superhydrophobic finishing via fluorosilane-coated titanium dioxide (TiO_2) nanoparticles. Selective plasma treatment via a patterned mask was then applied to create the gradient wettability porous channels across this hydrophobic fabric (Figure 3.1c). While these channels are served for one-way liquid flow, the predominantly superhydrophobic nature of the surface makes it repel the transported liquid or external liquid from the surface.

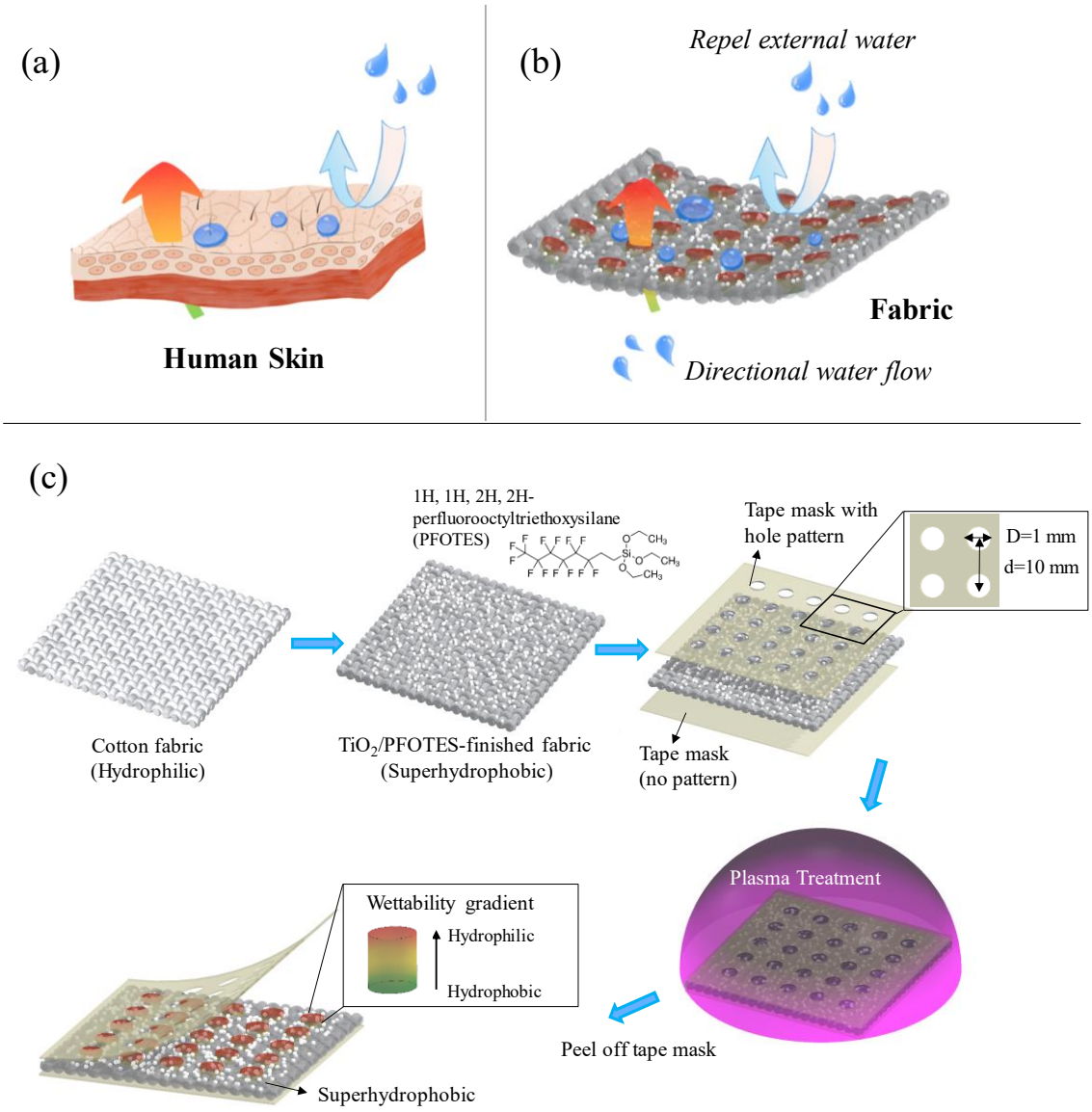

Figure 3.1 Schematic illustration and fabrication process of a "skin-like" fabric with both directional water transport property and water repellency. (a, b) Schematic demonstration of the dual properties of (a) human skin and (b) the designed "skin-like" fabric, respectively. (c) A combination of superhydrophobic finishing via fluorosilane-coated titanium dioxide (TiO_2) nanoparticles and selective plasma treatment via a patterned mask to create gradient wettability spot channels through the fabric thickness to endow the dual properties.

3.2 Experimental Section

3.2.1 Superhydrophobic finishing of cotton fabrics

The fabrics used for the experiment were woven cotton fabrics. They were treated via conventional desizing, scouring, and bleaching process prior to the use [47].

The superhydrophobic coatings were prepared using the following protocol [48]. 2.0 g 1H, 1H, 2H, 2H-Perfluorooctyltriethoxysilane ($C_{14}H_{19}F_{13}O_3Si$, 97%, Oakwood) (noted as PFOTES) was dissolved in 198 g ethanol via vigorous mixing for 2 hours. The solution was subsequently mixed with 10 g Degussa P25 titanium dioxide nanoparticles (TiO_2, Rutile: Anatase/85:15, 99.9%, 20 nm; Degussa) to form a suspension. The cotton fabrics with designed sizes were immersed in the coating suspension for 5 min, and dried in air for 10 min before testing.

3.2.2 Selective plasma treatment of the finished fabrics

One side of the superhydrophobic finished cotton fabric (notated as top side) was tightly covered by a layer of paper tape mask with laser-cut hole patterns (diameter varies from 0.5 to 3 mm, with a typical one of 1 mm, the intervals between holes is 10 mm), another side (notated as back side) was covered by the same tape mask without the hole patterns (Figure 3.1c). The masked fabric was placed into an oxygen gas plasma etcher (PE100RIE, Plasma Etch Inc.) and treated under O_2 flow rate of 50 cc/min and power of 300 W, for a certain time. Because of the patterned mask, only the hole spot area of the top side of the fabric was expected to be exposed to the plasma. After plasma treatment, the tape mask was peeled off from both sides of the fabric.

3.2.3 Characterization

Contact angle measurement: Contact angles (CA) of the fabrics were measured via the sessile drop method using a Movie Contact Angle (VCA) System (AST Products, Billerica, MA) equipped with the software (VCA Optima XE). The fabrics were cut into strips, and hung in the air by fixing two ends using a thick (~8 mm) epoxy putty tape on a glass slide. A 10 µL water droplet was placed on the fabric surface to check either its contact angle or the transport properties. At least five parallel measurements from both spot and non-spot areas on both sides of the fabrics were conducted on each specimen, and the results of either contact angles or transport time were averaged for each fabric sample.

Morphology analysis: Scanning electron microscopy (SEM, Tescan Mira3 FESEM) was used to study the microstructure of the cotton fabric before and after superhydrophobic and plasma selective treatments. The samples were coated with a thin layer of gold palladium before observation.

Chemical analysis: The surface chemical information of the cotton fabrics before and after superhydrophobic coating and plasma treatment were analyzed using X-ray photoelectron spectroscopy (XPS) (SSX-100, Surface Science Instruments) with operating pressure of ~2×10^{-9} Torr. Monochromatic Al Kα x rays (1486.6 eV) with 1 mm diameter beam size was used. Photoelectrons were collected at a 55 ° emission angle. Electron kinetic energy was determined by a hemispherical analyzer using a pass energy of 150 V for wide/survey scans ranging from 0 to 1100 eV. A flood gun was used for charge neutralization of all the samples. The data analysis was performed on CasaXPS software.

Thermal analysis: A thermogravimetric analyzer (TGA 500, TA Instruments) was used to determine the amount of TiO_2 nanoparticles deposited on the treated fabric. 5-10 mg of each sample was placed in an alumina ceramics crucible and thermally heated from 30 to 990 ^oC in a nitrogen gas medium with a heating rate of 10 ^oC/min. The weight percentage of TiO_2 nanoparticles was estimated by calculating the difference between the remaining weight of pristine cotton fabric and TiO_2/PFOTES-coated fabric.

Water dripping test: Water droplets of ~20 µL per droplet were dripped onto either top or back sides of the horizontally laid superhydrophobic finished fabrics after selective plasma treatment. Continuous water droplet supply from a syringe pump (SK-500 III, Shenzhen Shenke Medical, China) with a flow rate of 10 µL/min was dripped by a needle onto either top or back sides of the 45 ^{o} inclinedly laid fabrics.

Water flux test: A home-made device was set-up to measure the breakthrough pressure of the fabrics [38]. The device includes a water source from a syringe pump, a hollow syringe cylinder with the bottom end attached with the testing fabric and an underneath glass bottle collector. During the test, the fluid rate was set as 0.05, 0.09, 0.4 and 0.95 mL/min, respectively. The breakthrough pressure was recorded as the minimum pressure under which the water starts to pass through the fabric.

Water shower test: The water transport properties were further measured by a water shower test. A testing fabric was capped over on a 20 mL glass vessel loaded with ~ 1 g blue silica gel beads. The vessel was then showered by an eye shower for 10 s, and the color of inside silica gel beads was checked to find whether there was water transported through the fabric. Both top and back sides of the fabrics were tested to check the transport difference.

3.3 Results

3.3.1 Microstructure of the fabrics

We synthesized the predominantly superhydrophobic fabric with directional water transport property via TiO_2/PFOTES superhydrophobic finishing on a cotton fabric followed by selective plasma treatment (Figure 3.1c). We firstly checked the morphologies of the different fabrics. The pristine cotton fabric has a woven fibrous structure and smooth fiber surface (Figure 3.2a), and the TiO_2/PFOTES finished fabric showed a rougher fiber surface because of the TiO_2 nanoparticles (Figure 3.2b). The morphologies of both exposed top and unexposed back spot areas of the fabrics after selective plasma treatment differed from plasma treatment time (Figure 3.2c). The fabrics treated for 1 to 3 min still kept woven structure, while those treated for 5 or 10 min generated fuzzy surfaces, especially the one after 10 min has almost non-woven structure on both top and back spot areas, though the unexposed back spot was less severe. Higher magnifications reveal all the fiber surfaces were still rough, but the fibers became broken and discontinuous by the 5 and 10 mins' treatment (Figure S3.1). All the non-spot areas on both top and back surfaces did not change morphologies (Figure S3.2) compared with untreated fabric (Figure 3.2b). These indicates plasma, besides the surface treatment on the top spot areas, can penetrate through the thickness via spot channels and damage the fibers in different extents, especially after longer treatment (Apparently, 10 min was too long); however, it does not affect the completely covered non-spot areas on either top or back sides of the fabrics.

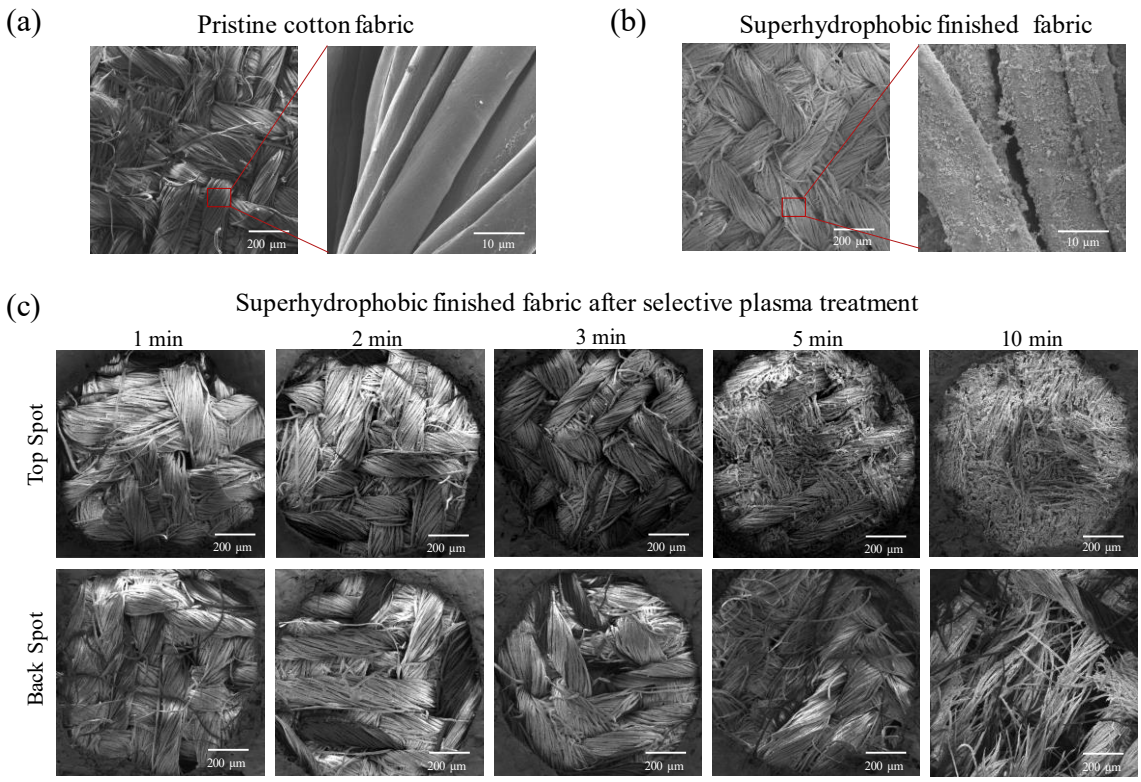

Figure 3.2 SEM morphologies of the cotton fabrics under different treatment conditions. (a) Pristine cotton fabric, (b) superhydrophobic finished fabric, and (c) exposed top spot areas and unexposed back spot areas of the superhydrophobic finished fabric after selective plasma treatment (300 W) for 1 to 10 min, respectively.

3.3.2 Wettability of the fabrics

Contact angle measurement was then used to investigate the wetting behavior of the fabrics before and after superhydrophobic finishing and successive selective plasma treatment. The superhydrophobic finished fabric showed a contact angle of 152 ^{o} (Figure 3.3a and Figure S3.3) while that of the pristine cotton fabric is 0 ^{o} (superhydrophilic, Figure S3.3). The increased hydrophobicity was caused by the surface nanostructures of the perfluorosilane-coated titanium dioxide nanoparticles [48]. When the fabric was treated by the plasma etcher, the contact angles have a significant difference between exposed spot areas and unexposed non-spot areas . The CAs of the non-spot areas on both top and back

sides of the fabrics only decreased slightly and still stayed at high values (e.g. ~141 ^{o} and ~140 ^{o} on the non-spots of both top and back sides after 5 mins' treatment, respectively). This is due to a complete coverage of the tape mask which prevents the O_2 plasma going inside the fabrics and therefore less chance to endow hydrophilicity [49]. On the contrary, the CAs of the exposed spot areas on both top and back sides of the fabrics decreased dramatically with the increase of plasma treatment time. For instance, 1 min's treatment brought the CA of the spot areas on the top side of the fabric down to 135 ^{o}, which further decreased to 114 ^{o} after 2 min, 97 ^{o} after 3 min, and 44 ^{o} after 5 min, respectively. The CA change of the spot areas on the back side of the fabrics was more interesting, which dropped down to 141 ^{o} after 1 min, but was no longer measurable (N/A, noted as 0 ^{o}) after 2 min or longer time. This is because the water droplets were found to quickly transport from the back spot areas to the top spot areas (Figure 3.3a, inset images, and Figure S3.3), therefore a zero CA values were recorded. The water transport time from the back spots to the top spots was also recorded with the treatment of plasma, as shown in Figure 3.3b. For the fabric selectively treated with plasma for 2 min, it took ~ 5 s for the water droplet to transport through the thickness; while the time for transport was about and below ~ 1 s for the fabrics after plasma treatment of 3 and 5 min, respectively.

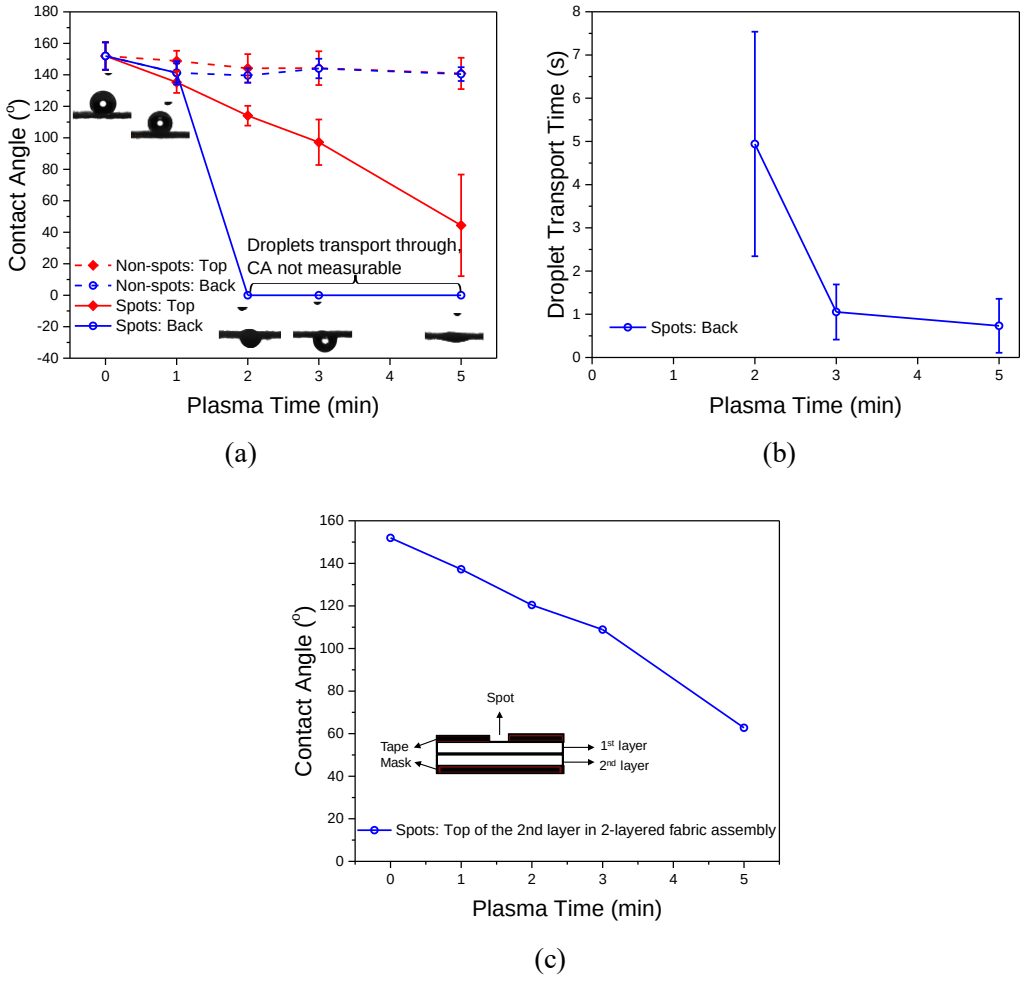

Figure 3.3 Wetting behavior of the superhydrophobic finished fabric after selective plasma treatment. (a) Contact angles of the spot and non-spot areas of both top and back sides of the superhydrophobic finished fabric after plasma treatment for 0 to 5 min; insets are droplet images when dripped onto the back spot areas. (b) Water transport time from the back spot area to the top spot area. (c) Contact angle of a two-layer fabric assembly to prove the wettability gradient.

An initial guess for the reason of the water transport was that either differentiated wettability or wettability gradient along the vertical direction of the spot areas occurred through the fabric thickness. To verify the cause, the “real” CAs of the spot areas on the back side of the fabrics need to be “measured”. To do this, we assembled two layers of the superhydrobic fabrics, then covered the top and back sides of the assembly with the

patterned tape mask (Figure 3.3c, inset image), and treated it again with plasma. We then measured the CAs of the spot area on the top side of the second layer and used it as the "real" CAs of the spot area on the back side of the first layer, with the assumption that they should be similar as the two layers are closely contacted [23, 50]. Figure 3.3c shows that CAs decreases gradually along with the plasma prolongation, but they are far over "zero", e.g. 109 ^{o} for the sample after 3 min's plasma treatment. This means the plasma penetrates into the spot channels, and decreases the hydrophobicity to different degrees, therefore a wettability gradient should be formed through the fabric thickness. Notice, for the samples with less than 3 min's treatment, both top and back spots are still hydrophobic (CA over 90 ^{o}), while the sample with 5 min's treatment turns to be hydrophilic on both sides through the spot (also see Figure S3.3). This may explain the hanging round droplet appearances for the transported water droplets on the opposite (top) side for the 2 and 3 min's samples, while a spreading shape for the 5 min's sample (Figure 3.2a, inset images, and Figure S3.3). The contact angles and transport times of the plasma treated fabrics were also measured after 7 days' aging at room temperature (Figure S3.4a, b), and they showed the similar trends as those in Day 0 (Figure 3.3a, b), indicating the samples were stable. Overview images of multiple water droplets on either side of the treated fabric at Day 0 and Day 7 can be found in Figure S3.4c. Combining the SEM morphologies (Figure 3.2c) and water transport screening by the contact angle test (Figure 3.3), we chose the superhydrophobic fabric after selective plasma treatment under 300 W for 3 min for further studies.

3.3.3 Chemical analysis of the fabrics

XPS was used to investigate the chemical elements of the cotton fabrics before and after superhydrophobic finishing and plasma treatment (300W, 3 min). As shown in the Table 3.1, both the titanium (Ti) and fluorine (F) content increased after the TiO_2/PFOTES superhydrophobic finishing on the cotton fabric. After selective plasma treatment, the Ti content kept stable on both top and back spots, which coincides with the TGA data (Figure S3.5) and identical rough morphology on the corresponding areas (Figure 3.2b, c). However, there was a significant difference in F content, which decreased from 34.53% to 0.91% and 15.36% on the exposed top and unexposed back spot areas, respectively. This indicates the fluorine-based hydrophobic silane chains on the exposed top spot areas might be severely etched away by the plasma [51], and those underneath the spots were also damaged by the penetration of the plasma through the thickness via spot channels, but in a less severe extent. Similar observation was also reported by Wang et al. [50, 52]. The indication of plasma penetration coincides with the SEM morphology (Figure 3.2c), contact angle trend either for the one layer (Figure 3.3a) or two-layer structures (Figure 3.3c) , and should be the reason for the gradient wettability across the fabric thickness.

Table 3.1 Atomic contents of C, O, Ti, Si and F on different fabric surfaces from XPS results

Sample	C (%)	O (%)	Ti (%)	Si (%)	F (%)
Pristine cotton fabric	62.89	35.17	0.16	1.11	0.67
Superhydrophobic finished fabric	28.18	28.42	7.88	0.99	34.53
Superhydrophobic finished fabric after plasma 3 min (Top Spot)	42.77	47.51	7.37	1.43	0.91
Superhydrophobic finished fabric after plasma 3 min (Back Spot)	40.39	35.89	6.41	1.95	15.36

3.3.4 Water transport properties of the fabrics

The directional water transport ability was first found when the fabrics were measured for the surface wettability via CA test (Figure 3.3a). Figure 3.4 shows a series of typical images taken from CA Movie when 10 µL water droplet was placed on top and back spot areas of the plasma (300 W, 3 min) treated superhydrophobic finished fabric, respectively. When water was dripped onto the plasma-exposed top spot area, the droplet stayed on the surface steadily for 3 s and longer time (not shown) (Figure 3.4a), with an average CA of 97 º (Figure S3.3). However, when it was dropped onto the reverse side (unexposed back spot area), the droplet quickly transported through to the other side (top side) of the fabric (Figure 3.4b). This difference indicates the directional water transport ability of the plasma selectively treated fabric through the spot channels from back to top side. A dynamic process of directional water transport can also be viewed through Movie S3.1a, b, where a 20 µL water was manually dropped from the pipette onto top and back spot areas of the fabric, respectively.

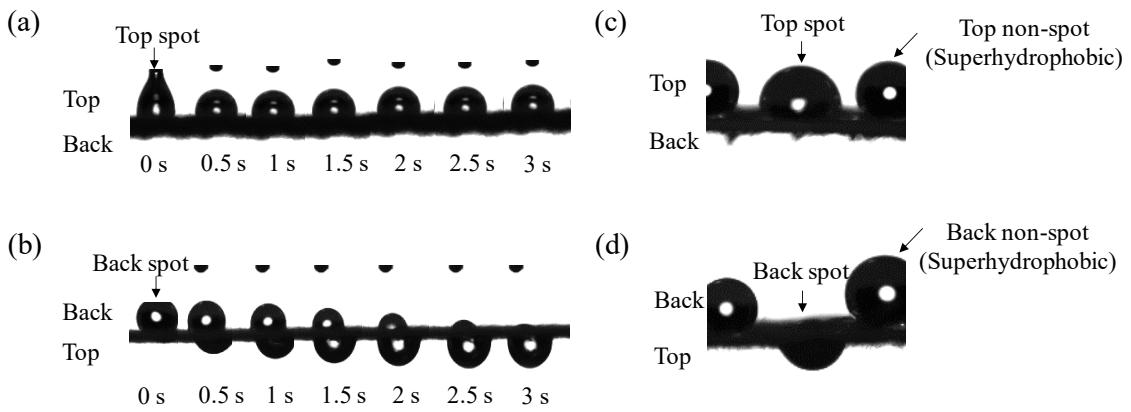

Figure 3.4 Directional water transport property of the superhydrophobic finished fabric after selective plasma treatment (300 W, 3 min). (a, b) Typical water droplet motion on (a) exposed top spot and (b) unexposed back spot areas of the fabric for 3 s on a horizontally laid fabric during the contact angle test, respectively. (c, d) Typical droplet images on both spot and non-spot areas of (c) top side and (d) back side of the fabric, respectively.

In order to confirm the dual directional flow property and water repellency, the fabrics were placed inclinedly with an angle of 45 ^{o}, and water was dripped from either top or back spot areas of the fabric by a needle connecting with a continuous water source at a flow rate of 10 µL/min. Figure 3.5 shows a series of photos captured during these experiments (Movie S3.2a, b). When water was dripped from top side of the fabric, it firstly adhered to the spot area, e.g. first droplet at 5.0 s; during the continuous supply with water, the droplet grew and after the last droplet at 280.8 s, it was big enough (~46 µL) to roll off from the fabric; through the entire process, no water transport was observed (Figure 3.5a). On the reserve direction, when the first droplet contacted the back spot area, it spontaneously transported from the pin of the needle to the other side after 10.0 s;and after accumulating to a similar volume at 248.5 s, the large droplets roll off again from the top surface (Figure 3.5b). While the directional water transport property was further proved in this test, the detachment of water droplets indicates the water repellency of the fabric, which is clearly due to the superhydrophobicity of the predominant non-spot areas of the both surfaces

surrounding the gradient wettability spot areas. From this test, we can estimate the maximum flow rate of each channel to be 46/248.5=0.185 μL/s. In one of our test specimens, the spatial distance of the channels is 1 cm, so the maximum water transport rate is 0.185 × 0.001 g × 3600 /0.0001 m^2/ h =6660 g/m^2/h, which far exceeds the maximum sweating rate of an average person under strenuous activity and is about 15 times greater than that of the best commercial Gore-Tex fabric [3].

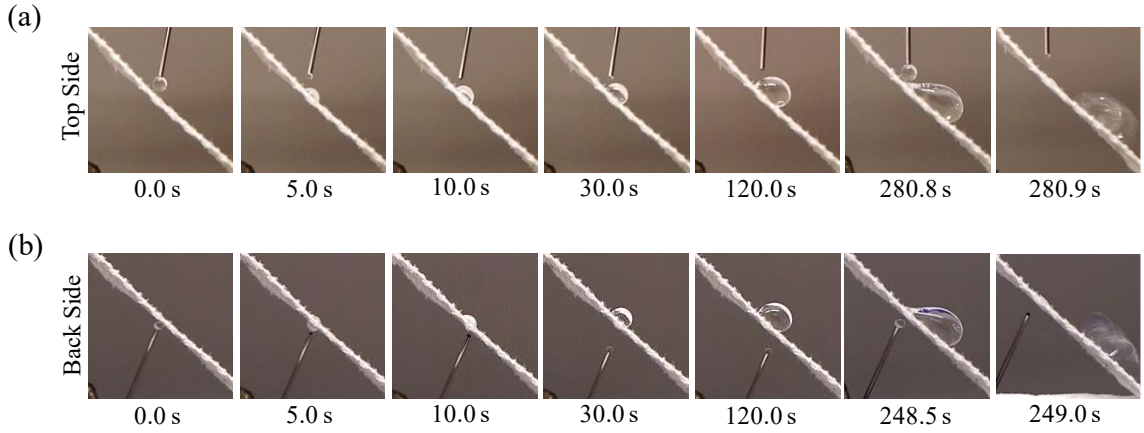

Figure 3.5 Directional water transport property and water repellency of the superhydrophobic finished fabric after selective plasma treatment (300 W, 3 min). Still frames taken from videos when water was dripped onto an inclinedly laid (45 °) plasma selectively treated superhydrophobic finished fabric on (a) exposed top spot and (b) unexposed back spot, at a flow rate of 10 μL/min, respectively.

The breakthrough pressures of the top and back sides of the designed fabric having one spot were also experimentally examined via a water flux test by placing a plastic hollow cylinder on the either side to hold water (Figure S3.6a) [38]. To avoid leaking, the edge of the fabric was sealed together with the bottom edge of the plastic cylinder using a silicone adhesive. Water droplets were pumped into the cylinder by a needle at different flow rates. We firstly examined the fabrics with different spot sizes at a flow rate of 0.4 mL/min, as shown in Figure 3.6a. Apparently, there're significant difference of the breakthrough

pressures for the top and back sides of the fabric. For the top sides, the pressures were higher and decreased with the increase of the spot sizes, i.e. the smallest spot size (diameter) of 0.5 mm generated a 4.7 cm H_2O pressure, the medium size of 1 mm reduced the pressure to 3.76 cm H_2O (also see Movie S3.3a), and the biggest size of 3 mm further reduced to 1.8 cm H_2O. This is reasonable, as a bigger plasma-exposed area would enlarge the channels for the water to pass through, thereby lower breakthrough pressure. When the fabrics were placed inversely (back sides), the supplied water droplets can quickly transport through, resulting a very low breakthrough pressure, ~0.2 cm H_2O (see Movie S3.3b for the sample of spot size 1 mm). This discrepancy was accordant with the horizontal and inclined water transport results in Figure 3.4 and 3.5 (also see Movie S3.1 and S3.2), and triply-confirmed the directional water transport properties of the designed fabric. Besides, we tested the fabric with a spot size of 1 mm at different flow rates, and found the pressure increased with the increase of the water flow rates (Figure 3.6b), which should be caused by the delay of liquid penetration considering the predominantly flow resistance of the fabrics [38]. In addition, we also recorded the droplet sizes of the water transported through the spots and found they increased with the spot enlargement (Figure S3.6b).

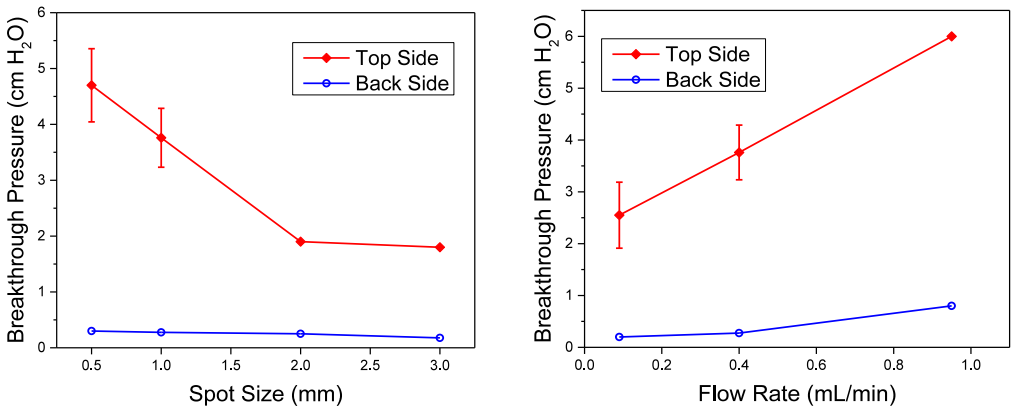

(a) (b)

Figure 3.6 Breakthrough pressures of both top and back sides of the superhydrophobic finished fabric after selective plasma treatment (300 W, 3 min). (a) At different sizes (diameters) of spot areas under a flow rate of 0.4 mL/min, and (b) at different flow rates through a spot diameter of 1 mm, respectively.

The directional water transport ability was further proved via another test by showering either top or back side of the fabric capping over a glass vessel loaded with blue silica gel beads (Figure S3.7a). After the vessel being showered under an eye wash shower for 10 s, the color of the inside beads did not change when top side of the fabric was capped upside (Figure S3.7b), while it partially turned to pink when back side was capped upside, indicating a water transport through the fabric (Figure S3.7c).

3.4 Mechanism Understanding and Discussion

Theoretical analysis has been conducted to explain why the directional water transport occurs consistently, and quantify the dependence of the flow directionality and the breakthrough pressure on the microstructure and wettability of the fibrous systems. The release of water drops from the fabric face has also been clarified. The previous studies have summarized the possible reasons for the flow directionality, such as water

evaporation[6], hydrostatic pressure [27], and combined effect of hydrophobic, hydrophilic and gravitational forces [13]. However, the significant affecting factors including the dynamic flow process between fibers or yarns, the impact of geometrical microstructures (e.g. elliptical cross-sectional shape of the yarns), and the detachment behavior of the water drops from the fibrous materials have been less investigated, which are critical to reveal the underlying mechanism of the directional water transport. Beyond directional water movement inside fibrous channels, it is of importance that the water drops can be effectively released rather than being absorbed and held in the hydrophilic region or simply escaping in form of evaporation. Water transport by liquid drops is much faster than that by evaporative diffusion of vapors, as one water drops contains millions of vapor molecules.

The underlying mechanism of the fluid directionality in the porous spot with gradient wettability is illustrated in Figure 3.7a. Here, the Gibbs pinning criterion, which has been successfully correlated to the flow directionanlity in the fibrous fluid diodes with varied geometry [38], is extended to describe the directional water transport inside the hollow channels between yarns with both gradient wettability and varied microstructure. Since the channel between the yarns varies in size along the flow direction, an expansion/contraction angle (α) is used to characterize the degree of the expansion or contraction of flow path (Figure 3.7b). When the channel is uniform in size, α becomes zero. And α approaches 90 ^{o} or -90 ^{o}, respectively, at the bottom and the top of the fibrous material in the flow direction. More specifically, the contact line gets pinned with the breakthrough angle $\alpha + \theta$ beyond 90 ^{o} based on the Gibbs pinning condition [38]. On the contrary, the advancement of the liquid continues when the air-liquid interface is concave and the dragging force exists towards the flow direction. As such, continuous advancement of the liquid water can be

satisfied, when the direction angle β as a function of contact angle θ and the expansion/contraction angle α is satisfied as follows,

$$\beta = \alpha + \theta - \frac{\pi}{2} < 0, \tag{3.1}$$

It can also been seen from Figure 3.7b that the water will flow inversely if $\beta > 0$, as the driving force on the basis of surface tension becomes opposite to the intended flow direction. Assume the yarns are elliptical, their surface can be described as the locus of all points that satisfy the equations, viz., $x = a\cos\omega$, and $y = b\sin\omega$, where x and y are the coordinates of any point on the ellipse, a and b are the semi-axes in the $\mathrm{x}-$ and $\mathrm{y}-$ directions, respectively, ω is the angle of eccentric anomaly, which ranges from $\pi/2$ to $-\pi/2$ radians in Figure 3.7b. The value of α can be determined by the slope of the tangent line at ($a\cos\omega$, $b\sin\omega$) to the ellipse, viz., $\alpha = \arctan\left(\frac{1}{k}\right)$, where $k = -\frac{b}{a}\frac{\cos\omega}{\sin\omega}$.

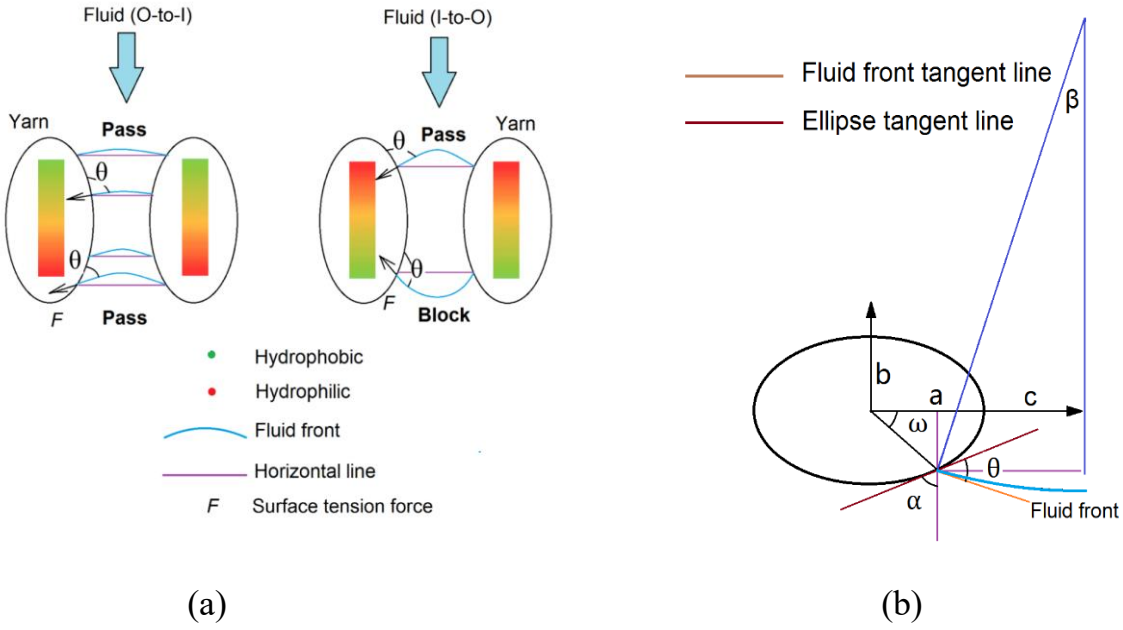

(a) (b)

Figure 3.7 Mechanism of directional water transport. Schematic illustration of (a) directional water transport through the spot channel between elliptical yarns with gradient wettability, and (b) an axisymmetric water fluid front between elliptical yarns, where, a and b are the semi-principal axes in x- and y-directions, respectively, c is the half distance between yarns, θ is the contact angle, ω is the eccentric anomaly, α is the expansion/contraction angle, and β is the direction angle, respectively.

It has been shown in Figure 3.3c that the bottom surface (back side) of the porous spot becomes less hydrophobic with increasing time of plasma treatment. Here, a linear gradient of wettability is assumed from the hydrophilic (simplified as 'I') top spot surface with contact angle at 0° when $\omega = \pi/2$ to the hydrophobic (simplified as 'O') bottom surface with contact angle at θ_0 when $\omega = -\pi/2$, with $\theta = \theta_{IO} = -\frac{\theta_0}{2}\sin\omega + \frac{\theta_0}{2}$. In the opposite flow direction, the contact angles will be $\theta_{OI} = \frac{\theta_0}{2}\sin\omega + \frac{\theta_0}{2}$ with contact angle at 0° when $\omega = -\pi/2$ to the bottom surface with contact angle at θ_0 when $\omega = \pi/2$. The maximum value of the contact angle on the face away from plasma exposure has found to be $\theta_0 = 109^o$ for the sample with 3 min's treatment (Figure 3.3c). The dependence of the diode effect (pass or block) on ω that indicates the water advancement is illustrated in Figure

3.7a, where the sign "block" indicates the flow ceases or retreats at the local area while the sign "pass" means that the flow can continue moving. It is found that the values of a and b in Eq. (3.1) are approximated as $80\ \mu m$ and $50\ \mu m$, and the half distance between yarns, c, is approximately 50 μm, respectively (Figure S3.8). Note the surface tension force is always along the flow direction at $\beta < 0$, when the water flows from the hydrophobic side to the hydrophilic side as seen in Figure 3.8a. It can be readily understood that the effect of dramatic contraction leading to high α (negative) overcomes that of the fair hydrophobicity with $\theta_{OI} > 90^{o}$ at the beginning stage and in the rest of flow process, the condition of $\beta < 0$ is always satisfied with reduction of θ_{OI}. In the opposite flow direction, the condition of $\beta < 0$ is also secured at the beginning with $\alpha < 0$ and $\theta_{IO} \sim 0$. However, β eventually becomes positive and the surface tension force is opposite to the main flow direction, with continuously increasing α (positive) and θ_{IO} during the progress of water movement. As such, the asymmetric flow behaviors from different flow directions result from the changes of geometrical structures and gradient wettability of the fibrous systems, based on the theoretical model of Eq. (3.1) and experimental findings in Figure 3.4-3.6. The dependence of direction angle on eccentric anomaly of the elliptical yarns in different flow directions has been further studied in Figure S3.9, when the semi-major axis and semi-minor axis vary at different values of the maximum contact angles of one surface of the porous spot (i.e., $\theta_0 = 109^{o}$ and $\theta_0 = 170^{o}$). It is interesting to note that both flows can be hindered from two different directions for $\theta_0 = 170^{o}$ when $b = 80$ μm and $a = 50$ μm, because the contact angle is always high in a wide range, where the expansion/contraction angles keep close to zero.

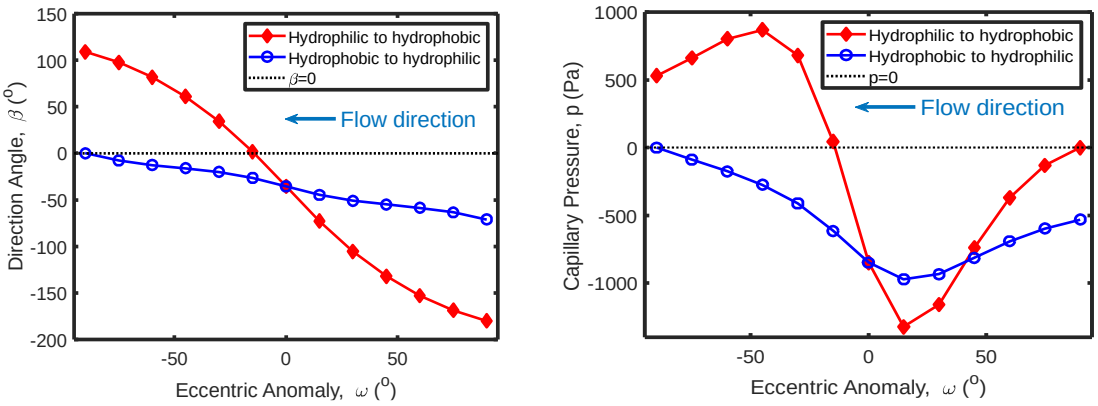

(a) (b)

Figure 3.8 Dependence of (a) direction angle and (b) capillary pressure on the eccentric anomaly of the elliptical yarns in different flow directions, respectively.

The detachment of water drops is essential to the continuous directional water transport process. In this work, patterned hydrophilic porous spots are distributed on the predominantly superhydrophobic surface for easy water removal. The size and wettability of the spots are related to the breakthrough pressure and detachment of water drops. It is noted that the capillary pressure varies at different positions of fluid fronts, and the maximum value of capillary pressure that blocks the water transport will be equal to the breakthrough pressure when the gravitation force is negligible. Here, the capillary pressure within the channel between yarns is determined by the Young–Laplace equation,

$$p = \frac{\gamma \sin(\alpha+\theta-\frac{\pi}{2})}{L} \tag{3.2}$$

where, $L = a + c - a\cos\omega$ is the half distance of the width of the fluid front and c is the half distance between yarns. It is clear that the capillary pressure is all negative in the OL flow direction in Figure 3.8b (and Figure S3.10a), so the breakthrough pressure will be equal to zero consistently with the advance of the liquid water. From the opposite flow

direction, a positive capillary pressure is found, with the maximum value of 800 Pa (8.16 cm water head), which is higher than 3.76 cm water head as found in Figure 3.6, possibly because some porous spots contain larger channels with greater c (see red arrow in Figure S3.8b), leading to the reduction in capillary pressure. With increasing a while keeping b and c as constants, Figure S3.10b reveals that a flatter shape of elliptical yarn results in a lower breakthrough pressure. Besides, more hydrophobic porous spots with higher θ_0 leads to increase in breakthrough pressures, as seen in Figure S3.10c.

With increasing water supply, the volume of water drop enhances until falling off from the porous spot when the gravitational force overcomes the surface tension force. The contacting circle line between the water drop and the fabric cannot enlarge due to the repellence of the surrounding hydrophobic area (Figure 3.9a). Thus the corresponding surface tension force is equal to $F_a = 2\pi r\sigma \sin\theta$, where r is the radius of the hydrophilic porous spot and $\theta < 90^o$. Then the contact angle will be enhanced by balance with the gravitational force of the growing water drop, which has a weight as $G = \rho g(4\pi R^3/3)$. Thus we have the scaling law accounting for the relationship between r and R, viz.,

$$r \sim R^3 \tag{3.3}$$

which holds until the detachment of water drops. Eq. (3.3) has been well verified by the experimental results of detachment of water drops at different sizes of porous spots (Figure 3.9b, also see Figure S3.6b).

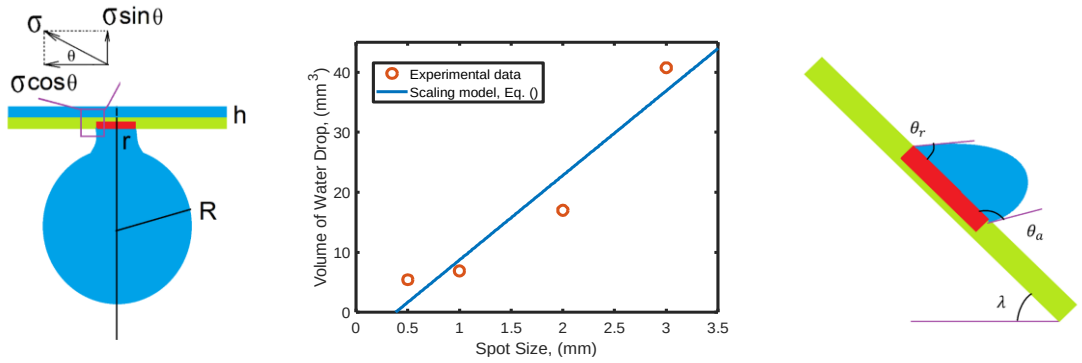

(a) (b) (c)

Figure 3.9 Mechanism of water droplet detachment. (a) Mechanical analysis of the water drop hung under the porous spot of the horizontally placed fibrous layer with increasing water supply. (b) Relationship between the size of the porous spot and the volume of the dripped water drop. (c) Mechanical analysis of the water drop attached on the porous spot of the inclined fibrous layer at an incline angle of λ.

When the fibrous layer is placed at an incline angle at $\lambda = 45\ ^{o}$, the surface tension force becomes the combined forces caused by the hydrophilic and hydrophobic areas together, $F_a = \pi\gamma R_f(\cos\theta_r - \cos\theta_a)$, where θ_a and θ_r are the advancing and receding contact angle, respectively (Figure 3.9c). The hydrophilic force in the upper area of the porous spot holds the water drop and the hydrophobic force in the lower region repels and impedes the water drop from rolling off. The gravitation force of the water drop is close to $mg\sin\lambda$, which will be equal to the capillary forces at the detachment condition, viz.,

$$mg\sin\lambda \sim \pi\gamma R_f(\cos\theta_r - \cos\theta_a) \tag{3.4}$$

where the mass of water drop scales with the cubic drop radius R_f, viz., $m \sim R_f^3$. Analogous to the phenomenon described in Eq. (3.3), the increase in m is much faster than that of R_f in Eq. (3.4), which explains the detachment of growing water eventually drops. The directional water transport will stop if the Laplace pressure of the supplied water drop is

equal to the hydrostatic pressure of the water column or water drop generated in the other side of the fabric [53]. However, this condition cannot be met in reality as the water drop will fall off when growing slightly big.

3.5 Conclusion

In summary, we have developed a novel "skin-like" fibrous materials with both directional water transport and water repellent properties. We created distributed porous spot channels with gradient wettability across the thickness of hydrophobic fabrics via a combination of superhydrophobic finishing and selective plasma treatment. While these channels serve for directional liquid transport, the predominantly untreated surface area remained superhydrophobic, therefore repels external liquid contaminants. The mechanism of directional flow is explained by the Gibbs pinning criterion. The technology might be applicable for all kinds of fabrics. Either the hydrophobic pre-finishing or selective plasma treatment is simple and efficient, therefore will be very feasible for the commercial applications. The proposed fibrous materials can have a direct application in developing smart and high performance clothing, especially for sportswear. It has a high significance to the apparel industry, for bringing both directional water transport property and water repellency, therefore would bring a huge value for the industry players and market end-users. The technology can also be leveraged into other fabric or membrane applications, such as liquid separation and purification, fuel cells, wound dressing, and flexible microfluidic devices.

3.6 Supporting Information

Microstructure of superhydrophobic finished fabric after selective plasma treatment

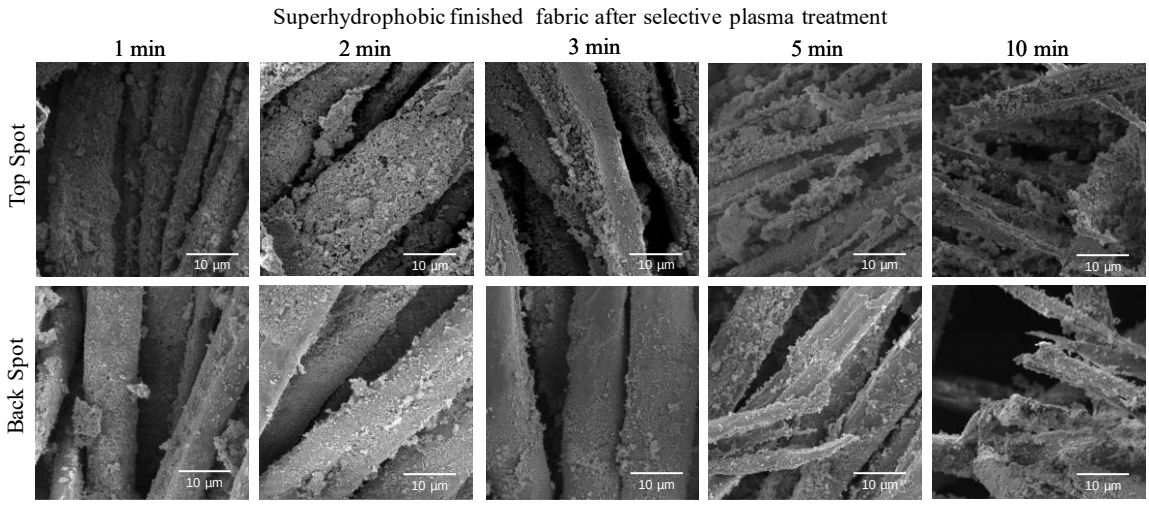

Figure S3.1 High magnifications of SEM images of the exposed top spot areas and unexposed back spot areas of the superhydrophobic finished fabric after selective plasma treatment for 1 to 10 min.

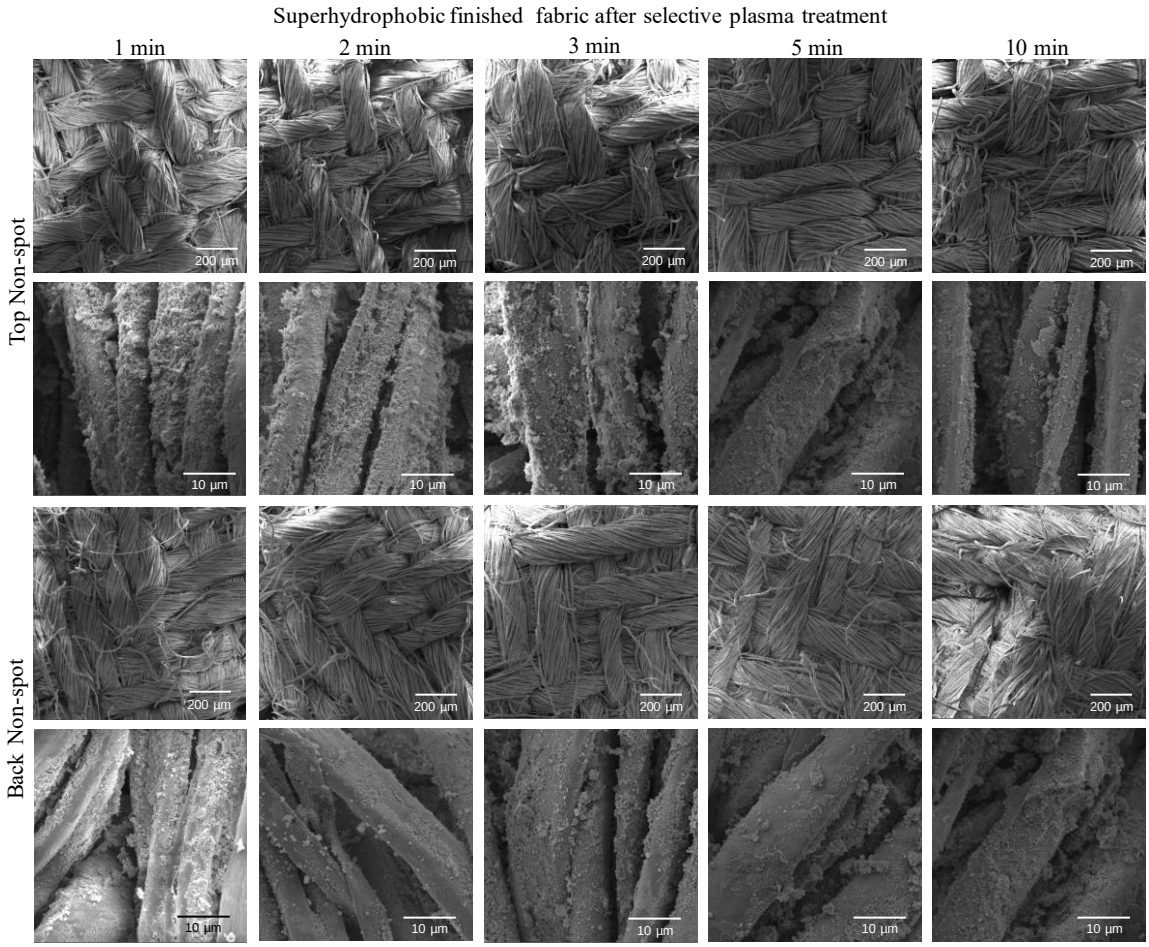

Figure S3.2 SEM morphologies of unexposed top non-spot areas and unexposed back non-spot areas of the superhydrophobic finished fabric after selective plasma treatment for 1 to 10 min. Images in Line 2 and 4 are high magnifications of Line 1 and 3, respectively.

Wetting behavior of the fabrics under different treatment conditions

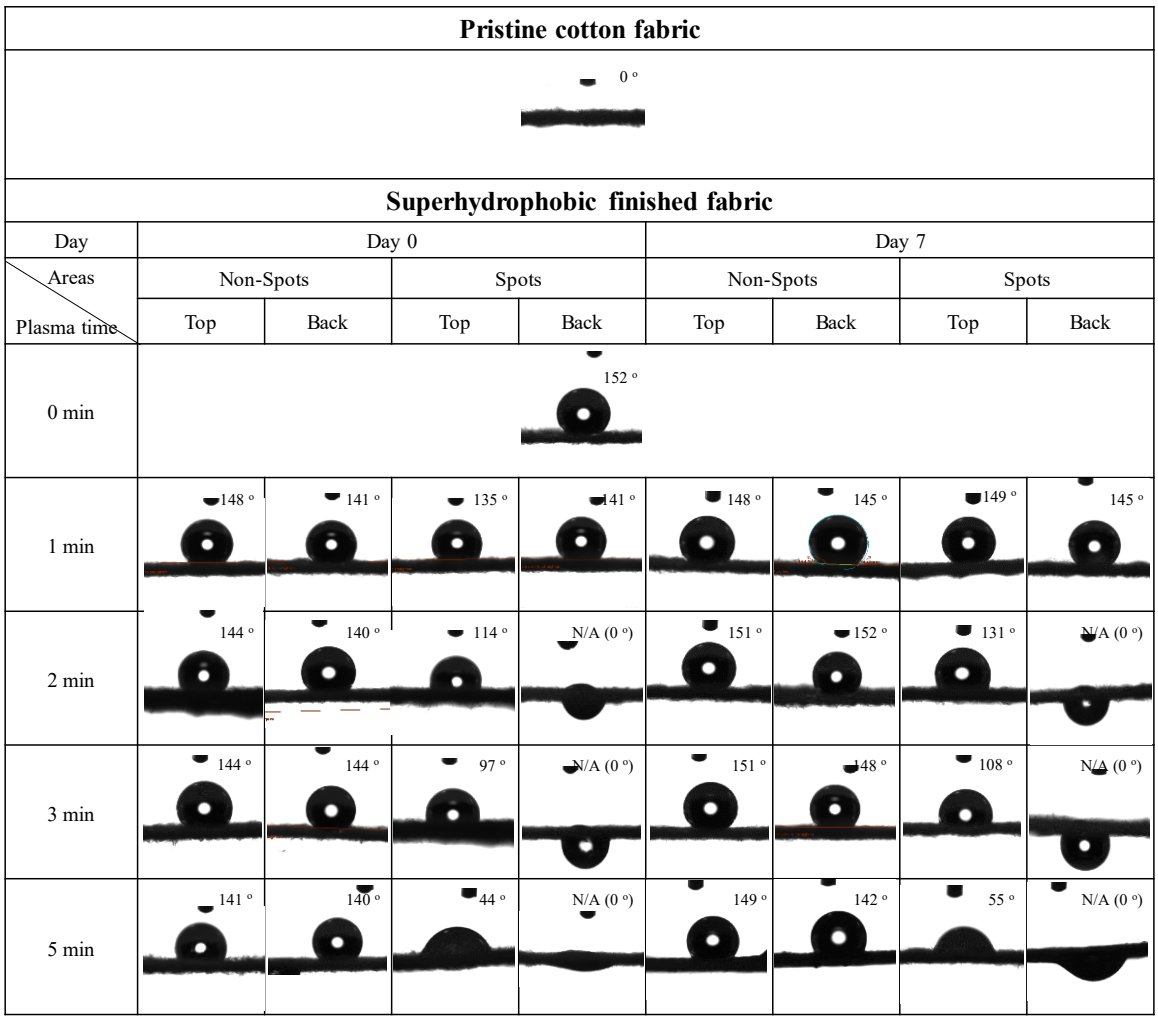

Figure S3.3 Water droplet images (from contact angle test) on pristine cotton fabric, and both spot areas and non-spot areas from both top and back sides of the superhydrophobic finished fabric before and after selective plasma treatment for 1 to 5 min.

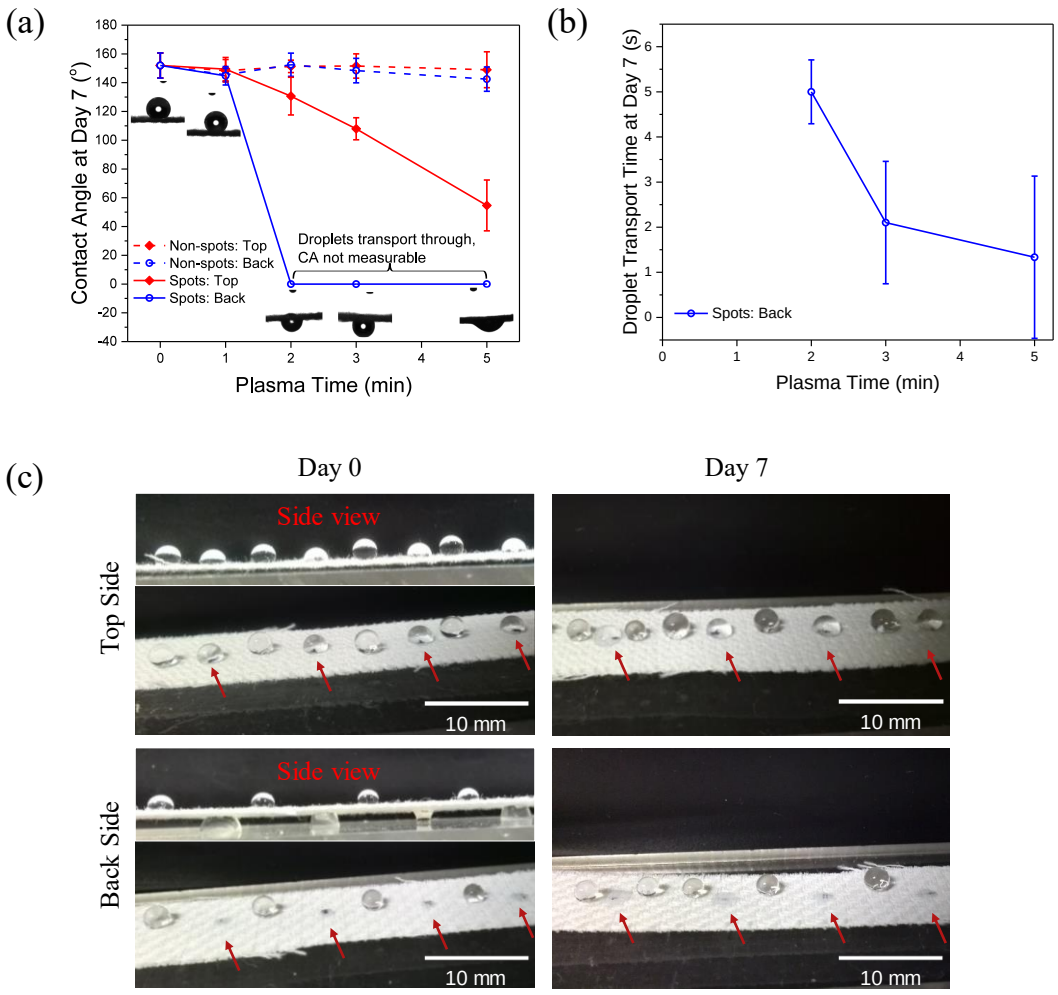

Figure S3.4 Wetting durability of the superhydrophobic finished fabric after selective plasma treatment. (A) Contact angles of the spot and non-spot areas of both top and back sides of the superhydrophobic finished fabric after plasma treatment for 0 to 5 min at Day 7; insets are droplet images when dripped onto the back spot areas. (B) Water transport time from the back spot area to the top spot area at Day 7. (C) Overview images of multiple water droplets on either side of the superhydrophobic finished fabric after selective plasma treatment (300 W, 3min), at Day 0 and Day 7. Red arrows indicate the spot channels marked in black dots on the fabrics. Insets in as-prepared samples are side views of the fabrics and droplets.

Thermal analysis of the fabrics under different treatment conditions

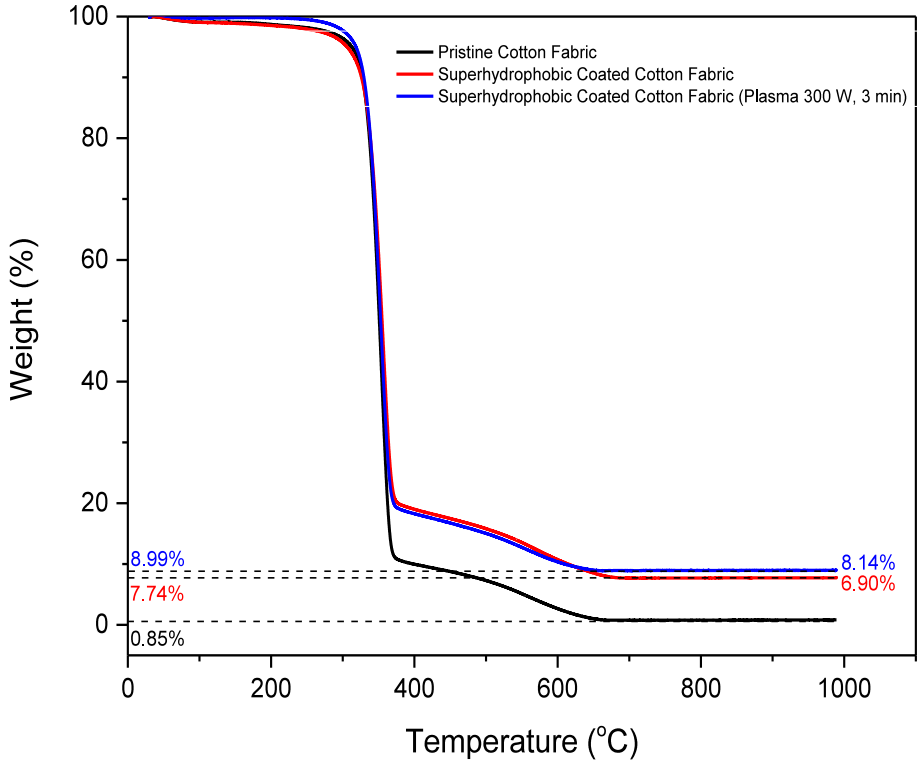

Figure S3.5 Thermogravimetric analysis (TGA) spectra of pristine cotton fabric, superhydrophobic finished fabric before and after plasma treatment (300 W, 3 min).

Breakthrough pressure test

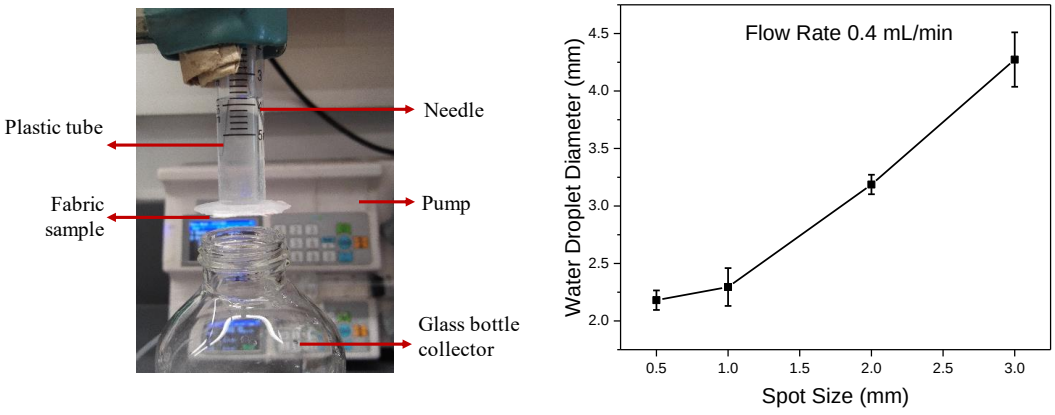

(a) (b)

Figure S3.6 Breakthrough pressure test. (a) Experimental set-up for measuring breakthrough pressure of the fabrics. (b) Water droplet diameters transported through different sizes (diameters) of spot areas under a flow rate of 0.4 mL/min.

Water shower test

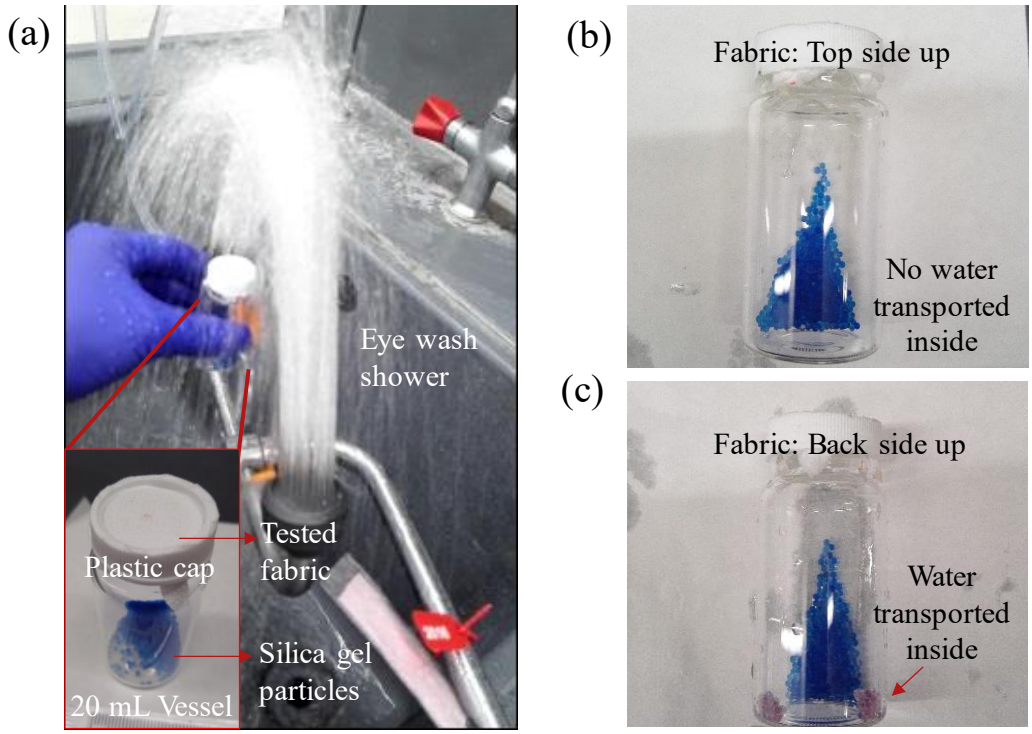

Figure S3.7 Water shower test. (a) A water shower test to measure the water transport through the different sides of the plasma selectively treated (300 W, 3 min) superhydrophobic finished fabric. Water (b) did not and (c) did transport (red arrow) through the fabric after 10 s when (b) the top side and (c) back side of the fabric were up contacting the shower, respectively.

Additional microstructure of superhydrophobic finished fabric for mechanism understanding

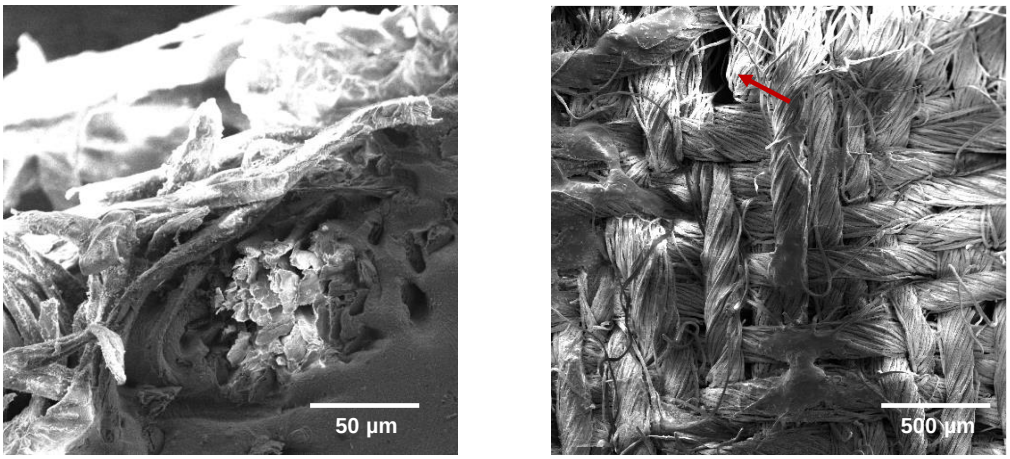

(a) (b)

Figure S3.8 SEM morphologies to measure the semi-axes *a*, *b* and *c* of the superhydrophobic finished fabric. (a) Cross-section showing the semi-axes *a* and *b* of the yarn are approximately 80 µm and 50 µm, respectively. (b) Low magnification of a fabric image in Figure 3.2b, showing a half distance *c* is approximately 50 µm and a big pore with greater *c* (red arrow) exists between yarns of the superhydrophobic finished fabric.

Mechnism understanding: Relationship of direction angle and capillary pressure with eccentric anomaly of the elliptical yarns

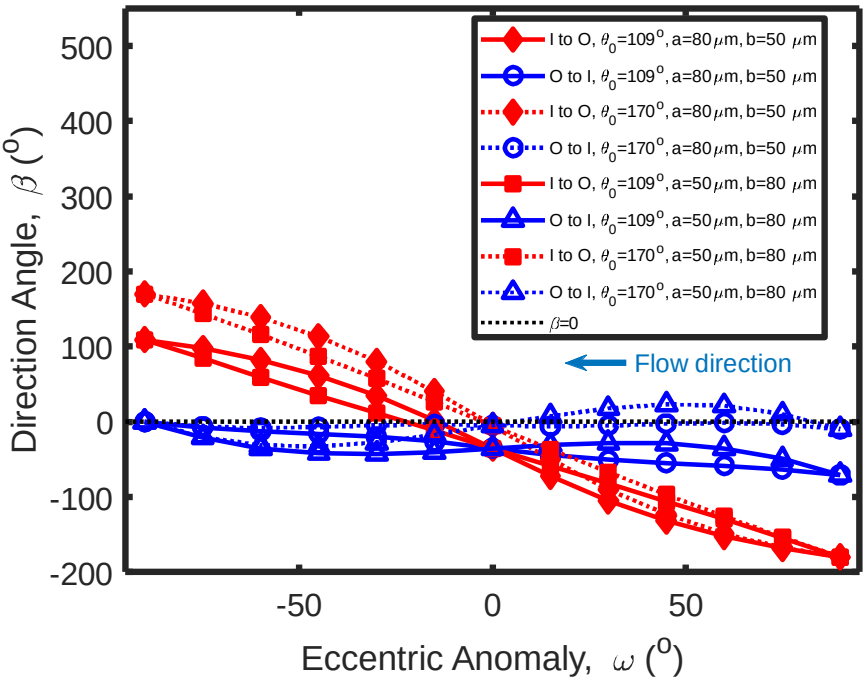

Figure S3.9 Dependence of direction angle on eccentric anomaly of the elliptical yarns in different flow directions. The semi-major axis and semi-minor axis vary at different values of the maximum contact angles on one side of the porous spot.

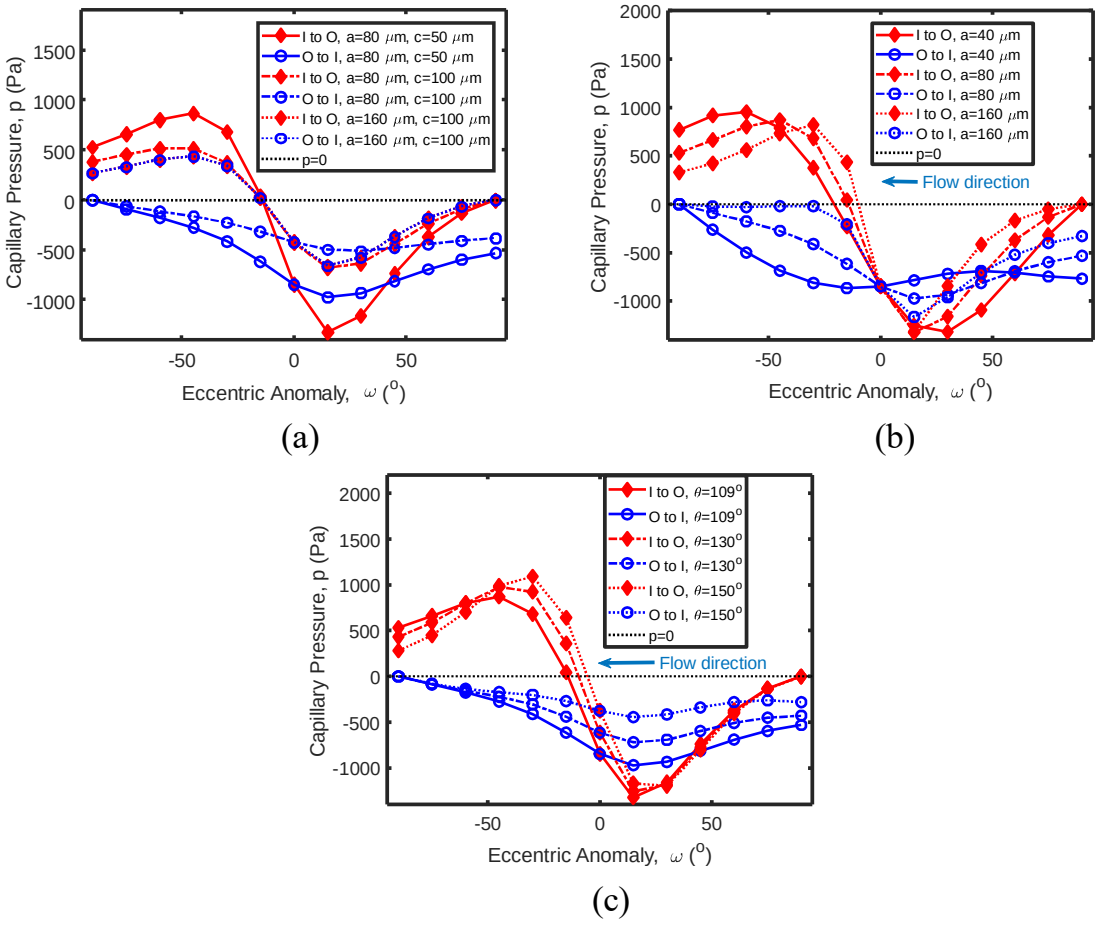

Figure S3.10 Dependence of capillary pressure on eccentric anomaly of the elliptical yarns. (a) At different semi-principal axes in different flow directions. The semi-principal axes and the half-distance between yarns vary in three groups as follows: $a = 80$ μm, $b = 50$ μm, $c = 50$ μm ; $a = 80$ μm , $b = 50$ μm, $c = 100$ μm ; and $a = 160$ μm , $b = 100$ μm, $c = 100$ μm. (b) At different shapes of elliptical yarns in different flow directions. The semi-principal axes and vary in three groups as follows: $a = 40$ μm, $b = 50$ μm; $a = 80$ μm, $b = 50$ μm; and $a = 160$ μm, $b = 50$ μm. (c) At different maximum contact angles in different flow directions. The contact angles vary in three groups as follows: $\theta_0 = 109^o$; $\theta_0 = 130^o$; and $\theta_0 = 150^o$.

Movie S3.1a: Water droplets (20 µL per droplet) on the **top** spot area of a horizontally laid superhydrophobic finished cotton fabric after selective plasma treatment (300 W, 3 min).

Movie S3.1b: Water droplets (20 µL per droplet) on the **back** spot area of a horizontally laid superhydrophobic finished fabric after selective plasma treatment (300 W, 3 min).

Movie S3.2a: Continuous water droplet supply (10 µL/min) by a needle on the **top** spot area of a 45 ^{o} inclinedly laid superhydrophobic finished fabric after selective plasma treatment (300 W, 3 min).

Movie S3.2b: Continuous water droplet supply (10 µL/min) by a needle on the **back** spot area of a 45 ^{o} inclinedly laid superhydrophobic finished fabric after selective plasma treatment (300 W, 3 min).

Movie S3.3a: Continuous water flux (0.4 mL/min) by a needle to test the breakthrough pressure on the **top** side of the superhydrophobic finished fabric after selective plasma treatment (300 W, 3 min) having one spot diameter of 1 mm by placing a plastic hollow cylinder on the fabric.

Movie S3.3b: Continuous water flux (0.4 mL/min) by a needle to test the breakthrough pressure on the **top** side of the superhydrophobic finished fabric after selective plasma treatment (300 W, 3 min) having one spot diameter of 1 mm by placing a plastic hollow cylinder on the fabric.

REFERENCES

[1] M. Manshahia, A. Das, High active sportswear - A critical review, *Indian J Fibre Text* **39**(4) (2014) 441-449.

[2] R. Paul, High performance technical textiles, First ed., *Wiley* 2019.

[3] D.J. Gohlke, J.C. Tanner, Gore-Tex® waterproof breathable laminates, *J Coated Fabrics* **6**(1) (1976) 28-38.

[4] A. Mukhopadhyay, V.K. Midha, A review on designing the waterproof breathable fabrics Part II: construction and suitability of breathable fabrics for different uses, *J Ind Text* **38**(1) (2008) 17-41.

[5] J.T. Fan, Y.S. Chen, Measurement of clothing thermal insulation and moisture vapour resistance using a novel perspiring fabric thermal manikin, *Meas Sci Technol* **13**(7) (2002) 1115-1123.

[6] Y. Zhao, H.X. Wang, H. Zhou, T. Lin, Directional fluid transport in thin porous materials and its functional applications, *Small* **13**(4) (2017).

[7] A.R. Parker, C.R. Lawrence, Water capture by a desert beetle, *Nature* **414**(6859) (2001) 33-34.

[8] L. Zhai, M.C. Berg, F.C. Cebeci, Y. Kim, J.M. Milwid, M.F. Rubner, R.E. Cohen, Patterned superhydrophobic surfaces: Toward a synthetic mimic of the Namib Desert beetle, *Nano Lett* **6**(6) (2006) 1213-1217.

[9] Y. Zheng, H. Bai, Z. Huang, X. Tian, F.-Q. Nie, Y. Zhao, J. Zhai, L. Jiang, Directional water collection on wetted spider silk, *Nature* **463**(7281) (2010) 640-643.

[10] J. Ju, H. Bai, Y. Zheng, T. Zhao, R. Fang, L. Jiang, A multi-structural and multi-functional integrated fog collection system in cactus, *Nat Commun* **3** (2012) 1247.

[11] D. Miao, Z. Huang, X. Wang, J. Yu, B. Ding, Continuous, spontaneous, and directional water transport in the trilayered fibrous membranes for functional moisture wicking textiles, *Small* **14**(32) (2018) e1801527.

[12] X. Wang, Z. Huang, D. Miao, J. Zhao, J. Yu, B. Ding, Biomimetic fibrous murray membranes with ultrafast water transport and evaporation for smart moisture-wicking fabrics, *ACS Nano* **13**(2) (2019) 1060-1070.

[13] H. Zhou, H.X. Wang, H.T. Niu, T. Lin, Superphobicity/philicity Janus fabrics with switchable, spontaneous, directional transport ability to water and oil fluids, *Sci Rep* **3** (2013) 2964.

[14] M.Z. Ge, C.Y. Cao, J.Y. Huang, X.N. Zhang, Y.X. Tang, X.R. Zhou, K.Q. Zhang, Z. Chen, Y.K. Lai, Rational design of materials interface at nanoscale towards intelligent oil-water separation, *Nanoscale Horiz* **3**(3) (2018) 235-260.

[15] D.H. Liang, Z. Lu, H. Yang, J.T. Gao, R. Chen, Novel asymmetric wettable agnps/chitosan wound dressing: in vitro and in vivo evaluation, *ACS Appl Mater Inter* **8**(6) (2016) 3958-3968.

[16] L. Shi, X. Liu, W. Wang, L. Jiang, S. Wang, A self-pumping dressing for draining excessive biofluid around wounds, *Adv Mater* **31**(5) (2019) e1804187.

[17] S.M. Montgomery, K.L. Adams, L. Rebenfeld, Directional inplane permeabilities of geotextiles, *Geotext Geomembranes* **7**(4) (1988) 275-292.

[18] A. Miszkowska, S. Lenart, E. Koda, Changes of permeability of nonwoven geotextiles due to clogging and cyclic water flow in laboratory conditions, *Water* **9**(9) (2017) 660.

[19] J.S. Feng, J.P. Rothstein, One-way wicking in open micro-channels controlled by channel topography, *J Colloid Interface Sci* **404** (2013) 169-178.

[20] E. Fu, S.A. Ramsey, P. Kauffman, B. Lutz, P. Yager, Transport in two-dimensional paper networks, *Microfluid Nanofluidics***10**(1) (2011) 29-35.

[21] B.Q. Xiao, J.T. Fan, F. Ding, A fractal analytical model for the permeabilities of fibrous gas diffusion layer in proton exchange membrane fuel cells, *Electrochim Acta* **134** (2014) 222-231.

[22] C. Zeng, H.X. Wang, H. Zhou, T. Lin, Directional water transport fabrics with durable ultra-high one-way transport capacity, *Adv Mater Interfaces* **3**(14) (2016).

[23] H.X. Wang, J. Ding, L.M. Dai, X.G. Wang, T. Lin, Directional water-transfer through fabrics induced by asymmetric wettability, *J Mater Chem* **20**(37) (2010) 7938-7940.

[24] Y.Y. Kong, Y.Y. Liu, J.H. Xin, Fabrics with self-adaptive wettability controlled by "light-and-dark", *J Mater Chem* **21**(44) (2011) 17978-17987.

[25] H. Zhou, H. Wang, H. Niu, T. Lin, Superphobicity/philicity Janus fabrics with switchable, spontaneous, directional transport ability to water and oil fluids, *Sci Rep* **3** (2013) 2964.

[26] Y. Zhang, M. Barboiu, Dynameric asymmetric membranes for directional water transport, *Chem Comm* **51**(88) (2015) 15925-15927.

[27] J. Wu, N. Wang, L. Wang, H. Dong, Y. Zhao, L. Jiang, Unidirectional water-penetration composite fibrous film via electrospinning, *Soft Matter* **8**(22) (2012) 5996-5999.

[28] H.X. Wang, H. Zhou, H.T. Niu, J. Zhang, Y. Du, T. Lin, Dual-layer superamphiphobic/superhydrophobic-oleophilic nanofibrous membranes with unidirectional oil-transport ability and strengthened oil-water separation performance, *Adv Mater Interfaces* **2**(4) (2015).

[29] X.L. Tian, H. Jin, J. Sainio, R.H.A. Ras, O. Ikkala, Droplet and fluid gating by biomimetic janus membranes, *Adv Funct Mater* **24**(38) (2014) 6023-6028.

[30] F.X. Sun, Z.Q. Chen, L.C. Zhu, Z.Q. Du, X.G. Wang, M. Naebe, Directional trans-planar and different in-plane water transfer properties of composite structured bifacial fabrics modified by a facile three-step plasma treatment, *Coatings* **7**(8) (2017).

[31] H. Liu, J.Y. Huang, F.Y. Li, Z. Chen, K.Q. Zhang, S.S. Al-Deyab, Y.K. Lai, Multifunctional superamphiphobic fabrics with asymmetric wettability for one-way fluid transport and templated patterning, *Cellulose* **24**(2) (2017) 1129-1141.

[32] H.J. Wang, W.Y. Wang, H. Wang, X. Jin, J.L. Li, Z.T. Zhu, One-way water transport fabrics with hydrophobic rough surface formed in one-step electrospray, *Mater Lett* **215** (2018) 110-113.

[33] Y.F. Si, L.W. Chen, F.C. Yang, F. Guo, Z.G. Guo, Stable Janus superhydrophilic/hydrophobic nickel foam for directional water transport, *J Colloid Interface Sci* **509** (2018) 346-352.

[34] L.L. Hou, N. Wang, X.K. Man, Z.M. Cui, J. Wu, J.C. Liu, S. Li, Y. Gao, D.M. Li, L. Jiang, Y. Zhao, Interpenetrating Janus membrane for high rectification ratio liquid unidirectional penetration, *ACS Nano* **13**(4) (2019) 4124-4132.

[35] J.T. Fan, M.K. Sarkar, Y.C. Szeto, X.M. Tao, Plant structured textile fabrics, *Mater Lett* **61**(2) (2007) 561-565.

[36] Q. Chen, J.T. Fan, M.K. Sarkar, Biomimetics of branching structure in warp knitted fabrics to improve water transport properties for comfort, *Text Res J* **82**(11) (2012) 1131-1142.

[37] M. Sarkar, J.T. Fan, Y.C. Szeto, X.M. Tao, Biomimetics of plant structure in textile fabrics for the improvement of water transport properties, *Text Res J* **79**(7) (2009) 657-668.

[38] D. Shou, J. Fan, An all hydrophilic fluid diode for unidirectional flow in porous systems, *Adv Funct Mater* **28** (2018) 1800269.

[39] K. Bal, J.T. Fan, M.K. Sarkar, L. Ye, Differential spontaneous capillary flow through heterogeneous porous media, *Int J Heat Mass Transf* **54**(13-14) (2011) 3096-3099.

[40] D. Shou, J. Fan, Structural optimization of porous media for fast and controlled capillary flows, *Phys Rev E Stat Nonlin Soft Matter Phys* **91**(5) (2015) 053021.

[41] J. Fan, D. Shou, Flow asymmetricity in fibrous constructs, *Fiber Society Spring Conference* 2015.

[42] D. Shou, L. Ye, J. Fan, K. Fu, Optimal design of porous structures for the fastest liquid absorption, *Langmuir* **30**(1) (2014) 149-155.

[43] D. Shou, L. Ye, J. Fan, K. Fu, M. Mei, H. Wang, Q. Chen, Geometry-induced asymmetric capillary flow, *Langmuir* **30**(19) (2014) 5448-5454.

[44] D. Shou, J. Fan, Structural optimization of porous media for fast and controlled capillary flows, *Physical Review E* **91**(5) (2015) 053021.

[45] E. Arens, H. Zhang, The skin's role in human thermoregulation and comfort, *Thermal and Moisture Transport in Fibrous Materials* (2006) 560-602.

[46] E. Proksch, J.M. Brandner, J.M. Jensen, The skin: an indispensable barrier, *Exp Dermatol* **17**(12) (2008) 1063-1072.

[47] K.P. Tang, J.T. Fan, J.F. Zhang, M.K. Sarkar, C.W. Kan, Effect of softeners and crosslinking conditions on the performance of easy-care cotton fabrics with different weave constructions, *Fiber Polym* **14**(5) (2013) 822-831.

[48] Y. Lu, S. Sathasivam, J.L. Song, C.R. Crick, C.J. Carmalt, I.P. Parkin, Robust self-cleaning surfaces that function when exposed to either air or oil, *Science* **347**(6226) (2015) 1132-1135.

[49] A. Tourovskaia, T. Barber, B.T. Wickes, D. Hirdes, B. Grin, D.G. Castner, K.E. Healy, A. Folch, Micropatterns of chemisorbed cell adhesion-repellent films using oxygen plasma etching and elastomeric masks, *Langmuir* **19**(11) (2003) 4754-4764.

[50] C.X. Wang, Y. Ren, Y.P. Qiu, Penetration depth of atmospheric pressure plasma surface modification into multiple layers of polyester fabrics, *Surf Coat Tech* **202**(1) (2007) 77-83.

[51] J.D. Wu, Z.W. Mao, L.L. Han, J.B. Xi, Y.Z. Zhao, C.Y. Gao, Directional migration of vascular smooth muscle cells guided by synergetic surface gradient and chemical pattern of poly(ethylene glycol) brushes, *J Bioact Compat Pol* **28**(6) (2013) 605-620.

[52] C.X. Wang, Y. Liu, H.L. Xu, Y. Ren, Y.P. Qiu, Influence of atmospheric pressure plasma treatment time on penetration depth of surface modification into fabric, *Appl Surf Sci* **254**(8) (2008) 2499-2505.

[53] M.Y. Cao, K. Li, Z.C. Dong, C.M. Yu, S. Yang, C. Song, K.S. Liu, L. Jiang, Superhydrophobic "pump": continuous and spontaneous antigravity water delivery, *Adv Funct Mater* **25**(26) (2015) 4114-4119.

CHAPTER 4

BREATHABLE FABRICS WITH SMART PORES TO MIMIC LEAF STOMATA[*]

Abstract

Smart moisture responsive materials with tunable moisture permeability in response to wearers' physiological demands and environmental conditions are highly desirable for personal thermal regulation and comfort. In this study, we have designed and fabricated novel artificial leaf stomata on a fabric surface, the pores of which open and close depending on the surrounding humidity. Its working mechanism is based on the differential swelling and bending of the "guard cells" as that in the real leaf stomata. The moisture permeability of the fabric with artificial leaf stomata increased by 56% when the pores opened under wet condition in comparison with that when the pores are closed under dry condition. This moisture responsive fabric can have a direct application in smart functional clothing such as sportswear. The concept can be further extended to develop smart materials for controlled nutrient or drug release and other relevant industrial applications.

[*] **Lihong Lao**, Yuen Shing Wu, Jintu Fan. Artificial Leaf Stomata for Personal Thermal Regulation. ***Submitted***. 2019.

4.1 Introduction

Recently, smart breathable fabrics or membranes have attracted more and more attentions, especially in protective clothing as well as other applications such as medical care products, food packing, drug release and liquid separations [1-4]. The concept is unique in that the fabric or membrane is able to respond according to the environmental stimuli, i.e. the system can regulate shape, moisture or liquid transport under the stimuli such as light, temperature, pressure, electricity, magnetite, chemicals, etc. Depending on the different stimuli types and applications, the constituent materials (e.g. fiber, yarn, fabric, finishing and coating) will require specific chemical or physical features that can achieve these functionalities [5].

A stomata is a pore or opening in the epidermis of plant leaves, through which carbon dioxide is received for photosynthesis and water vapor is transpired [6]. A stomata consists of two guard cells, having thicker and inextensible inner walls as well as thinner and extensible outer walls [7]. The stomata open and close in response to changing conditions, such as light intensity, humidity, and carbon dioxide concentration [8, 9]. Under a high light intensity and high humidity (wet), the two guard cells are swollen and bowed apart from one another, creating an open pore to draw water in; Conversely, when the plant senses a water shortage, the cells are shorted, resulting in the closure of the pore to prevent the water loss (Figure 4.1a). The size of stoma lengths ranges from 10 to 80 μm and the width ranges from a few to 50 μm [10].

In apparel industry, there is always a demand to have smart materials functioning like the leaf stomata [11], which are able to regulate the moisture/vapor evaporation or even liquid

transport according to the body humidity, i.e. pores can automatically open under higher humidity (wet) and close under lower humidity (dry) without any other energy input. This will be particularly useful to maximize the barrier protection and thermal comfort for a wearer's changing physiological conditions [12].

Currently, most existing smart materials are based on the response to the temperature, chemicals, light, electricity and magnetite. For example, Hu et al. [13] constructed a dual-layer hydrogel composed of polyacrylamide (PAAm) and PAAm-Poly (N-isopropylacrylamide) (PNIPAAm) interpenetrating polymer network (IPN), and found a shape change ability of the system under an elevated temperature from 30 ^{o}C to 38 ^{o}C, which was above the lower critical solution temperature (LCST) of PNIPAAm. Similarly, Topham et al. [14] constructed a two-gel structure with polyacid and polybase PH-sensitive triblock copolymers, and observed the gel motion under different acidic and neutral/basic conditions. Kim et al. [15, 16] and Park et al. [17] applied the concept of leaf stomata to fabricate a membrane with thermo-responsive PNIPAAm hydrogel, and enable the constructed pore to open or close by swelling or shrinking of the materials under different temperatures. Gargava et al. [18] also prepared a hydrogel-based valve with PAAm and poly (N,N-dimethylacrylamide) (PDMAA) to mimic the stomata, but the regulation of the middle pore was based a stimulus of acetone solvent. Besides, Akzo Nobel markets a rubber membrane product under the name of Stomatex®, which is claimed to mimic the opening and closure of the leaf stomata according to user's different levels of physical activity [19]. Stomatex® is a synthetic rubber membrane having a pattern of dome-shaped vapor chambers, each with a tiny pore in the center. Yet, unlike the moisture responsiveness

of leaf stomata, it enlarges the pores by the flexing of the material caused by body motion [20] and strictly speaking, it is not environment-responsive.

Only a few studies have been reported for the materials' sensitivity to the water or moisture for opening and closing the pores. Wang et al. [21] formed a heterogeneous biohybrid film with a layer of special living cells attaching on another humidity-inert layer, and achieved reversible shape change in response to the environment humidity; the films were further embedded into garment design as ventilating flaps to modulate the ventilation of the body under different humidity levels. Using the same dual-layer and flap concepts, Mu et al. [22] attached a commercial perfluorosulfonic acid ionomer (PFSA) film on an inert substrate of polyethylene glycol terephthalate (PET) film, and integrated into commercial sports shirt to facilitate the formation of two-dimensional or three-dimensional geometrical changes of the flaps in response to vapor stimuli. However, in both designs, the flap substrates are less stretchable and the bending actuations are through-planes, which can adversely affect both the comfort (e.g. tactile comfort) and appearance of the clothing. Therefore, further development in the humidity-sensitive smart materials is needed.

As demonstrated in this work, we have developed a breathable fabric with smart pores to mimic the structure and function of leaf stomata for regulating the pore open and close behavior under different humidity conditions. We used only one material, polyacrylamide (PAAm) hydrogel, with two different crosslinking levels to form a three-layer system and integrated it into a stretchable knitted nylon fabric (Figure 4.1b). Because of the different swelling, the two hydrogel have different expansion abilities under humid condition, with an outer layer of less crosslinked (LC) PAAm hydrogel having a swelling more than 100

times of that of an inner layer of highly crosslinked (HC) counterpart after the full expansion. When the constructs were coated on the fabric pore window areas, the swelling difference led to an asymmetric bending towards outer layer direction under higher humidity (wet), and therefore the middle slit (pore) opens. While under the normal humidity (dry), the pore stays closed status. In both conditions, the fabric maintains a flat surface without buckling, which has little effect on the overall dimension of the fabric.

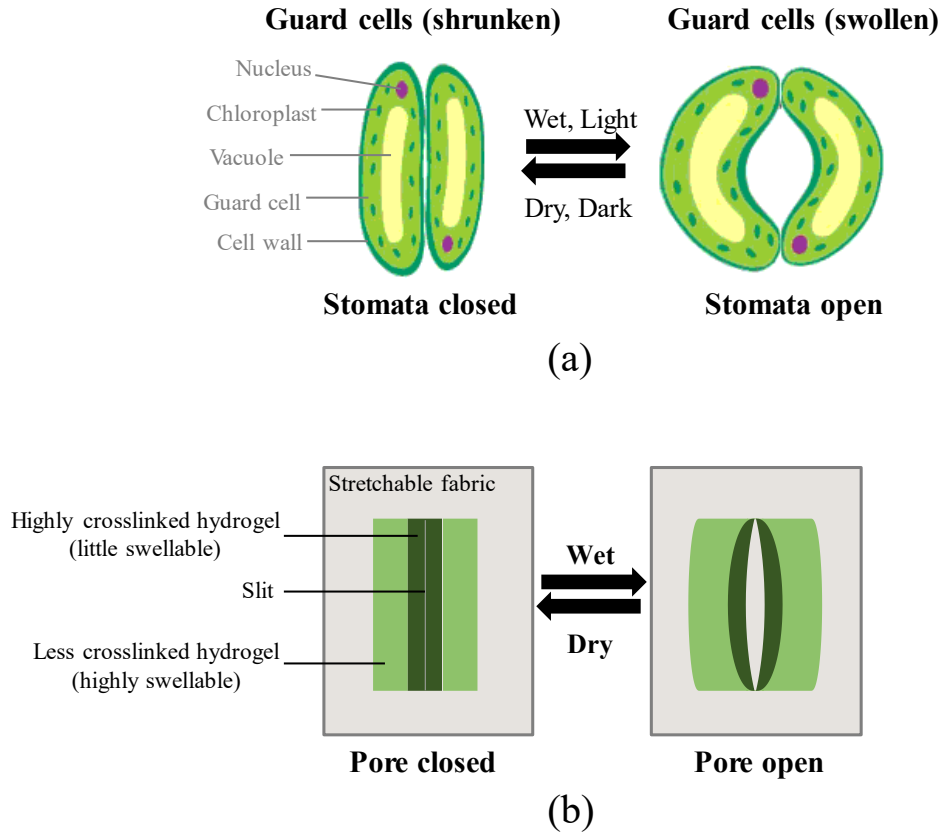

Figure 4.1 Scheme to show the design of stretchable fabrics with smart pores to mimic leaf stomata structure and function. (a) An illustration of guard cells (pore) open and close of leaf stomata. (b) Design of "artificial stomata" on a stretchable fabric with pore areas coated by a three-layer hydrogel system with a slit, where the inner layer was composed of highly crosslinked (HC) little swellable hydrogel and outer layer composed of the less crosslinked (LC) highly swellable hydrogel. The artificial stomata was hypothesized to open the pores under wet condition, and close the pores under dry condition.

4.2 Experimental Section

4.2.1 Preparation of PAAm hydrogel

The polyacrylamide hydrogels were synthesized using the following protocol [23]. 12 wt % of acrylamide monomer (AAm; Sigma-Aldrich, A8887) was dissolved in deionized (DI) water with 17% (4 M) LiCl (Alfa Aesar). The solution was subsequently mixed with a photoinitiator, Darocur® 1173 (BASF) at 0.2 wt% of the solution and a crosslinker, N,N′-methylene bisacrylamide (MBA; Sigma, M7279) at either 0.12 wt% or 1.2 wt% of the solution, for the less crosslinked (LC) and highly crosslinked (HC) hydrogels, respectively. For some solutions, 1.2 wt% PAAm polymer (Sigma-Aldrich, M_w~5×10^6) was also added as a comparison [24]. The solutions were stirred overnight at room temperature, until it was homogeneous. They were then poured into a microtome embedding mold (Electron Microscopy Sciences, 15 mm wide × 7 m high × 4 mm deep) and cured via exposure to 365 nm ultraviolet (UV) light (UVP Blak-Ray™ B-100AP High-Intensity UV Inspection Lamps) for 10 minutes.

4.2.2 Preparation of three-layer sandwiched hydrogel with slit

The three-layer sandwiched hydrogel was prepared by step-by-step stacking and curing three hydrogel solutions in the same mold, with the outer layers having the less crosslinked (LC) hydrogel formula and the inner layer having the highly crosslinked (HC) hydrogel formula. For the first layer, 400 µL of the LC solution having a low amount of MBA crosslinker (0.12 wt%) was injected into the mold, and was photo-polymerized via exposure to 365 nm UV light for 10 min. After the first layer has been completely cured, the 400 µL of second HC solution having the high amount of MBA (1.2 wt%) was injected

into the mold on top of the first layer, and cured under the same condition. Finally, the 400 μL of first LC solution was injected into the mold onto the second layer, and cured to form the third layer.

4.2.3 Coating three-layer hydrogel on pore areas of the fabric

Knitted nylon fabrics were supplied by Nanjing Yuyuan Textile Co Ltd (100% Nylon, NNP 32003). The fabrics were washed, immersed into 5 wt% benzophenone (BP, Alfa Aesar, A10739)/ethanol solution for pre-activation [25]. For hydrogel coating, the BP pre-treated fabric was covered by a tape mask with patterned pore structure grooves. The pore area has three windows, with the inner and two outer windows having widths of 2 mm and 2.5 mm, respectively. The height of the pore is 9 mm. The horizontal and vertical distances between each pore area are 6 mm and 4 mm, respectively. A water-soluble glue viscous solution (Elmer's School Glue) was pasted into the grooves. After the glue has solidified and the tape mask has been peeled off, the stomata pore template with three windows was formed on the fabric. The different hydrogel formulas were then injected and cured into the template windows in orders, i.e. the inner middle window filled with HC solution and cured first, followed by LC solution curing in the two outer windows. A slit was then cut in the middle of the HC hydrogel. Finally, the fabric was immersed into a water bath to wash away the glue template, and air dried at room temperature.

4.2.3 Characterization

Morphology analysis: Scanning electron microscopy (SEM, Tescan Mira3 FESEM) was used to study the microstructure of the different crosslinked PAAm hydrogels and the nylon

fabrics before and after hydrogel coating in the pore areas. The samples were frozen-dried and coated with a thin layer of gold palladium before observation.

Water response (swelling) of single hydrogel: Pieces of PAAm hydrogels (4 mm wide × 7 mm high × 1 mm thick) having the different amounts of the MBA cross-linker was immersed into the water. They were taken out at the desired time intervals, wiped superficially with a filter paper to remove the surface water and weighed (W_t). The uptake ratio was defined as $(W_t - W_0)/W_0$, where W_0 is the initial weight before the water immersion [26]. The results from three similar specimens were averaged for each hydrogel sample.

Water response of hydrogels with slits: The pieces of LC PAAm hydrogel, HC hydrogel and three-layer sandwiched hydrogel (4 mm wide × 7 mm high × 1 mm thick) with a middle slit (6 mm high) were was also immersed into the water for 10 min and checked the response behavior. Each piece of the samples was cut cross-sectionally from the molded hydrogels, on which the slits were cut in the middle position.

Water response of fabric with the pore areas coated with hydrogels: The nylon fabrics with hydrogel coating in the pore areas were also immersed into the water for 10 min and checked the pore responses. Different combinations of the hydrogel formulas were investigated. Optical microscopy (Olympus BX51, Olympus Corporation) was used to observe the pore behaviors.

Evaluation of water vapor transmission rate (WVTR): The WVTR was measured with an upright cup method according to BS 7209 [27, 28], with a modified temperature at 35 ^{o}C.

Various samples were cut into circular sharps with a diameter around 90 mm, and attached firmly to the edge of the standard aluminum cups (an inner diameter of 83 mm, an outer diameter of 90 mm, inner cup thickness of 18.5 mm, and outer cup thickness of 20 mm) via an adhesive. Each cup contained ~60 g of DI water inside and a triangular support was used underneath the samples to prevent them sagging into the cup. Samples were then placed on a heater at the temperature of 35 ^{o}C, and tested over 1 h to determine the water mass loss over the time as the water vapor transmission rate. All the fabric samples were placed in a standard atmosphere (65 ± 2% relative humidity, and a temperature of 20 ± 2 ^{o}C) for at least 24 hours prior to testing. The results were averaged from three parallel tests.

Evaluation of air permeability: Air permeability for various fabrics were tested via a gas permeability module on a Capillary Flow Porometer 7.0 (Porous Materials Inc., USA, CFP-1100-AEHXL) [29]. Samples were cut into circular sharps with a diameter of ~25 mm, placed gently in the chamber, and fixed by the seal O-ring (an inner diameter 18.3 mm and an outer diameter 25 mm) and the adapter plates. During the test, the air pressure will increase and the flow through and pressure drop across the sample will be measured. From the affiliated software, an average Darcy's Permeability Constant will be obtained for each sample according to sample thickness, diameter, air flow and the pressure. All the samples were placed in a standard atmosphere (65 ± 2% relative humidity, and a temperature of 20 ± 2 ^{o}C) for at least 24 hours prior to testing. The results were averaged from three parallel tests.

The experimental data were analyzed using ANOVA. The significance level was set at $p<0.05$. Results were reported as mean ± standard deviation.

4.3 Results

4.3.1 Study of differently crosslinked PAAm hydrogels

We used UV photo-polymerization to synthesize the polyacrylamide hydrogels using a previous protocol with a crosslinker, N,N′ -methylene bisacrylamide (MBA) and a photoinitiator, Darocur® 1173 [23]. We adjusted the formula with different crosslinker loadings. The less crosslinked (LC) hydrogel having the MBA crosslinker of 0.12 wt% showed a transparent appearance, while the highly crosslinked (HC) sample with MBA of 1.2 wt% turned to a white color (Figure 4.2a). The microstructure did not vary, with both showing a porous morphology after frozen-dry (Figure 4.2b). The water uptake (swell ratios) differed between different samples (Figure 4.2c). The LC sample easily absorbed water and swelled, and reached almost 130% of the original weight after 120 min (p<0.05); the HC samples did not swell and was stable in its weight (the images can be found in Figure S4.1).

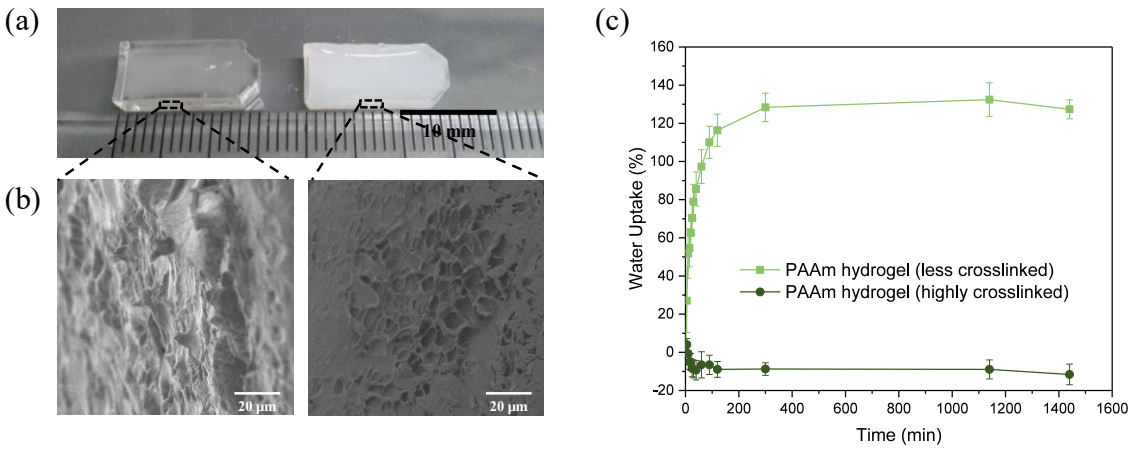

Figure 4.2 Images, microstructure and water behavior of polyacrylamide (PAAm) hydrogels with different crosslinker loadings. (a) Photo images and (b) SEM morphologies of less crosslinked (left) and highly crosslinked (right) PAAm hydrogels, respectively. (c) Water uptake profiles (swell ratios) of these two hydrogels.

4.3.2 Study of three-layer sandwiched hydrogel

We then applied a step-by-step UV cure of the two hydrogel solutions and fabricated a three-layer hydrogel composite in a mold (15 mm wide × 7 m high × 4 mm deep). The cross-section view of the sample (4 mm wide × 7 mm high × 1 mm thick) clearly demonstrated the sandwiched structure (Figure 4.3a), with the inner layer of white HC and two outer layer layers of transparent LC PAAms, respectively (noted as LC/HC/LC sandwiched hydrogel composite), corresponding to the appearance in the neat samples (Figure 4.2a). We then used a knife to cut a slit (6 mm) in the middle of the inner layer on a piece of the three-layer composite, and compared the water response of the slit (pore) with those cut in same length in the two neat hydrogel pieces with the same shape and thickness (Figure 4.3b). When the samples were contacted with water for 10 min, the slits in the two neat sample did not change, with only the whole piece of the LC hydrogel swelling (Figure 4.3c, left); however, the sandwiched hydrogel composite responded, with the inner HC hydrogel walls separated, leading to the slit enlarged (Figure 4.3c, right). When most of the external water was evaporated for 1 h (not completely dry, because hydrogels contain water), the inner HC hydrogel walls closed up (Figure 4.3d, right). This phenomenon was illustrated by the nearby schemes, which was similar as pore behavior in leaf stomata, i.e. the pores open in wet (humid) and close in dry conditions, respectively.

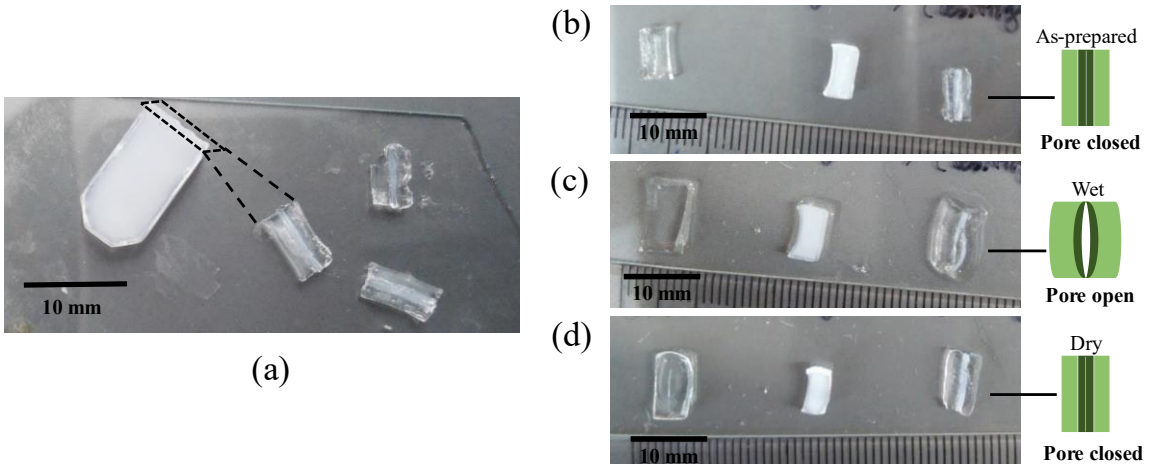

Figure 4.3 Images and water behavior of three-layer sandwiched PAAm hydrogel composite. (a) The surface and cross views of the three-layer sandwiched hydrogel composite. (c-d) Water behavior of the pores (slits) cut in the middle of less crosslinked (left), highly crosslinked (middle) and three-layer (right) PAAm hydrogel pieces with the same dimensions (4 mm wide × 7 mm high × 1 mm thick) in (b) as prepared, (c) wet (contacting with water for 10 min) and (d) dry conditions, respectively; the right schemes explain the response of the pore in the three-layer hydrogel piece.

4.3.3 Coating of three-layer hydrogel on pore areas of the fabric

We then tried to create leaf stomata-mimicking pores with the three-layer hydrogel structure on a knitted nylon fabric following the scheme process in Figure 4.4 (also Figure S4.2, for real sample processing). The clean fabrics were first pre-activated by a benzophenone (BP)/ethanol solution [25]. To prevent hydrogel solutions spreading on the fabric, we firstly patterned a glue template with three parallel windows (total 7 mm wide × 9 mm high, inner window 2 mm wide, outer window 2.5 mm wide) on the fabric via extruding and solidifying the glue under an assistance of a laser-cut patterned tape mask. We then injected the HC hydrogel precursor in the inner window of the glue templates, and cured it under 365 nm UV for 10 min, and successively injected and cured the LC hydrogels in the outer windows for another 10 min. After all the hydrogels has been cured, we cut a

slit with the same length of 9 mm in the middle of the inner HC hydrogel layer, and washed away the glue resists under a water bath.

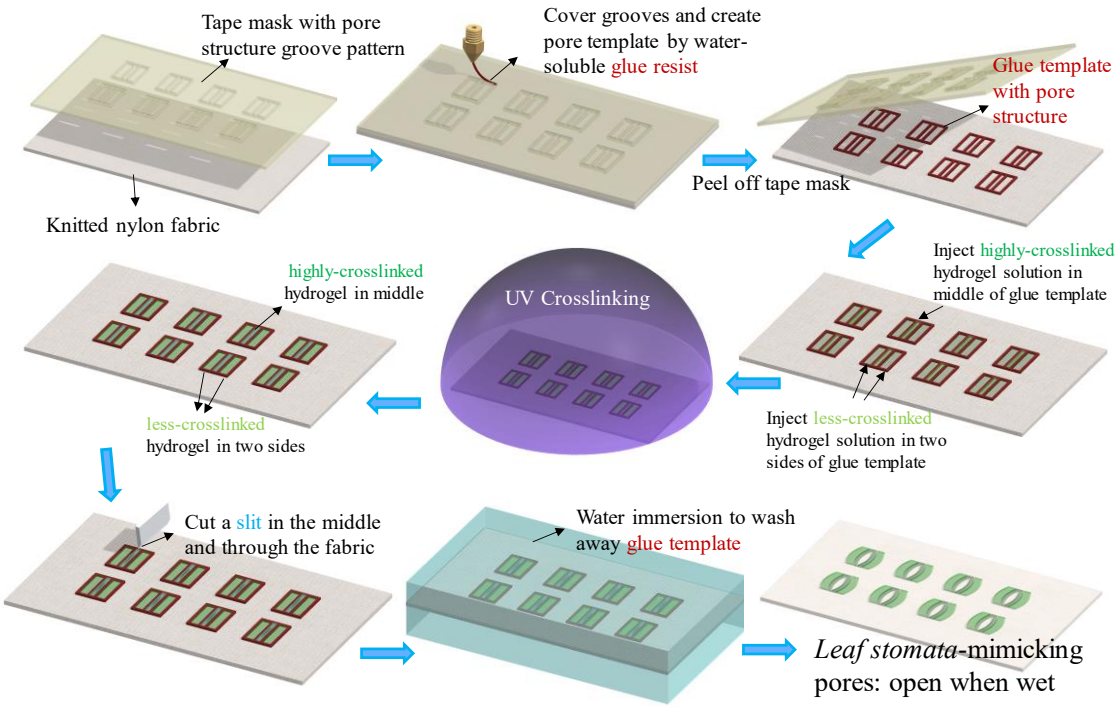

Figure 4.4 Scheme to show the process of creating three-layer hydrogel coated pores on a nylon fabric to mimic leaf stomata.

We screened the water behaviors for the pores coated by different combinations of LC and HC PAAm hydrogels (Table 4.1, and Figure S4.3). We also compared the effect with the addition of PAAm polymer in the hydrogel solutions (noted as LCP and HCP for less crosslinked and highly crosslinked solutions, respectively) [24]. It was found the pores did not response to the water if only the inner window was coated either by the LC, HC, LCP or HCP hydrogels. The pores slightly opened when only the two outer windows were filled with LC and LCP hydrogels, however did not response either when filled with HC and HCP hydrogels. When the inner windows were coated with LC or LCP hydrogels, and the outer windows were coated with HC or HCP hydrogels, the pores enlarged slightly when

contacting with water, however they remained open when the fabrics were dry. Only when the windows were coated in reversed order, i.e. inner with HC or HCP, and outer with LC or LCP hydrogels, the pores can be largely open when getting wet and closed when back to dry (circled in Table 4.1). The addition of PAAm polymer did not make difference, even receded the closing for LCP/HCP/LCP sample (HCP for inner and LCP for two outer windows, respectively). In this matter, we chose HC and LC hydrogel combination for the inner and outer window coatings (LC/HC/LC), respectively, for further experiments, as noted * in the table.

Table 4.1 Summary of water response of the pore window areas coated by different combinations of hydrogels. The combinations include no hydrogel (0), less crosslinked hydrogel (LC), highly crosslinked hydrogel (HC), less crosslinked hydrogel plus PAAm polymer (LCP) and highly crosslinked hydrogel plus PAAm polymer (HCP).

Condition	Wet					Dry				
	Outer layer					Outer layer				
Inner layer	None (0)	AAm & PAAm (LCP)	AAm (LC)	AAm & PAAm (HCP)	AAm (HC)	None (0)	AAm & PAAm (LCP)	AAm (LC)	AAm & PAAm (HCP)	AAm (HC)
None (0)	-	+	+	-	-	-	-	-	-	-
AAm & PAAm (LCP)	-			+	+	-			+	-
AAm (LC)	-			+	+	-			+	+
AAm & PAAm (HCP)	-	++	++			-	+	-		
AAm (HC)	-	++	++*			-	-	-*		

The symbols -, + and ++ represent pore close, slightly open, and largely open, respectively.
Red circles showed good combinations for pore open and close behaviors.
* represents the hydrogel combination used in the following experiments.

Figure 4.5c showed a typical fabric sample with the pore windows (7 mm wide × 9 mm high) coated with the three-layer PAAm hydrogel (LC/HC/LC combination). The fabric

kept a flat, non-buckling surface. The horizontal and vertical distances between each window are 6 mm and 4 mm, respectively. Figure 4.5b showed SEM morphologies for the fabric before and after hydrogel coating. Both the neat and BP pre-treated knitted nylon fabrics showed a smooth fiber surface, whereas the hydrogel coated window areas turned to a rougher fiber surface, with hydrogel materials connecting between fibers. The hydrogel solutions also penetrated through the fabric, as the back side of the both window areas also showed rough morphologies (Figure S4.4b). No significant difference was found between the HC and LC hydrogel coated inner and outer window areas, respectively.

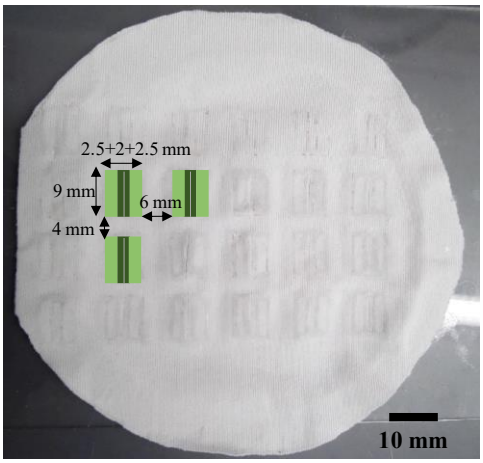

(a)

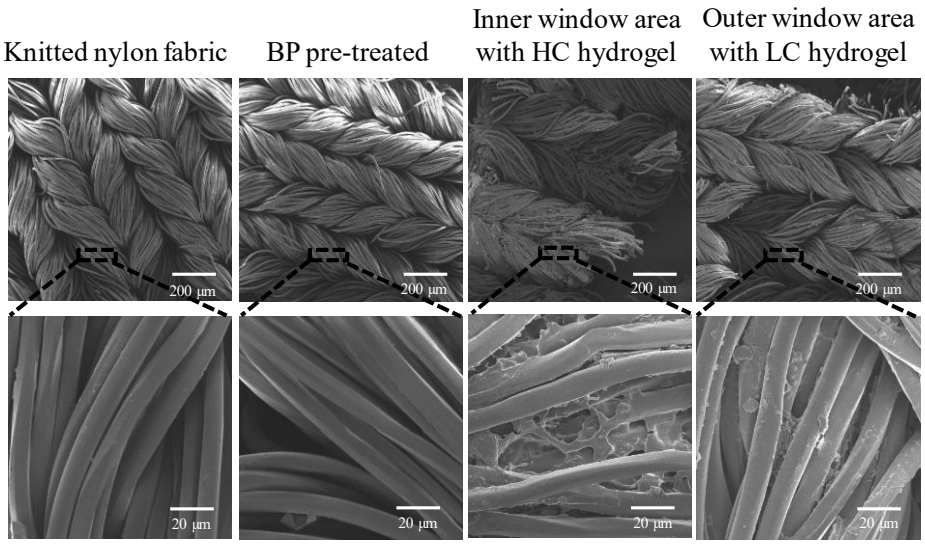

(b)

Figure 4.5 Structure of knitted nylon fabrics under different treatment conditions. (a) An image of a typical knitted nylon fabric with three-layer LC/HC/LC hydrogel coated pore structures; insets are schemes of the designed coating and dimension of the windows on the pore area. (b) SEM images of the neat nylon fabric, BP pre-tread fabric, the inner and outer window areas in the designed three-layer hydrogel coated pores on the nylon fabric.

4.3.4 Performance of the fabric with three-layer hydrogel coated pore structure

The water response of the fabric with the pore windows coated with the three-layer LC/HC/LC PAAm hydrogels were further studied, in terms of dimension change, and effect to vapor and gas permeability. When the sample was contacted with water for 10

min, the slits enlarged leading to pores open (Figure 4.6a, left). The optical microscopy reveals the average pore size increased to 0.72 mm (Figure S4.5a), with the largest pore over 1.30 mm (Figure 4.6b, left), as compared to 0.20 mm that of the as-prepared sample (data not shown). After the sample was dried at room temperature for 1 h, the pores closed to an average of 0.2 mm (Figure 4.6a, b, rights, and Figure S4.5a), similarly as the original size. The control fabric and fabric with slit only did not change the pore and slit dimensions (Figure S4.5).

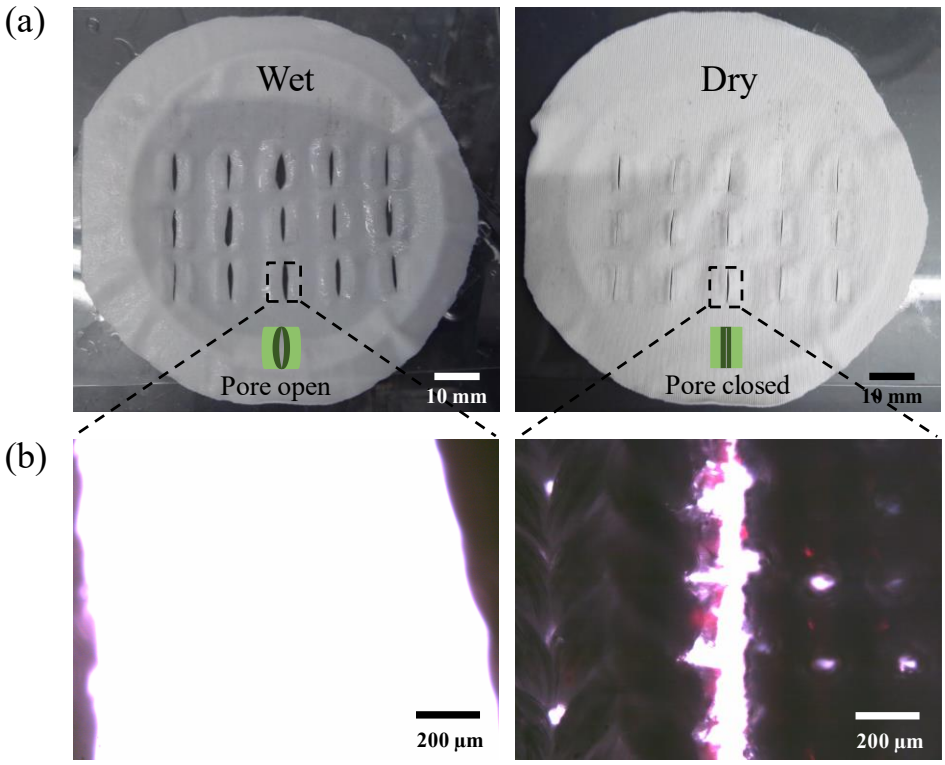

Figure 4.6 Water response of a knitted nylon fabric with the pore areas coated by three-layer PAAm hydrogels. (a) Images of a typical knitted nylon fabric with three-layer LC/HC/LC hydrogel coated pore structures under wet (left) and dry (right) conditions, respectively; insets are schemes to show the pore responses. (b) Optical images of the pore responses under wet (left) and dry (right) conditions, respectively.

The breathability of the designed fabric with hydrogel coated pores was evaluated by measuring either water vapor or air permeability. For measurement of water vapor transmission rate (WVTR), an upright cup method was employed according to BS 7209 standard, however a heater was used to elevate temperature to 35 ^{o}C to simulate the human skin temperature (Figure S4.6a) [27, 28]. The neat nylon fabric with and without slit cut were also tested as controls (Figure S4.6b, c). The WVTR was calculated using the following equation:

$$WVTR = \frac{M}{At} \tag{4.1}$$

where *WVTR* is the transmission rate of water vapor (g/m^2/h), *M* the loss in mass (g), *t* the time duration (h), and *A* the area of the exposed test fabric which is equal to the internal area of the dish (m^2). The results were averaged from three parallel tests.

From Figure 4.7a, we found the fabric with the slits (15 slits on a 90 mm circular sample) regardless of hydrogel coating had a similar vapor transmission rate as the control fabric (280-306 g/m^2/h) (p>0.05) under initial dry condition. This means the gaps between the yarns by the slits did not affect too much on the permeability, probably because the knitted fibrous system has already been very breathable as it was very porous (Figure S4.5b). When all the fabrics were wet, the transmission rates all increased, which should be attributed to the surface vapor evaporation. However, compared with both control samples (372 and 375 g/m^2/h), the sample with the hydrogel coated pores showed a much higher permeability (477 g/m^2/h) (p<0.05), being 56% greater than that at the dry condition. Obviously, it was because the openness of the pores under the wet condition increased the chance for the underneath vapor to transmit out (Figure S4.6g).

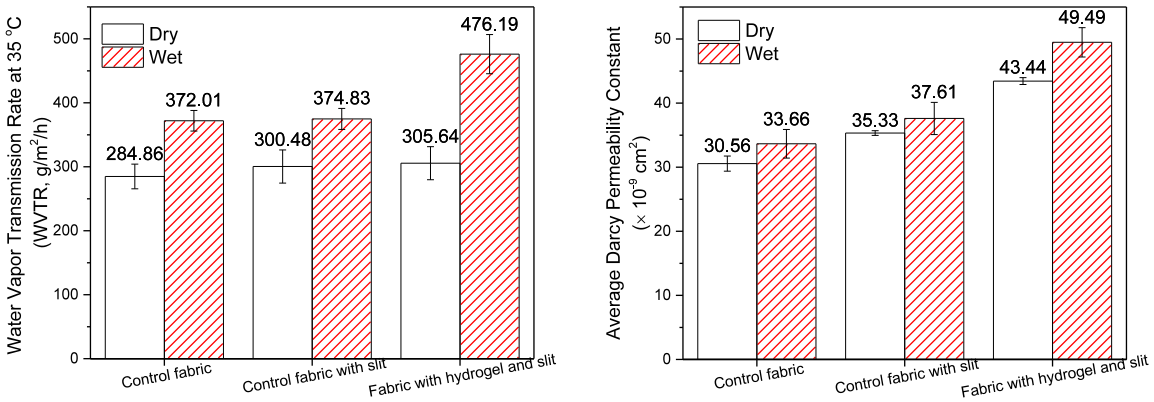

(a) (b)

Figure 4.7 The effect of water response on vapor or air permeability of knitted nylon fabrics with the pore areas coated by three-layer PAAm hydrogels. (a) Water vapor transmission rates and (b) air permeability profiles of control knitted nylon fabric, control fabric with slit, and fabric with slit and pore areas coated with three-layer hydrogels under both dry and wet conditions, respectively.

The air permeability was tested via a gas permeability module on a Capillary Flow Porometer [29]. Similarly, a circular area (18.3 mm) of fabric with two slits coated with three-layer hydrogels was compared with the control fabric and the fabric with only two slits, both under dry and wet atmospheres (Figure S4.7). The generated results were Darcy's Permeability Constant, calculated using the following equation:

$$C = \frac{8FTV}{\pi D^2(P^2-1)} \tag{4.2}$$

where C is Darcy's Permeability Constant (Darcy or cm², 1 Darcy = 9.87 × 10^{-9} cm²), *F* the air flow (CC/s), *T* the sample thickness (mm, measured 0.39 mm for the nylon fabrics), *V* the air viscosity (0.0185 CP for air), *D* the sample diameter (mm), and *P* the pressure (atmospheres, psi). The results were averaged from three parallel tests.

As shown in Figure 4.7b, the trend of the air permeability constant was similar as that of the WVTR test, i.e. the designed fabric with pores coated with three-layer hydrogels have a higher permeability ($> 43 \times 10^{-9}$ cm^2) than the control two fabrics ($< 38 \times 10^{-9}$ cm^2), both under dry and wet conditions ($p<0.05$); and the permeability increased under wet condition ($\sim 50 \times 10^{-9}$ cm^2) compared with that under dry condition (43×10^{-9} cm^2) ($p<0.05$). This again proved the enlargement of the pores benefited the air flow through the fabric, thereby a higher breathability.

4.4 Discussion

Breathable fabrics are widely used in protective clothing as well as many other applications such as wound dressings, food packaging, roofing and filtration/separation [19], owing to their ability in protecting from liquid penetration, yet allowing the transmission of moisture vapor. While a resting body produces about 30 g/m^2/h insensible perspiration, a person in active sports may produce as much as 1000 g/m^2/h of sweat [30]. In order to maximize the barrier protection and thermal comfort, it is therefore highly desirable to have smart or intelligent breathable fabrics, the water vapor permeability of which can change depending on the wearer's physiological and environmental conditions [12].

The present study demonstrated environmental-responsive permeability of a fabric can be achieved by creating moisture sensitive pores on the fabric, where the inner wall of the pores was coated with highly crosslinked (HC) PAAm hydrogel, and the outer windows of the pore were coated with less crosslinked (LC) hydrogels. The basis of this idea was to closely mimic the mechanism of the opening and closure of the leaf stomata in nature. In these artificial stomata on a knitted nylon fabric, the outer layers of LC hydrogels were

functioning as the drive of the “guard cells”, which swelled largely under higher humidity (wet). Due to the connection with the inner less swellable HC hydrogel, the dimension change of the “guard cells” occurred asymmetrically during the swelling, i.e. the outer LC part would swell more than the interconnected restricting HC part, which led to the bending of the “guard cells” toward the outer side. Because the knitted fabric substrate is very stretchable, the outwards bending of the two “cells” bowed apart from each other, leading to the middle slit in the hydrogel (and the fabric) enlarged, therefore the pore of the artificial stomata opened. The openness of the pores under wet condition enhanced the vapor permeability to 477 $g/m^2/h$ at 35 ^oC, which was 56% higher than the unmodified fabric at the same condition, and 100% higher than that of reported PFSA film-based shirt having semilunar patterns (237 $g/m^2/h$) [22], respectively. Conversely, when humidity decreased (dry), the evaporation of the water turned the swelling hydrogels to their original dimensions, therefore no bending occurred and the pores closed again, without affecting the original permeability level.

The opening and closure of the artificial stomata on the fabric can be very beneficial to meet the wearer’s physiological demand in different conditions. For instance, when the wearer is resting under a cold and dry condition, the artificial stomata keeps a closed status so as to retain heat and maximize barrier protection; on the other hand, when the wearer sweats profusely as a result of either physical activity or exposure to hot and humid environment, the pores of the designed fabrics are enlarged so as to increase moisture transmission for improved thermal comfort. Beside the protective clothing, the smart breathable fabrics can also have wide applications in smart medical care products, controlled nutrient or drug release and other industrial products.

Our concept of artificial stomata can be further improved by reducing the dimension of each artificial stomata and scaling up the coating process of patterned hydrogels on the fabric or membrane surface. If the dimension of the moisture responsive pores are reduced to microscales, the fabric or membrane would have greater barrier protection for heat retention or water repellency when the pores are closed [19] . To commercialize the proposed technique, it is also necessary to automate or scale up the process, which may be achieved by screen printing or 3D printing.

4.5 Conclusion

In summary, we have created smart moisture responsive pores on a commercial nylon fabric to mimic the leaf stomata. The "pores" are slits on the fabric coated by a special hydrogel system, with the inner and outer layers having different swelling behaviors, which functionalized as "guard cells" to regulate the dimensions. Under high humidity (wet), the outer layers of the "guard cell" swell in larger extent than the inner layers, which lead the slits enlarged and the "pores" open; under dry condition, both layers do not swell, therefore the slits ("pore") closed. The open and close behaviors of the pores have been confirmed by the images and optical microscopy. The microstructure of hydrogels was observed under SEM. Because of the opening of the pores under wet condition, both water vapor permeability and air permeability have greatly increased for the designed fabric compared with the control fabric. The smart breathable fabric can be directly used for functional clothing to meet the wearer's different physiological demands. Besides, it can also be applied in other areas, such as would dressings, controlled nutrition/drug release, and other relevant industrial products.

4.6 Supporting Information

Water behavior of polyacrylamide (PAAm) hydrogels with different crosslinker loadings

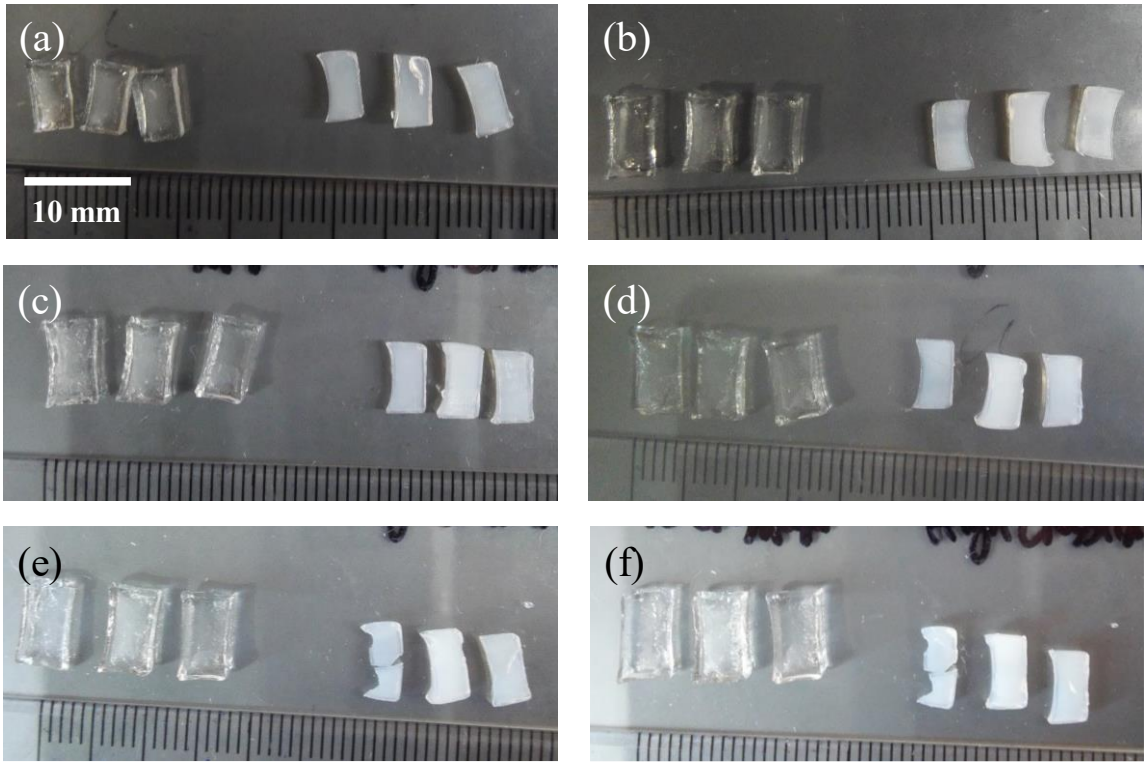

Figure S4.1 Images of three parallel samples for less crosslinked (left) and highly crosslinked (right) PAAm hydrogels after water uptake for different time. (a) 0 min, (b) 10 min, (c) 20 min, (d) 40 min, (e) 60 min and (f) 120 min, respectively.

Coating of three-layer hydrogel on pore areas of the fabric

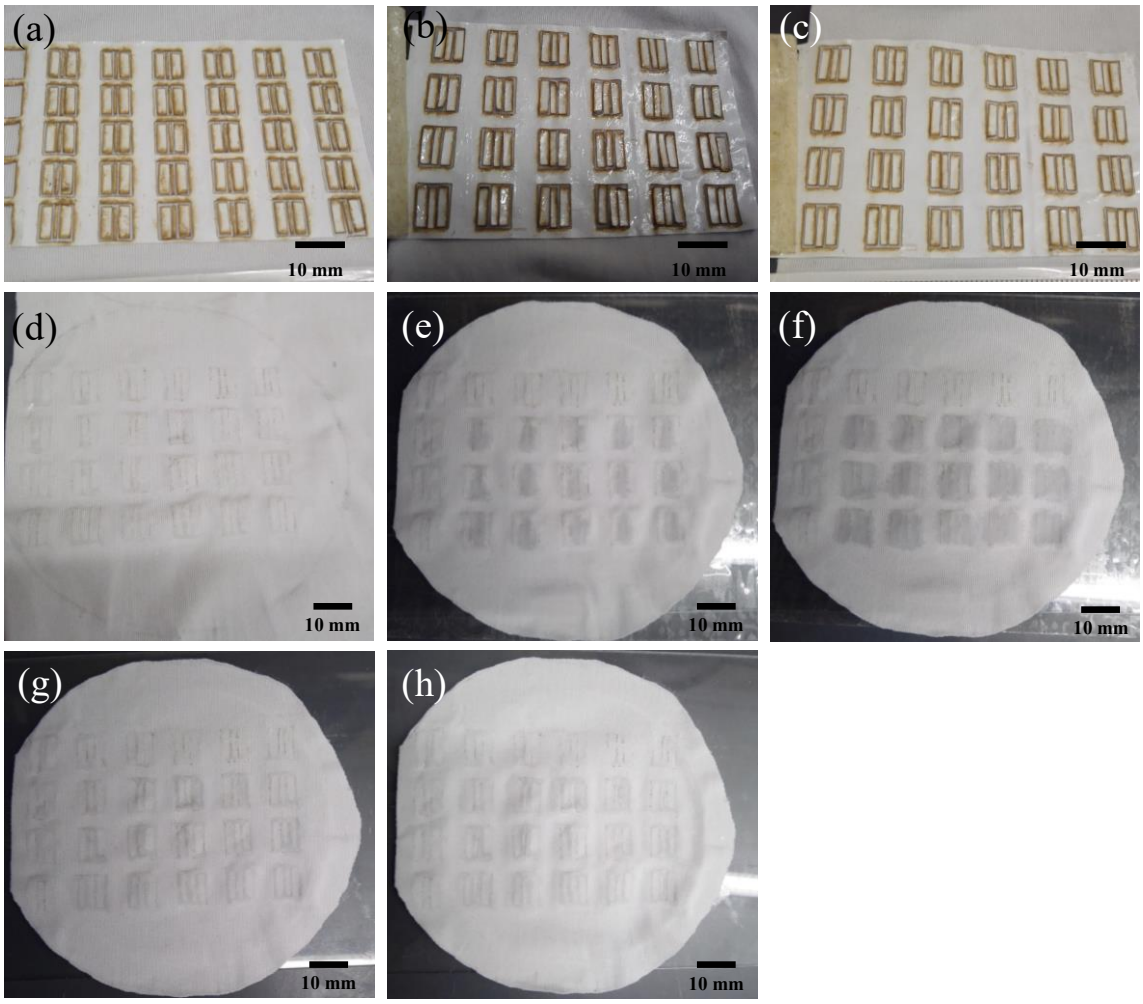

Figure S4.2 Fabrication process to create a knitted nylon fabric with the pore areas coated by three-layer PAAm hydrogels. (a) Cover nylon fabric with a laser-cut tape mask with patterned window structure. (b) Extrude a glue resist into the grooves of the window patterns. (c) Solidify the glue in air. (d) Form the glue template with patterned windows after peeling off the mask. (e) Inject and cure the highly crosslinked hydrogel (HC) hydrogel solution in the inner window of the glue templates. (f) Inject and cure the less crosslinked hydrogel (LC) hydrogel in the two outer windows of the glue templates. (g) Form the three-layer hydrogel coated windows after hydrogel completely curing. (h) Cut slits in the middle of the inner HC hydrogel layer to form leaf stomata-mimicking pores.

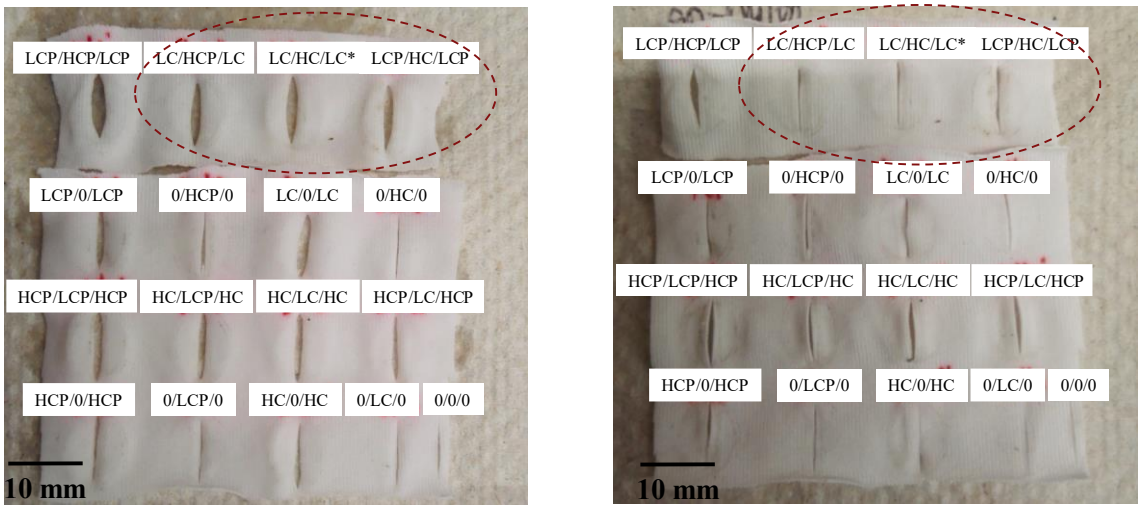

(a) (b)

Figure S4.3 Water response of the pore areas coated by different combinations of hydrogels. Combinations include no hydrogel (0), less crosslinked hydrogel (LC), highly crosslinked hydrogel (HC), less crosslinked hydrogel plus PAAm polymer (LCP) and highly crosslinked hydrogel plus PAAm polymer (HCP) under (a) wet and (b) dry conditions, respectively. Red circles showed good combinations for pore open and close behaviors.

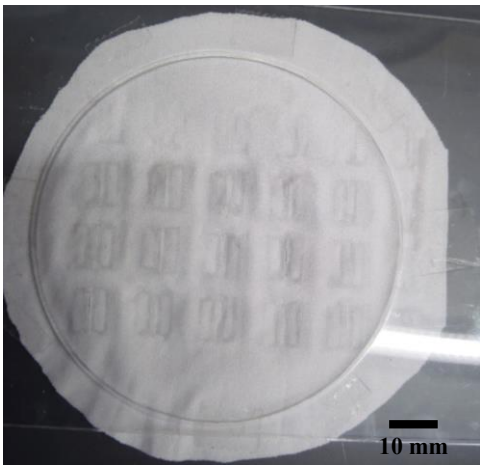

(a)

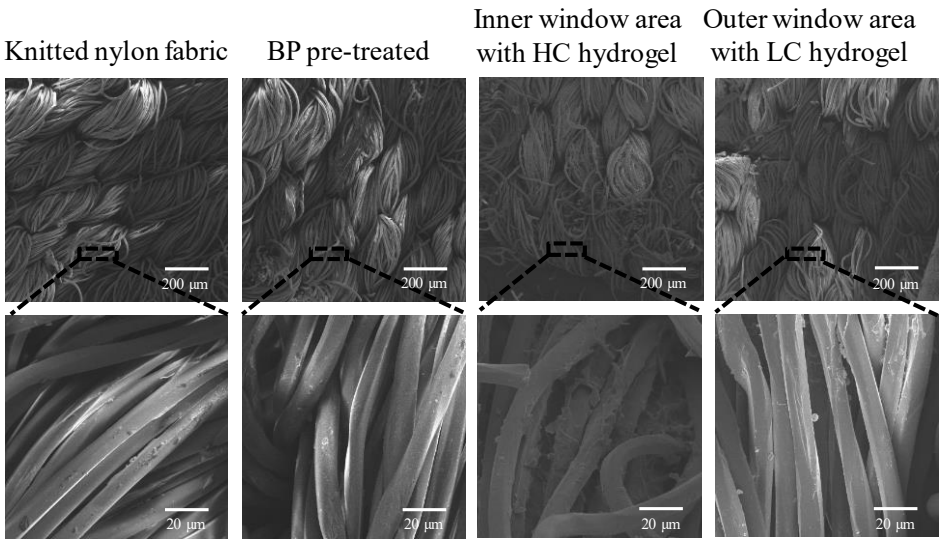

(b)

Figure S4.4 Structure of back side of knitted nylon fabrics under different treatment conditions. (a) An image of back side of a typical knitted nylon fabric with three-layer LC/HC/LC hydrogel coated pore structures. (b) SEM images of back side of the neat nylon fabric, BP pre-tread fabric, the inner and outer window areas of the three-layer hydrogel coated pores on the nylon fabrics.

Performance of the fabric with three-layer hydrogel coated pore structure

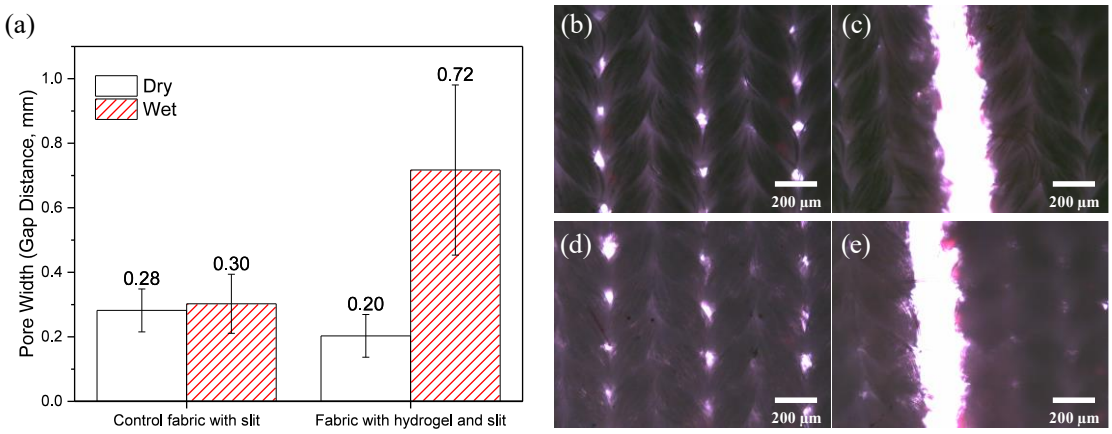

Figure S4.5 Water response of control knitted nylon fabric, control fabric with slits and fabric with slits coated with three-layer hydrogels. (a) Pore width (slit gap distance) of control fabric with slits, and fabric with slit (pore areas) coated with three-layer hydrogels under both dry and wet conditions, calculated from optical microscopy. (b-e) Optical images of the pore responses of (b, d) control knitted nylon fabric and (c, e) control fabric with slits under (b, c) dry and (d, e) wet conditions, respectively.

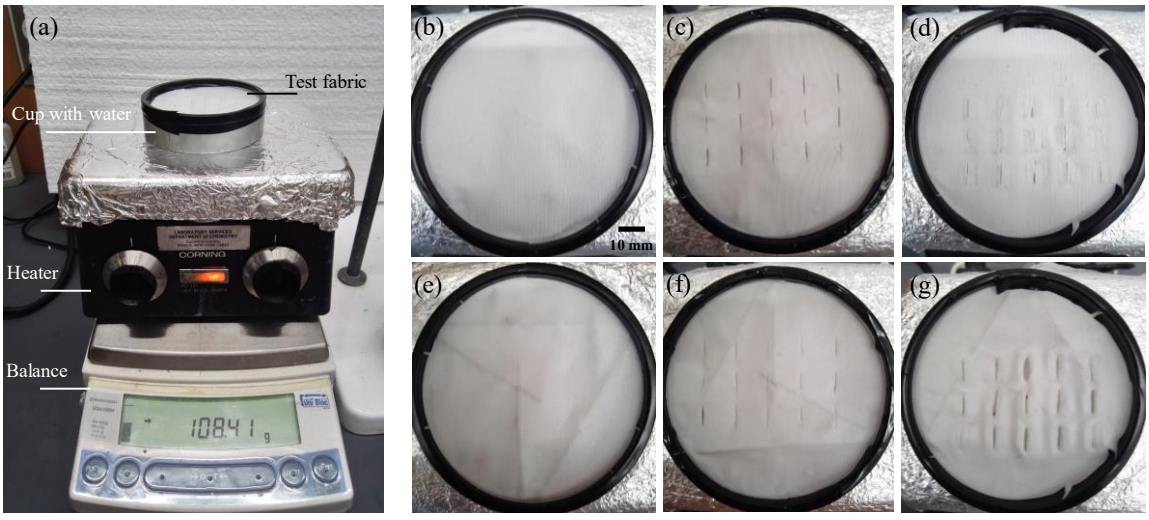

Figure S4.6 Cup method to test water vapor transmission rate (WVTR) of the fabrics. (a) Experimental set-up for measuring WVTR of the fabrics at 35 ^{o}C. (b, e) Control knitted nylon fabric, (c, f) control fabric with slits and (d, g) fabric with slits coated with three-layer hydrogels. The fabrics were covered on the cups for tests under (b-d) dry and (e-g) wet conditions, respectively.

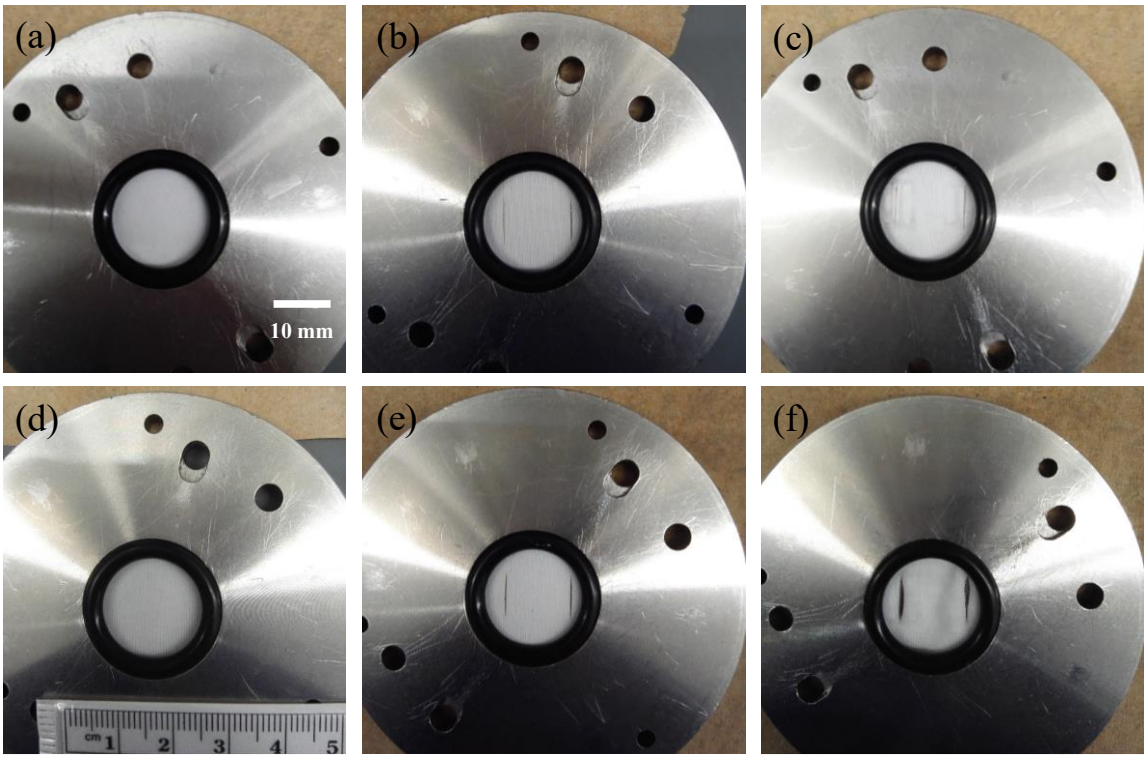

Figure S4.7 Fabric samples fixed in the capillary flow porometer chambers for air permeability test. (a, d) Control knitted nylon fabric, (b, e) control fabric with slits and (c, f) fabric with slits coated with three-layer hydrogels, under (a-c) dry and (d-f) wet conditions, respectively.

REFERENCES

[1] S.L.P. Tang, G.K. Stylios, An overview of smart technologies for clothing design and engineering, *Int J Cloth Sci Tech* **18**(1-2) (2006) 108-128.

[2] J.L. Hu, H.P. Meng, G.Q. Li, S.I. Ibekwe, A review of stimuli-responsive polymers for smart textile applications, *Smart Mater Struct* **21**(5) (2012).

[3] A. Gugliuzza, E. Drioli, A review on membrane engineering for innovation in wearable fabrics and protective textiles, *J Membrane Sci* **446** (2013) 350-375.

[4] D. Jocic, Polymer-based smart coatings for comfort in clothing, *Tekstilec* **59**(2) (2016) 107-114.

[5] J. McCann, R. Hurford, A. Martin, A design process for the development of innovative smart clothing that addresses end-user needs from technical, functional, aesthetic and cultural view points, *Ninth IEEE International Symposium on Wearable Computers, Proceedings* (2005) 70-77.

[6] E. Pennisi, EVOLUTION How plants learned to breathe Even early plants likely had sophisticated pores to regulate water and swap gases with their environment, *Science* **355**(6330) (2017) 1110-1111.

[7] N.S. Christodoulakis, J. Menti, B. Galatis, Structure and development of stomata on the primary root of Ceratonia siliqua L, *Ann Bot* **89**(1) (2002) 23-9.

[8] O.L. Lange, R. Losch, E.D. Schulze, L. Kappen, Responses of stomata to changes in humidity, *Planta* **100**(1) (1971) 76-86.

[9] M.R.G. Roelfsema, R. Hedrich, In the light of stomatal opening: new insights into 'the Watergate', *New Phytol* **167**(3) (2005) 665-691.

[10] M. Fricker, C. Willmer, Stomata, *Springer Netherlands* (2012) 18. ISBN 978-94-011-0579-8. Retrieved 15 June 2016.

[11] J.T. Fan, M.K. Sarkar, Y.C. Szeto, X.M. Tao, Plant structured textile fabrics, *Mater Lett* **61**(2) (2007) 561-565.

[12] E. Kamalha, Y.C. Zeng, J.I. Mwasiagi, S. Kyatuheire, The comfort dimension; a review of perception in clothing, *J Sens Stud* **28**(6) (2013) 423-444.

[13] Z.B. Hu, X.M. Zhang, Y. Li, Synthesis and application of modulated polymer gels, *Science* **269**(5223) (1995) 525-527.

[14] P.D. Topham, J.R. Howse, C.J. Crook, S.P. Armes, R.A.L. Jones, A.J. Ryan, Antagonistic triblock polymer gels powered by pH oscillations, *Macromolecules* **40**(13) (2007) 4393-4395.

[15] H. Kim, S.J. Lee, Stomata-inspired membrane produced through photopolymerization patterning, *Adv Funct Mater* **25**(28) (2015) 4496-4505.

[16] H. Kim, S.J. Lee, Fabrication of triple-parted stomata-inspired membrane with stimulus-responsive functions, *Sci Rep-Uk* **6** (2016) 21258.

[17] Y. Park, M.P. Gutierrez, L.P. Lee, Reversible self-actuated thermo-responsive pore membrane, *Sci Rep-Uk* **6** (2016) 39402.

[18] A. Gargava, C. Arya, S.R. Raghavan, Smart hydrogel-based valves inspired by the stomata in plants, *Acs Appl Mater Inter* **8**(28) (2016) 18430-18438.

[19] A. Mukhopadhyay, V.K. Midha, A review on designing the waterproof breathable fabrics Part I: fundamental principles and designing aspects of breathable fabrics, *J Ind Text* **37**(3) (2008) 225-262.

[20] Stomatex® Technology, *http://www.stomatex.com/faqs.htm#what*

[21] W. Wang, L.N. Yao, C.Y. Cheng, T. Zhang, H. Atsumi, L.D. Wang, G.Y. Wang, O. Anilionyte, H. Steiner, J.F. Ou, K. Zhou, C. Wawrousek, K. Petrecca, A.M. Belcher, R. Karnik, X.H. Zhao, D.I.C. Wang, H. Ishii, Harnessing the hygroscopic and biofluorescent behaviors of genetically tractable microbial cells to design biohybrid wearables, *Sci Adv* **3**(5) (2017).

[22] J. Mu, G. Wang, H. Yan, H. Li, X. Wang, E. Gao, C. Hou, A.T.C. Pham, L. Wu, Q. Zhang, Y. Li, Z. Xu, Y. Guo, E. Reichmanis, H. Wang, M. Zhu, Molecular-channel driven actuator with considerations for multiple configurations and color switching, *Nat Commun* **9**(1) (2018) 590.

[23] L.H. Lao, S.S. Robinson, B. Peele, H.C. Zhao, B.C. Mac Murray, J.K. Min, B. Mosadegh, S. Dunham, R.F. Shepherd, Selective mineralization of tough hydrogel lumens for simulating arterial plaque, *Adv Eng Mater* **19**(1) (2017).

[24] S. Li, B.N. Peele, C.M. Larson, H.C. Zhao, R.F. Shepherd, A stretchable multicolor display and touch interface using photopatterning and transfer printing, *Adv Mater* **28**(44) (2016) 9770-9775.

[25] H. Yuk, T. Zhang, G.A. Parada, X.Y. Liu, X.H. Zhao, Skin-inspired hydrogel-elastomer hybrids with robust interfaces and functional microstructures, *Nat Commun* **7** (2016).

[26] H.P. Tan, J.D. Wu, L.H. Lao, C.Y. Gao, Gelatin/chitosan/hyaluronan scaffold integrated with PLGA microspheres for cartilage tissue engineering, *Acta Biomater* **5**(1) (2009) 328-337.

[27] BS 7209, Specification for water vapour permeable apparel fabrics, *British Standard* (1990).

[28] M. Kim, Y.S. Wu, E.C. Kan, J. Fan, Breathable and flexible piezoelectric Zno@PVDF fibrous nanogenerator for wearable applications, *Polymers-Basel* **10**(7) (2018).

[29] J.A. Fernando, D.D.L. Chung, Pore structure and permeability of an alumina fiber filter membrane for hot gas filtration, *J Porous Mat* **9**(3) (2002) 211-219.

[30] J.T. Fan, Y.S. Chen, Measurement of clothing thermal insulation and moisture vapour resistance using a novel perspiring fabric thermal manikin, *Meas Sci Technol* **13**(7) (2002) 1115-1123.

CHAPTER 5

CONCLUSIONS AND SUGGESTIONS FOR FURTHER WORK

5.1 Summary

This dissertation reported several advances in improving the moisture and liquid transport properties of clothing fabrics for thermal comfort. These advances are summarized below:

Wettability improvement: Chapter 2 reports a new approach to endow superhydrophilicity on a wrinkle-free cotton fabric through a combination of plasma treatment followed by the attachment of specially engineered silica nanoparticles. Wettability is optimized by screening different power and time of the plasma treatment. Through aging, laundering and abrasion tests, it was found the fabric achieved durable superhydrophilicity after the nanoparticle treatment. In the meantime, the treated fabric does not have any detrimental effect on the wrinkle-free performance, mechanical property and abrasion resistance. The technology solves the dilemma of achieving both the wrinkle-free property and superhydrophilicity on a cotton fabric in a conventional wrinkle-free finishing process, therefore would bring a huge value for the industry players and market end-users.

Directional liquid transport: Chapter 3 reports a "skin-like" fabric with both directional water transport and water repellent properties. Spatially distributed porous channels with gradient wettability was created through the thickness of a superhydrophobic finished fabric via a selective plasma treatment with patterned masks. While these channels were served for directional liquid transport, the predominantly untreated surface remained

superhydrophobic, therefore could repels external liquid contaminants. The properties were validated by water dipping tests on either contact angle tester or a home-made device. The mechanism can be theoretically analyzed by the Gibbs pinning criterion and correlated with the structure and wettability. The technology has a high significance to the apparel industry, for bringing directional water transport property and water repellency simultaneously on a fabric. It can also be leveraged into other fabric or membrane applications, such as liquid separation and purification, fuel cells, wound dressing, and flexible microfluidic devices.

Moisture-responsive breathability: Chapter 4 reports a breathable nylon fabric with moisture responsive pores to mimic leaf stomata. The function is realized by coating a special hydrogel system on the slits (pores) of the fabrics functioning as "guard cells", in which the inner layer has a highly crosslinked component and the outer layer has a less crosslinked component. Because of the different swelling, the pores are able to enlarge under wet condition, while stay closed under normal dry condition. The opening of the artificial stomata in wet environment improved both water vapor transmission and air permeability compared with the control fabric. The smart breathable fabric can have a potential application as interactive functional clothing for different physiological demands. In addition, it may be also extended to other potential applications such as smart medical care devices, food packaging, controlled nutrient or drug release and other industrial products.

5.2 Future Work

Despite the several progresses reported in this dissertation, there are still space for further work.

Performance Evaluation: In this work, evaluations of the developed fabrics are based on the key properties via basic objective methods in the lab. Other non-relevant but still important properties should also be evaluated so as to meet wearer's diverse need. For example, the superhydrophilic finished wrinkle-free fabric was found not as soft as the pristine fabric. Evaluations by, for example, Kawabata evaluation system (KES-F) should be conducted to compare the fabric handle or softness with the industrial standards. To evaluate the overall thermal comfort of clothing made of the developed fabrics, testing on a sweating manikin is recommended. Human subjective evaluation can further be considered when the fabric samples can be scaled up.

Scalability: Most of the process and fabrication of the fabrics are based on manual operation. The development of an automated process is essential for scaling up the fabrication process. For example, the spot channels for the directional water transport fabric may be continuously created during the chemical finishing process. The artificial stomata (hydrogels) may be coated onto the fabric via screen printing or 3D printing, and a smaller scale slit could be generated by laser cutting. With the automatization, it would be possible to prepare larger sample for further human subjective tests. It is also expected the preciseness and scalability of the fabrication process will also be greatly improved by the automated process.

Extension: The current functions of the fabrics are targeted on water, viz. liquid or vapor form. It is possible to investigate other liquids, such as oil, based on the similar material design principles. For example, silica nanoparticles have the flexibility to be functionalized as hydrophobic, oleophobic, omniphilic and omniphobic. While oleophobic fluoro-free coatings are also being investigated in the lab, it is good to form a platform to manipulate the surface of silica through the chemistry approaches for different fabric applications. Directional water transfer fabrics can also be extended to oil transfer systems for developing efficient separation or filtration membranes.